February

Many-body theory of Electric Dipole Moments of Atoms and it's implications for the Standard Model of Particle Physics

A thesis

submitted for the degree of

Doctor of Philosophy

In

The Faculty of Science

University of Mangalore, Mangalore

by

K. Venkata Phani Lata

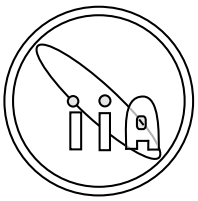

Indian Institute of Astrophysics

Bangalore 560 034, INDIA

February 2006

To my dearest mother, Smt. Shantha Kumari

DECLARATION

I hereby declare that the matter contained in this thesis is the result of the investigations carried out by me at the Indian Institute of Astrophysics, Bangalore, under the supervision of Prof. Bhanu Pratap Das. This thesis has not been submitted for the award of any degree, diploma, associateship, fellowship etc. of any university or institute.

Prof. Bhanu Pratap Das
(Thesis Supervisor)

K.Venkata Phani Lata.
(Ph.D. Candidate)

Indian Institute of Astrophysics
Bangalore 560 034, INDIA
August, 2005

CERTIFICATE

This is to certify that the thesis entitled **"Many body theory of Electric Dipole Moments of Atoms and it's implications for the Standard Model of Particle Physics"** submitted to the University of Mangalore by Ms.K. Venkata Phani Lata . for the award of the degree of Doctor of Philosophy in the faculty of Science, is based on the results of the investigations carried out by her under my supervision and guidance, at the Indian Institute of Astrophysics, Bangalore. This thesis has not been submitted for the award of any degree, diploma, associateship, fellowship etc. of any university or institute.

Prof. Bhanu Pratap Das
(Thesis Supervisor)

Indian Institute of Astrophysics
II Block, Koramangala
Karnataka
August, 2005

Acknowledgements

The following.

LIST OF PUBLICATIONS

1. Publications - (1)

2. Publications - (2)

3. Publications - (3)

4. Publications - (4)

5. Publications - (5)

Table of Contents

List of Tables

List of Figures

Many-body theory of Electric Dipole Moments of Atoms and it's implications for the Standard Model of Particle Physics

Chapter 1

Introduction

1.1 Atomic electric dipole moments(EDM)

The three discrete symmetry operations under which the laws of physics were thought to be invariant till the year 1957 are parity (P), time-reversal (T) and the charge conjugation (C). The search for violations of these symmetries could have profound implications for our understanding of particle physics. Of the three symmetries, P violation was observed by Wu.et.al.[1] in 1957. Some years later, CP violation was observed in the neutral kaon system [2]. The three symmtries are linked by the CPT theorem [1] from which it can be inferred that CP-violation implies T violation.

The origin of parity violation can be discerned within the frame work of the Standard Model (SM) of particle physics through the weak interactions, but there is no clear understanding of the origin of time-reversal violation in nature. The presence of a non-zero electric dipole moment on a non-degenerate physical system is a direct signature of parity (P) and time-reversal (T) symmetry violations [3]. The total angular momentum of a physical system is related to it's intrinsic EDM given by, $\mathbf{D} = d\,\mathbf{J}$, where $\mathbf{J}$ is the total angular momentum and $\mathbf{D}$ the intrinsic EDM and d is the proportionality constant. It will be shown at a later stage in the thesis that d is actually the coupling constant of the P and T violating interaction in question. Table.1.1 illustrates the consequences of $\hat{P}$ and $\hat{T}$ violations on the intrinsic EDMs. Under a parity transformation $\mathbf{D}$ being a vector changes sign and $\mathbf{J}$ being pseudo vector doesn't change sign, whereas under a time-

[1] While a physical system described by a local field theory may violate any of these symmetries independently, it is invariant under the combined operation of all three of them

Quantity	Parity	Time-reversal
$\mathbf{D}$	$\mathbf{D} = -\mathbf{D}$	$\mathbf{D} = \mathbf{D}$
$\mathbf{J}$	$\mathbf{J} = \mathbf{J}$	$\mathbf{J} = -\mathbf{J}$

Table 1.1: $\hat{P}$,$\hat{T}$ violation for a non-zero EDM

reversal tranformation $\mathbf{J}$ changes sign and $\mathbf{D}$ does not. The above table demonstrates in a simple way that for a system to have a non-zero EDM, both $\hat{P}$ and $\hat{T}$ have to be simulataneously violated. This can be rigorously proved for a non-degenerate physical system using some important ideas of quantum mechanics and is presented in Appendix *A*. Hence, it follows that atoms being non-degenerate physical systems can possess a non-zero intrinsic EDM if there are violations of P and T symmetries. They offer advantages from an experimental point of view, of being electrically neutral and hence can be subjected to external electric fields. In addition, atoms are rich sources of EDMs as we shall explain later in this chapter. They allow studies of CP or T violations in the leptonic, semi-leptonic and hadronic sectors. Searches for an atomic EDM can be broadly classified into the following catagories - EDM of paramagnetic atoms (atoms having open-shell structure) and EDMs of dia-magnetic atoms (atoms with closed electronic structure) and EDMs of nucleons, particularly that of the neutron. In this thesis, we discuss only the EDMs of diamagnetic atoms. Theoretical studies involve the parameterization of the atomic EDMs in terms of the CP-violating coupling constants at various levels as shown in Fig.1.1 [4]. Some of the extensions of the Standard Model, like the Multi-higgs, Super Symmetry (SUSY) and Left-right symmetric models, predict CP-violation at the level of elementary particles. The atomic EDMs can hence be expressed in terms of these coupling constants, with the knowledge of the CP-violating parameters of the intermediate - nuclear, nucleon and elementary particle sectors as shown in Fig.1.1.

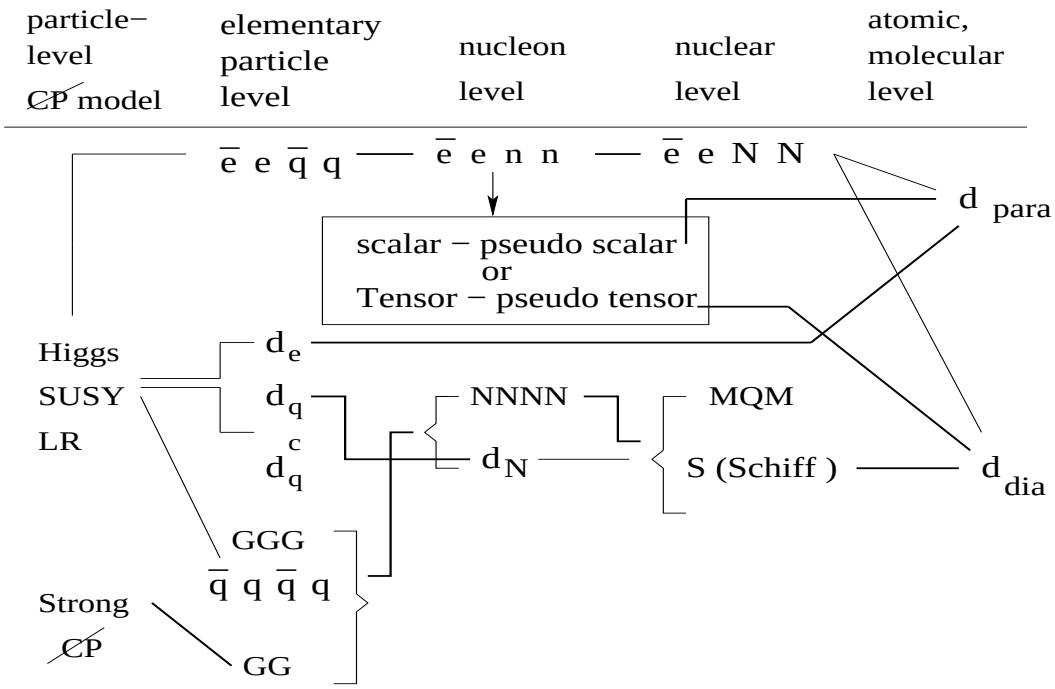

Figure 1.1: Origin of atomic EDM (Steve Barr, 1993).

1.1.1 Closed and open-shell atomic EDMs - their implications

The permanent EDM of a physical system is aligned along it's total angular momentum. This can be demonstrated by using the Wigner-Eckart theorem[2]. Since the EDM of a closed-shell atom has zero total angular momentum from the electronic sector, the atomic EDM must lie along the nuclear spin. This EDM arises primarily from the CP-violating electron-nuclear interactions and the Nuclear Schiff moment(NSM, S). The electron-nuclear interaction, which violate $\hat{T}$ and $\hat{P}$ are the tensor-pseudo tensor (T-PT)[3] or the scalar-pseudo scalar (S-PS)interactions, the NSM and the Magnetic Quadrupole Moment (MQM). In this thesis, we study atomic EDMs of closed-shell atoms which arise mainly from the T-PT electron-nuclear interactions and the Nuclear Schiff Moment. At the elementary particle level, the origin of closed-shell atomic EDMs is attributed to the $\hat{P}$ and $\hat{T}$ violating electron-quark interactions and quark-quark interactions which are

[2]Essentially which states that any vector pertaining to a system, must align with respect to the direction of the internal property of the system

[3]In $\bar{e}e - \bar{N}N$ interaction, we treat the electron and the nuclear currents as the tensor and pseudo tensor currents respectively, given by $\bar{\Psi}_e \sigma_{\mu\nu} \Psi_e$ and $\bar{\Psi}_N \sigma_{\mu\nu} \gamma^5 \Psi_N$

predicted by the lepto-quark models [4]. The limits on the T-PT coupling constant (C_T) has been obtained from the comparison of the most recent experimental result of ^{199}Hg atomic EDM [5, 6],

$$d(^{199}Hg) \;=\; (-1.06 \pm 0.49 \pm 0.40) \times 10^{-28}\text{ecm}$$

and the enhancement factor calculated by [7], using the Coupled-perturbed Hartree-Fock theory,

$$d(^{199}Hg) = -6.0 \times 10^{-22} C_T \sigma_N \text{e} - \text{m}$$

which gives the limit on C_T,

$$C_T = \Big(1.77 \pm 0.82 \pm 0.67\Big) \times 10^{-9} \sigma_N$$

A non-zero value of C_T would imply physics beyond the Standard Model. The accuracy of the calculations of enhancement factors would lead to a more stringent limit on C_T. Coupled-perturbed Hartree-Fock theory accounts for two-particle, two-hole kind of electron correlations to all orders in perturbation. In addition to these correlation effects, it is important to include a lot more effects which have not been accounted for by the Coupled-perturbed Hartree-Fock theory to all orders. A more accurate atomic theory should be able to treat all kinds of electron correlation to all orders in perturbation, which includes four-particle, four-hole, three-particle - one-hole, etc effects. It is a challenge for many-body atomic theorists to be able to account for these important correlation effects and in this thesis, we have attempted to address this problem.

As shown in the chart, Fig.1.1, the NSM(denoted by operator **S**) can be caused by the nucleon-nucleon interactions or a nucleon EDM, which at the elementary level could arise from the interaction between the quarks and the chromo electric dipole moments of the quarks. The coupling constants associated with these interactions can be predicted by Multi-higgs, SUSY [4, 8]. The dependence of the T-PT and NSM interactions on the nuclear spin makes closed-shell atoms, in particular, those having non-zero nuclear spin the best candidates to look for EDMs sensitive to the nuclear sector. Closed shell

atoms can also give information on the electron EDM and scalar-pseudo scalar electron-nuclear interaction by considering the hyperfine interaction as a perturbation [9], but the the limits on the corresponding coupling constants would not be as sensitive as those obtained from the paramagnetic atomic EDMs. For ^{199}Hg, the EDM induced by the NSM is calculated and parameterized in terms of the Schiff moment operator S. The most recent calculation by [10, 11], gives,

$$d_{Hg} = -2.8 \times 10^{-17} \left(\frac{S_{Hg}}{\text{efm}^3} \right) \text{ecm}$$

At the nucleon level, the operator S can be obtained in terms of the pion-nucleon coupling constants; pions being the dominant mediators of the nucleon-nucleon interactions (more detailed analysis is presented in Section.6.6 with results) [12, 13]:

$$d_{Hg} = 3.92 \times 10^{-25} \eta_{np} \text{ ecm}$$

This calculation involves non-trivial nuclear-many body physics, and it gives [14],

$$d_{Hg} = -3.92 \times 10^{-25} \times \left(\frac{G_F m_\pi^2}{\sqrt{2}} \right) g_{\pi NN} \, \bar{g}_{\pi NN} \text{ ecm}$$

From the above, the observable atomic EDM can be expressed interms of the chromo EDMs of quarks by,

$$d_{Hg} = -3.92 \times 10^{-25} \times \left(\frac{G_F m_\pi^2}{\sqrt{2}} \right) g_{\pi NN} \times 2 \left(\tilde{d}_u - \tilde{d}_d \right) \text{ecm}$$

where $\tilde{d}_d$ and $\tilde{d}_u$ are chromo EDMs of the d and the u quarks respectively which are predicted by SUSY and the left-right symmetric models. The constant $\bar{g}_{\pi NN}$ is also related to θ_{QCD}, the QCD vacuum angle,

$$\bar{g}_{\pi NN} \approx -0.027 \, \theta_{\text{QCD}}$$

This allows us to constrain the value of θ_{QCD} through the ^{199}Hg atomic EDM.

1.2 Experiments on Atomic EDMs

The atomic calculations involve the calculation of 'enhancement factor' which is the atomic EDM parameterized in terms of the $\hat{P}$ and $\hat{T}$ violating coupling constants (R

$= d_{atom}/C$). Comparing with the measured value of the atomic EDM, the value of C can be extracted. Atoms are very good candidates for the search for atomic EDMs. In particular, heavy atoms are preferred choices as the EDM scales as Z^2 or Z^3. If a physical system has an intrinsic EDM d, then it's interaction with the external field, in analogy with the interaction of the magnetic dipole moment μ is,

$$H_{\rm int} = -\left(d\vec{E} \ + \ \mu\vec{B}\right) \cdot \frac{\vec{J}}{J}$$

where $\vec{J}$ is the total angular momentum of the system. In the presence of an external electric and magnetic fields, the EDM d and the magnetic dipole moment μ precess about the field axes. This precession is referred to as the Larmor precession. The basic idea in an EDM experiment is to measure the difference in the Larmor precession frequency corresponding to the parallel and anti-parallel configurations of $\vec{E}$ with respect to $\vec{B}$ [3],

$$\begin{aligned}
\omega_1 &= \frac{2\mu|\vec{B}| \ + \ 2d|\vec{E}|}{\hbar} \\
\omega_2 &= \frac{2\mu|\vec{B}| \ - \ 2d|\vec{E}|}{\hbar} \\
\delta\omega &= \omega_1 \ - \ \omega_2 = \frac{2d|\vec{E}|}{\hbar}
\end{aligned}$$

Therefore,

$$d \ = \ \frac{\hbar \, \delta\omega}{2|\vec{E}|}$$

Owing to the precision to which the frequency is to be measured, the EDM experiments are susceptible to a number of systematic effects like the motional magnetic fields, which is one of the most important sources of error. Atoms moving in an external electric field experience magnetic field in their rest frame, known as the motional magnetic field, given by, $\mathbf{B_m} = \mathbf{v} \times \mathbf{E}/\mathbf{c}$. This field is odd in $\vec{E}$ and can mimic an EDM signal. The second important systematic effect comes from the leakage currents induced by the electric field. The leakage currents caused by high voltage are difficult to control and account for. Laser cooled atoms are excellent candidates for an EDM experiment. They offer the following advantages over the conventional beam and cell apparatus :

1. The environment is relatively perturbation free due to extremely low temperatures.

2. The velocities of the atoms in the sample is zero and hence there is zero, or negligible motional magnetic field effect.

3. They allow high coherence times as the atoms can maintain spin coherence for a relatively long time.

4. Low leakage curents

5. It is possible to apply high electric fields as high as 100 kV/cm, as the sample region is small.

They offer many more advantages, than the conventional cell and beam apparatus for measuring the atomic EDM.

1.3 Present status of the ^{199}Hg EDM experiment and other closed-shell atoms

To date, the EDM experiment on ^{199}Hg gives the most sensitive limits on $\hat{P}$ and $\hat{T}$ violating coupling constants [5, 6]. ^{199}Hg has a non-zero nuclear spin, $I = 1/2$ and hence is very sensitive to the $\hat{P}$ and $\hat{T}$ violating interactions in the nuclear sector as both the Nuclear Schiff moment, and the tensor-pseudo tensor interactions, depend on the nuclear spin. Also, with $Z = 80$ it is sufficiently heavy which would enhance the relativistic effects, in turn enhancing the EDM. Any non-zero result for the ^{199}Hg EDM would indicate physics beyond the Standard Model. To set limits on specific models of CP violation, using atomic theory, the atomic EDM must be related to the CP violating parameters at the level of elementary particles. Our aim in this work is to improve the present limits for T-PT coupling constant and the Schiff moment which would in turn help in obtaining more accurate limits for the $\hat{P}$ and $\hat{T}$ violating coupling constants at the level of quarks and electrons. Limits on S can also be used to set further limits on the nucleon EDMs [15]. The Table.1.3 summarizes the on-going EDM experiments on closed-shell atoms. For experiments on various other atomic systems, see [16].

Atomic system	Present limit of EDM measured —($d_{\rm atom}$)—(e cm)	Laboratory
^{1}99Hg	$< 2.1 \times 10^{-28}$	Univ. of Washington, Seattle
Xenon		Princeton University
Radium		Argonne National Laboratory
Ytterbium		Kyoto University
Radon isotopes		University of Michigan

Table 1.2: On-going experiments on closed-shell atoms

Using apparatus consisting of two cells, the EDM of ^{199}Hg was measured to be [5, 6]

$$d(^{199}Hg) \;=\; (-1.06 \pm 0.49 \pm 0.40) \times 10^{-28}\text{ecm}$$

There is further scope of improving the above result, using 4 cells, which could improve the sensitivity of the measurement by a factor of 4.

Chapter 2

Closed-shell Atomic Electric Dipole moments

Atomic EDM can arise from one/many of the following sources :

- EDM of an electron d_e.
- P,T-odd electron-nucleon interactions which could be 'scalar' (scalar-pseudoscalar), 'tensor'(tensor-pseudotensor) or 'pseudo-scalar' (pseudoscalar-scalar) couplings.
- P,T-odd electron-electron couplings(is negligible in contribution due to the strength of the interaction).
- EDMs originating in the nucleus (nuclear Schiff moment (NSM))due to the presence of $\hat{P}$ and $\hat{T}$ violating interactions at the level of quarks.

Electric dipole moments of closed shell atoms arise predominantly from the 'tensor' kind of the electron-nucleus interaction and the NSM produced by the nucleus [4]. Though the other sources listed above also contribute to the atomic EDM of closed-shell atoms, they are not dominant owing to the electronic and nuclear structure and related effects in closed shell atomic systems, which will be discussed in subsequent sections, which make the closed-shell atoms less sensitive to other P and T -odd interactions.

2.1 Atomic EDM induced by a tensor-pseudo tensor kind of electron-nuclear interaction

Consider the atomic EDM arising from P,T-odd electron-nucleon interactions and treat the nucleus non-relativistically. The interaction Hamiltonian has the form,

$$H_{e-N}^{EDM,T} = \frac{iG_F C_T}{\sqrt{2}} \sum_i \boldsymbol{\sigma_N} \cdot \boldsymbol{\gamma_i} \rho_N(r) \tag{2.1}$$

where, G_F is the Fermi's coupling constant, C_T represents the T-PT coupling constant, $\rho_N(r)$ is the nuclear density and β and γ_5 represent Dirac matrices. The operator σ_N is the nuclear spin which sometimes denoted by $\mathbf{I}$ in this thesis. This interaction is responsible for the mixing of opposite parity electronic states producing a non-zero atomic EDM and it is this dependence of the $H_{e-N}^{EDM,T}$ on the nuclear spin that makes closed-shell atoms having *non-zero* nuclear spin to be more sensitive to this interaction. The above form can be arrived at, starting from the second quantised form of the $H_{\rm EDM}$ operator,

$$H_{\rm EDM} \;=\; \frac{iC_T G_F}{\sqrt{2}} \left[\bar{\Psi}_N \sigma_{\mu\nu} \Psi_N\right] \left[\bar{\Psi}_e \gamma^5 \sigma_{\mu\nu} \Psi_e\right]$$

Consider the term, $\left(\bar{\Psi}_N \sigma_{\mu\nu} \Psi_N\right)$. We have, $\bar{\Psi}_N = \Psi_N^\dagger \gamma_0$. Hence,

$$\begin{aligned} \gamma_0\, \sigma_{\mu\nu} &= \gamma_0 \frac{i}{2} \left[\gamma_\mu \gamma_\nu - \gamma_\nu \gamma_\mu\right] \\ &= 0 \,{\rm if}\; \mu = \nu \\ &= i\, \gamma_0 \gamma_\mu \gamma_\nu \,{\rm if}\; \mu \neq \nu \end{aligned} \tag{2.2}$$

Using $\{\gamma_\mu, \gamma_\nu\} = 0$, we have,

$$\begin{aligned} \gamma_0\, \sigma_{\mu\nu} &= \gamma_0\; i\; \gamma_\mu \gamma_\nu \; (\mu \neq \nu) \\ i\; \gamma_0 \gamma_\mu \gamma_\nu &= i\; \gamma_0 \left[\gamma_0 \gamma_i \;+\; \gamma_i \gamma_\nu\right]_{(i \neq \nu)} \\ &= i\; \gamma_i \;+\; i\; \gamma_0 \gamma_i \gamma_\nu \\ &= i\; \gamma_i \;+\; i \alpha_i \gamma_\nu \\ &= i \left(\gamma_i \;+\; \alpha_i \gamma_\nu\right) \end{aligned} \tag{2.3}$$

Hence,

$$H_{\rm EDM} \;=\; \frac{iC_T G_F}{\sqrt{2}} \;\Big[i\;\Psi_N^\dagger\,(\gamma_i \;+\; \alpha_i\gamma_\nu)_{(i\neq\nu)}\,\Psi_N\Big] \;\;\big[\bar{\Psi}_e\gamma^5\sigma_{\mu\nu}\Psi_e\big]$$

Consider,

$$\begin{aligned}
\bar{\Psi}_e\gamma^5\sigma_{\mu\nu}\Psi_e &= \Psi_e^\dagger\gamma_0\gamma_5\,(i\gamma_\mu\gamma_\nu)\,\Psi_e \\
&= i\;\Psi_e^\dagger\gamma_0\gamma_5\gamma_\mu\gamma_\nu\Psi_e \\
&= -\,i\;\Psi_e^\dagger\gamma_5\gamma_0\gamma_\mu\gamma_\nu\Psi_e \\
&= -\,i\;\Psi_e^\dagger\gamma_5\,(\gamma_i \;+\; \alpha_i\gamma_\nu\Psi_e)^2
\end{aligned} \tag{2.4}$$

where $\big[\nu = 0, \alpha_i\gamma_0 = -\gamma_0\alpha_i = -\gamma_0\gamma_0\gamma_i = -\gamma_i\big]$

$$\begin{aligned}
H_{\rm EDM} &= \frac{iC_T G_F}{\sqrt{2}}\;\big[\Psi_N^\dagger\big(\gamma_i \;+\; \alpha_i\gamma_\nu\big)_{(i\neq\nu)}\Psi_N\big]\;\big[\Psi_e^\dagger\gamma_5\,(\gamma_i \;+\; \alpha_i\gamma_\nu)\,\Psi_e\big] \\
&= \frac{iC_T G_F}{\sqrt{2}}\;\big[\Psi_N^\dagger\big(\gamma_i \;+\; \alpha_i\gamma_0 \;+\; \alpha_i\gamma_j\big)\Psi_N\big]\;\big[\Psi_e^\dagger\gamma_5\big(\gamma_i \;+\; \alpha_i\gamma_0 \;+\; \alpha_i\gamma_j\big)\Psi_e\big] \\
&= \frac{iC_T G_F}{\sqrt{2}}\;\Big[\Psi_N^\dagger\;\alpha_i\gamma_j\Psi_N\Big]\;\big[\Psi_e^\dagger\gamma_5\;\alpha_i\gamma_j\Psi_e\big] \\
&= \frac{iC_T G_F}{\sqrt{2}}\;\big[\Psi_N^\dagger\;\beta\gamma_i\gamma_j\Psi_N\big]\;\big[\Psi_e^\dagger\gamma_5\;\beta\gamma_i\gamma_j\Psi_e\big] \\
&= \frac{iC_T G_F}{\sqrt{2}}\;\Big[\Psi_N^\dagger\;\alpha_i\beta\alpha_j\Psi_N\Big]\;\big[\Psi_e^\dagger\gamma_5\;\alpha_i\beta\alpha_j\Psi_e\big] \\
&= \frac{iC_T G_F}{\sqrt{2}}\;\Big[\Psi_N^\dagger\beta\alpha_i\alpha_j\Psi_N\Big]\;\big[\Psi_e^\dagger\gamma_5\beta\alpha_i\alpha_j\Psi_e\big]
\end{aligned} \tag{2.5}$$

Consider

$$\begin{aligned}
\alpha_i\alpha_j &= \begin{pmatrix} 0 & \sigma_i \\ \sigma_i & 0 \end{pmatrix} \times \begin{pmatrix} 0 & \sigma_j \\ \sigma_j & 0 \end{pmatrix} \\
&= \begin{pmatrix} \sigma_i\sigma_j & 0 \\ 0 & \sigma_i\sigma_j \end{pmatrix} \\
&= \sigma_i\sigma_j\,\mathbf{I}
\end{aligned} \tag{2.6}$$

Consider,

$$\begin{aligned}
\gamma^5\alpha^k &= \begin{pmatrix} 0 & -I \\ -I & 0 \end{pmatrix} \times \begin{pmatrix} 0 & \sigma_k \\ \sigma_k & 0 \end{pmatrix} \\
&= \begin{pmatrix} -\sigma_k & 0 \\ 0 & -\sigma_k \end{pmatrix} \\
&= -\begin{pmatrix} \sigma_k & 0 \\ 0 & \sigma_k \end{pmatrix} \\
&= i\,\epsilon_{ijk}\,\gamma^5\,\alpha^k \\
&= i\,(\,2\,\mathbf{I}\,) \qquad (2.7)
\end{aligned}$$

Treating the nucleus non-relativistically,

$$\begin{aligned}
H_{\rm EDM} &= \frac{iC_TG_F}{\sqrt{2}}\,[\,2\,\mathbf{I}\,]\left[\Psi_e^\dagger\gamma_5\beta\,\gamma_5\,\alpha_k\Psi_e\right]\rho_{\rm N}\,(r) \\
&= \frac{2iC_TG_F\sqrt{2}}{2}\,\beta\,\alpha\,\mathbf{I}\,\rho_{\rm N}\,(r) \\
&= (i\,C_T\,G_F)\,\left(\sqrt{2}\right)(\,\beta\,\alpha\cdot\mathbf{I}\,)\;\rho_{\rm N}\,(r) \qquad (2.8)
\end{aligned}$$

For an N-electron system, the above equation becomes,

$$H_{\rm EDM} = (i\,C_T\,G_F)\,\left(\sqrt{2}\right)\sum_i(\,\gamma_i\cdot\mathbf{I}\,)\;\rho_{\rm N}\,(r) \qquad (2.9)$$

From the above expression, it can be noted that the nuclear density $\rho_{\rm N}\,(r)$ is proportional to the atomic number Z. The product of the Dirac matrices, $(\,\beta\,\alpha)$ is an off-diagonal matrix and hence the matrix element of the $H_{\rm EDM}$ between the spinors which are proportional to $\sqrt{Z}$, and the dependence of the β matrix on Z, finally results in the scaling of the enhancement factor as Z^3 [1]. This suggests that heavy atoms are preferred candidates for EDM experiments.

2.2 Atomic EDMs arising from the Nuclear Schiff Moment

According to Schiff's theorem, the EDM of a point like nucleus is completely screened by the atomic electrons and hence it cannot be measured[sandars]. If a set of charged

[1] See Appendix D for $H_{\rm EDM}$ matrix elements

particles with edms, are in equilibrium under their mutual electrostatic forces, the first order correction to the energy due to the interaction of EDM with external field is zero. Consider an atom as a set of quantum mechanical charged particles, placed in an external field. The atom gets polarized and hence this induced charge distribution produces an internal field to cancel the external field. Hence, there can be no nett force on the atom or the nucleus. This cancellation of the internal and external fields is exact for a point nucleus, but not for a finite one. A nucleus with a structure means the $l = 0$ and $l = 1$ electron wavefunctions have a non-zero density inside the nucleus. The nuclear Schiff moment arises due to the P and T odd nuclear interations and is responsible for the mixing of the opposite parity electronic wavefunctions, particularly the states having $l = 0$ and $l = 1$ and resulting in an atomic EDM.

The electrostatic potential produced by the Schiff moment is of the form [12]

$$\Phi(\vec{R}) = 4\pi \vec{S} \cdot \vec{\nabla}\delta(\vec{R})$$

for non-relativistic electrons. Now the contact interaction $-e\Phi$ mixes the 's' and 'p' orbitals and produces EDMs in atoms. Using integration by parts and property of Dirac delta function, the matrix element

$$\left\langle S \middle| -e\Phi \middle| P \right\rangle = 4\pi e \vec{S} \cdot \left(\nabla \Psi_s^\dagger \Psi_p\right)_{R=0} = const.$$

is finite. The general P,T - odd electrostatic potential inside the nucleus, is derived by [17] and a detailed derivation is presented in the Chapter$F$.

According to the most recent work by [17] a more convenient expression for the nuclear potential arising from the nuclear Schiff moment is given by :

$$\Phi(\vec{R}) = -\,3\frac{\vec{S}\cdot\vec{R}}{B}\,\rho(\vec{R}) \tag{2.10}$$

where $B = \int R^4 \rho(\vec{R}) dR$ and R is the electron coordinate. The Hamiltonian of the interaction of electrons with this potential is

$$H_{\rm SM} = \,3\,e\,\frac{\vec{S}\cdot\vec{R}}{B}\,\rho(\vec{R}) \tag{2.11}$$

If $\rho(\vec{R})$ is consider as the normalised density function, which is 1 for $R < R_N - \delta$ and $R > R_N + \delta$,then the dimension of B is L^5. Substituting in Eq.2.11, we obtain the dimension of S as QL^3. If $\rho(\vec{R})$ is considered as the usual nuclear density (dimension L^3), then the dimension of B becomes $= R^4 \times R^3 \times R = L^8$. Substituting the dimensions of all quantities in Eq.2.11, the dimension of S becomes $= \frac{Q^2}{L} \times \frac{L^8}{L^4} = Q\ L^3$. Further, considering the quantisation direction as $\hat{z}$, the Eq.2.11 can be reduced to

$$= -\ 15\ \frac{S\ z}{R_N^5}\ \rho(\vec{R})$$

We retain the quantity $\rho(\vec{R})$ throughout our calculation.

$$= -\ 3\ \frac{S\ z}{B}\ \rho(\vec{R})$$

$$= -\ 3\ \frac{S\ R\ cos\theta}{B}\ \rho(\vec{R})$$

in spherical polar coordinates. $\vec{R}$ is the electron coordinate and $\rho(\vec{R})$ is the nuclear density at the sight of the electron inside the nucleus. The matrix elements of $H_{\rm SM}$ are given by[2],

$$\left\langle \Phi_{ks_{1/2}} \middle| H_{\rm SM} \middle| \Phi_{mp_{1/2}} \right\rangle = (-\ 3\ S\ e)\ \left(\frac{-1}{3}\right)$$

$$\int_0^\infty \left[P_a(r)\ P_b(r)\ +\ Q_a(r)\ Q_b(r) \right] \frac{\rho(\vec{R})}{B}\ R\ dR \tag{2.12}$$

The matrix element of the Schiff moment operator between the states $|mp_{1/2}\rangle$ and $|ks_{1/2}\rangle$ can be derived in similarly and is given by,

$$\left\langle \Phi_{mp_{1/2}} \middle| H_{\rm SM} \middle| \Phi_{ks_{1/2}} \right\rangle = (-\ 3\ S\ e)\ \left(\frac{-1}{3}\right)$$

$$\int_0^\infty \left[P_a(r)\ P_b(r)\ +\ Q_a(r)\ Q_b(r) \right] \frac{\rho(\vec{R})}{B}\ R\ dR \tag{2.13}$$

[2]See Appendix$E$ for derivation

Consider the interaction of the Schiff potential with an electron, $H_{SM} = -e\,\Phi(\vec{R})$. The atomic EDM induced by the Schiff moment is given by,

$$D_{\rm atom} \;=\; \sum_I \frac{\left\langle \Psi_0^{(0)} \;\middle|\; \vec{D} \;\middle|\; \Psi_I^{(0)} \right\rangle \left\langle \Psi_I^{(0)} \;\middle|\; \vec{H}_{SM} \;\middle|\; \Psi_0^{(0)} \right\rangle}{E_0^{(0)} \;-\; E_I^{(0)}} \tag{2.14}$$

where $\vec{D}$ and $E_i^{(0)}$ are the induced electric dipole operator and the atomic state energies respectively. We now derive the units of the Schiff operator S. Noting that from the Eq.2.14, the quantity

$$\left\langle \Psi_I^{(0)} \;\middle|\; \vec{H}_{SM} \;\middle|\; \Psi_0^{(0)} \right\rangle$$

must have the dimensions of energy, we have,

$$\frac{\left\langle \Psi_I^{(0)} \;\middle|\; \vec{H}_{SM} \;\middle|\; \Psi_0^{(0)} \right\rangle}{E_0^{(0)} \;-\; E_I^{(0)}} \;=\; \text{dimensionless}$$

Expanding $H_{SM} \;=\; S\;e\;\frac{R\,cos\theta}{B}\;\rho(\vec{R})$, neglecting the constants. The units of energy in the context of electrostatics is given by $\frac{Q^2}{L}$, where Q=units of charge in Coulombs and L=unit of length. The nuclear density is normalised, $\int_0^\infty 4\pi r^2\;\rho(r)\;dr \;=\; 1$ and hence is dimensionless, then, $H_{SM} \;=\; S\;e\;\frac{R\,cos\theta}{R_N^5}$. Expanding the terms on the RHS of H_{SM} in units, we get $S\;Q\;\;(L/L^5)$. The units of S are hence,

$$S = \left(\frac{L^4}{Q}\right)\;\frac{Q^2}{L} \;=\; Q\;L^3$$

Chapter 3

Coupled Cluster Theory and it's application to Atomic EDMs

Calculation of physical properties of many-body quantum systems primarily involves the calculation of many-body wavefunctions. The accuracy of such a calculation hence depends upon the accuracy of the many-body wavefunctions. Consider a system of N particles. Let $|\Psi_0\rangle$ be the ground state exact wavefunction of the system and E be the total exact energy. The exact state and the exact energy can be determined starting from the reference state of the physical system, constructed from the single particle wavefunctions of the N contituents. The best choice of a many-particle reference state is the Slater determinant, $|\Phi_0\rangle$. For an atom, the slater determinant describes the Fermi sea, constructed from the set of occupied orbitals which are determined from the Hartree-Fock equation under the independent particle model approximation and satisfy the Pauli's exclusion principle, described in [18]. The more realistic picture is that the particles are not moving independently due to their mutual interactions, termed as electron-electron correlation. Coupled-cluster theory (CCT) [19, 20, 21, 22] is a way to treat these correlations systematically, where the exact atomic state is realized as the state of the atom where all possible electron correlations to all orders in terms of exciting clusters are accounted for. The operators describing these excitations are known as the cluster operators. It can be imagined that two electrons in the occupied space, interact with each other and get excited to unoccupied space. This can be described mathematically where an operator T_2 acts on the Fermi sea wavefunction $|\Phi_0\rangle$, to produce a wavefunction $T_2|\Phi_0\rangle$, describing a double excitation giving rise to two 'holes' in the

Fermi sea and consequently two 'particles' outside the Fermi sea. A similar process can occur where two pairs of particles excite themselves independently. This can be achieved by acting T_2 twice on the reference state $|\Phi_0\rangle$, with the inclusion of a statistical weighing factor of $\left(\frac{1}{2!}\right)$ to avoid counting pairs twice. The resulting contribution to the exact state is now $\left(\frac{1}{2!}\right) T_2^2|\Phi_0\rangle$. This process of excitation of independent pair of particles from the Fermi sea can be obtained by $\left(\frac{1}{m!}\right) T_2^m|\Phi_0\rangle$ which describes the amplitude of excitation of m independent pairs. All the double excitation amplitudes can be superposed to give the total amplitude $\sum_{m=0}^{\infty}\left(\frac{1}{m!}\right) T_2^m|\Phi_0\rangle = \exp(T_2)|\Phi_0\rangle$. Similarly, the amplitudes for the simultaneous excitation of three particles can be described by $T_3|\Phi_0\rangle$ and the total contribution for all triple excitations can be obtained by summing all the independent triplets, $\sum_{n=0}^{\infty}\left(\frac{1}{n!}\right) T_3^n|\Phi_0\rangle$. Also, the simultaneous independent excitation of m pairs and n triplets is given by $\frac{1}{n!m!}T_2^m T_3^n|\Phi_0\rangle$. Summing over n and m, the total amplitude is given by $\exp(T_2+T_3)|\Phi_0\rangle$. Proceeding as above, for an N electron system, all possible single, double, triple,.... ntuple excitations can be obtained from the wavefunction $\exp(T_1 + T_2 + T_3 + ... + T_N)|\Phi_0\rangle$. The operator $\exp(T_1)$ produces single particle excitations and hence the total *exact* atomic wavefunction can be described by the wavefunction $|\Psi\rangle = exp\left(\sum_{n=1}^{N} T_n\right)|\Phi_0\rangle$. This is the exact atomic state in the coupled-cluster formulation. Throughout the thesis we consider only the correlations giving rise to single and double excitations, to all orders and the exact atomic Hamiltonian is the approximate relativistic Dirac-Coulomb Hamiltonian described in the next section. Also, the above formulation

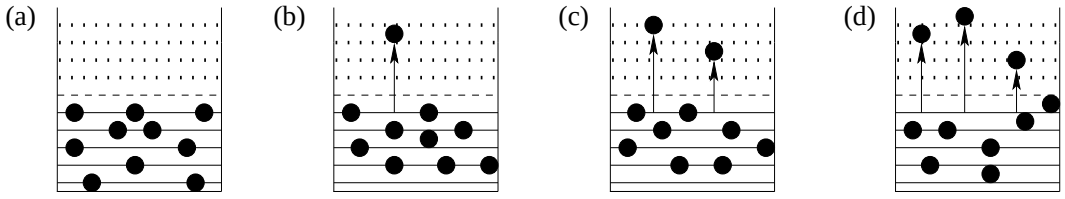

Figure 3.1: Physical realisation of the Coupled-cluster wavefunction - (a) represents Fermi vacuum, (b),(c),(d) represent single (T_1), double ($T_1^2/2!, T_2$) and triple ($T_1^3/3!, T_1T_2, T_3$) excitations respectively (Reference-Physics Today, March 1987).

of the many-body exact state is precisely valid for a closed-shell atomic system. The exact wavefunction of an atom having open-shell structure is obtained by partitioning the excitations into three parts - excitations from the core to virtual, core to valence

and valence to virtual shells. This is described by an additional operator S. The many-body state now becomes, $|\Psi\rangle = e^T e^S |\Phi_0\rangle$. This thesis deals only with the coupled-cluster theory applied to closed-shell atomic systems. See Ref.[23] for CCT applied to open-shell atomic systems.

3.1 CCT for closed-shell systems

3.1.1 Unperturbed CC equations

The starting point of setting up the coupled-cluster equations is the relativistic atomic Hamiltonian in the Dirac-Coulomb approximation is,

$$H = \sum_i \left[c\boldsymbol{\alpha_i} \cdot .\boldsymbol{p_i} + \left(\beta_{\mathbf{i}} - \mathbf{1}\right)c^2 + V(r_i)\right] + \sum_{i<j} \frac{1}{r_{ij}} \tag{3.1}$$

where, c is velocity of light, α and β are the Dirac matrices, r_{ij} is the Coulomb potential energy between two electrons, in atomic units ($m_e = 1$, $|e| = 1$ and $\hbar = 1$). In the above Hamiltonian, the rest mass energy is subtracted from the total energy eigen values. This is the Hamiltonian of an atomic system considering only the inter electron electrostatic interactions. The single particle equations are obtained by approximating the two-electron term in Eq.3.1 by a central field potential $U_{\mathrm{DF}}(r)$, known as the Dirac-Fock potential, then

$$H_{\mathrm{DC}} = \sum_i^N \left[c\boldsymbol{\alpha_i} \cdot \ \boldsymbol{p_i} + \left(\beta_{\mathbf{i}} - 1\right)c^2 + V(r_i) + U_{\mathrm{DF}}(i)\right] + \left(\sum_{i<j}^N \frac{1}{r_{ij}} - U_{\mathrm{DF}}(i)\right) \tag{3.2}$$

Define the residual Coulomb interaction V_{es} as,

$$V_{\mathrm{es}} = \left(\sum_{i<j} \frac{1}{r_{ij}} - U_{\mathrm{DF}}(i)\right)$$

The non-central (or) correlation effects are included by treating V_{es} as a perturbation. The single electron wavefunctions satisfy the Schroedinger equation [18, 24]

$$\left[c\boldsymbol{\alpha_i} \cdot .\boldsymbol{p_i} + \left(\beta - 1\right)c^2 + V(r_i) + U_{DF}(i)\right] \Big| \psi_a \Big\rangle = \epsilon_a \Big| \psi_a \Big\rangle \tag{3.3}$$

where $|\psi_a\rangle$ are the single electron wavefunctions in terms of the two component relativistic wavefunctions, given by

$$\left|\psi_a(\mathbf{r})\right\rangle = \frac{1}{r}\begin{pmatrix} P_a(r)\chi_{\kappa_a,m_a}(\theta,\phi) \\ i\,Q_a(r)\chi_{-\kappa_a,m_a}(\theta,\phi) \end{pmatrix} \tag{3.4}$$

where P_a and Q_a are the large and small components of the single electron wavefunction and the angular part is a product of the orbital and spin angular momenta of the electrons, given by

$$\chi_{\kappa_a,m_a}(\theta,\phi) = \sum_{m_a^l,m_a^s} |l_a, m_a^l\rangle \times |s_a, m_a^s\rangle \langle l_a, m_a^l, s_a, m_a^s | J_a, M_a\rangle$$

l_a and s_a are the orbital angular momenta, m_a^l, m_a^s, their respective projections, J_a, M_a, the total angular momentum and it's projection and a denotes the quantum numbers needed to specify the electron. The quantity $\langle l_a, m_a^l, s_a, m_a^s | J_a, M_a\rangle$ are the Clebsch-Gordan coefficients, the orbital part are the spherical harmonics and the terms involving spin are the Dirac spinors. These wavefunctions are simultaneous eigen functions of J, J_z, L and S. κ is the relativistic quantum number, given in terms of j and l, $\kappa = -\left(j+\frac{1}{2}\right)a$, where $a = +1$ for $l = \left(j-\frac{1}{2}\right)$ and $a = -1$ for $l = \left(j+\frac{1}{2}\right)$ [25, 26]. The many-electron wavefunctions of an atomic system with the above Hamiltonian are the Slater determinants obtained by constructing the linear combinations of the single particle wavefunctions respecting the Pauli's exclusion principle, given by

$$\left|\Psi\right\rangle = \sqrt{\frac{1}{N!}}\begin{vmatrix} \psi_a(1) & \psi_a(2) & \cdots \psi_a(N) \\ \psi_b(1) & \psi_b(2) & \cdots \psi_b(N) \\ \cdots & \cdots & \cdots \\ \cdots & \cdots & \cdots \\ \psi_n(1) & \psi_n(2) & \cdots \psi_n(N) \end{vmatrix} \tag{3.5}$$

where the coefficient $\sqrt{1/N!}$ is the normalisation constant, and a single particle orbital $\psi_i(j)$ represents the wavefunction of electron with the space coordinate j and specified by the set of quantum numbers i. Throughout the thesis, we denote $a, b, c, \cdots$ for occupied orbitals (holes) and $p, q, r, s, \cdots$ for unoccupied orbitals (particles). The challenging problem in atomic many-body theory is to solve the Hamiltonian Eq.3.2 with $V_{\rm es}$ as perturbation to all orders. Solving Eq. 3.2 variationally by minimising the energy

functional with respect to the form of orbitals and by imposing orthonormality condition [18], we get Hartree-Fock equation

$$\left(h^0 + g^0 - \epsilon_a^0\right)\left|\psi_a^0\right\rangle = 0; \tag{3.6}$$

where h^0 and g^0 are the single and two-particle operators respectively in Eq.3.2 , together termed as the Fock operator f^0. The operator g^0 is the central field approximation of the two-electron Coulomb interaction

$$g^0\left|\psi_a^0\right\rangle = \sum_{b=1}^{N_{\rm occ}}\left[\left\langle\psi_b^0\right|v\left|\psi_b^0\right\rangle\left|\psi_a^0\right\rangle - \left\langle\psi_b^0\right|v\left|\psi_a^0\right\rangle\left|\psi_b^0\right\rangle\right]$$

where $v = 1/r_{ij} = 1/r_{12}$ is the two-electron operator and the sum runs over all occupied orbitals. Substituting for g^0, the Eq.3.6 becomes

$$h^0\left|\psi_a^0\right\rangle + \sum_{b=1}^{N_{\rm occ}}\left[\left\langle\psi_b^0\right|v\left|\psi_b^0\right\rangle\left|\psi_a^0\right\rangle - \left\langle\psi_b^0\right|v\left|\psi_a^0\right\rangle\left|\psi_b^0\right\rangle\right] - \epsilon_a^0\left|\psi_a^0\right\rangle = 0 \tag{3.7}$$

Eq.3.7 is the Hartree-Fock equation. The perturbed equations are obtained by introducing the CP violating tensor-pseudo tensor interaction Hamiltonian in addition to the residual Coulomb interaction

$$H_{\rm T-PT} = \sqrt{2}\; C_T\; G_F\; \beta\; \alpha\; \cdot\; I\; \rho(r)\; e\; a_0 \tag{3.8}$$

where C_T, G_F and $\rho(r)$ are the tensor-pseudo tensor coupling constant, Fermi coupling constant and nuclear density respectively, β and α are the Dirac matrices and I is the nuclear spin. The wavefunctions and the Hamiltonian are perturbed by this interaction thereby giving the perturbed Hartree-Fock equations demonstrated in in the next few pages.

The many-body Schroedinger equation of the Dirac-Coulomb Hamiltonian for an atomic system, in a state $|\Psi\rangle$ is given by

$$H\left|\Psi\right\rangle = E\left|\Psi\right\rangle \Rightarrow He^T\left|\Phi_0\right\rangle = Ee^T\left|\Phi_0\right\rangle$$

Operating from left side by e^{-T}

$$e^{-T} H e^{T} \Big| \Phi_0 \Big\rangle = E \Big| \Phi_0 \Big\rangle$$

Expressing H in normal ordered form, $H = H_N + E_{HF}$, where $E_{HF} = \langle \Phi_0 | H | \Phi_0 \rangle - \langle \Phi_0 | H_N | \Phi_0 \rangle$ is the Dirac-Fock energy. Then,

$$e^{-T} \Big(H_N + E_{HF} \Big) e^{T} \Big| \Phi_0 \Big\rangle = E \Big| \Phi_0 \Big\rangle \tag{3.9}$$

Projecting Eq.3.9 with singly and doubly excited states $\langle \Phi_a^r |$ and $\langle \Phi_{ab}^{rs} |$ and restricting T to $T = T_1 + T_2$, the single and double excitation cluster amplitude equations are obtained. The second quantized form of these operators is

$$T_1 = \sum_{\mathrm{a,p}} a_p^\dagger \, a_a \, \mathbf{t}_a^p \Big| \Phi_0 \Big\rangle$$

and

$$T_2 = \sum_{\mathrm{a,p,b,q}} \frac{1}{2!} \, a_p^\dagger \, a_q^\dagger \, a_b \, a_a \, \mathbf{t}_{ab}^{pq} \Big| \Phi_0 \Big\rangle$$

Expanding $\Big(e^{-T} H_N e^{T} \Big)$ using Campbell-Baker-Hausdorf expansion,

$$e^{-T} \, H_N \, e^{T} = H_N + \Big[H_N, T \Big] + \frac{1}{2!} \Big[\Big[H_N, T \Big], T \Big] + \frac{1}{3!} \Big[\Big[\Big[H_N, T \Big], T \Big], T \Big] \tag{3.10}$$

$$+ \frac{1}{4!} \Big[\Big[\Big[\Big[H_N, T \Big], T \Big], T \Big], T \Big]$$

Examining the Eq.3.10, the first term H_N is a *connected* term as it contains only one vertex of H_N. The second term $[H_N, T]$ is also connected[1], using $[H_N, T] = \Big\{ \overbrace{H_N T} \Big\} - \Big\{ \overbrace{T H_N} \Big\}$. Considering a general term, $[H_N, T]^{(n)} = \Big[[H_N, T]^{(n-1)}, T \Big]$. Any nth commutator would consist of all connected terms, provided the $(n-1)$th commutator is connected. Hence the term $\left(e^{-T} \, H_N \, e^{T} \right)$ is built from only connected terms. Using

[1]For any two objects A, B we have $\overbrace{AB} = AB - \Big\{ \overbrace{AB} \Big\}$

$\left\{\overbrace{T H_N}\right\} = 0$, we get,

$$\begin{aligned} e^{-T} H_N e^T &= H_N + \left\{\overbrace{H_N T}\right\} + \left\{\overbrace{H_N T\, T}\right\} + \left\{\overbrace{\overbrace{H_N T\, T}\, T}\right\} + \left\{\overbrace{\overbrace{\overbrace{H_N T\, T\, T}\, T}}\right\} \quad (3.11) \\ &= \left(H_N e^T\right)_{\mathrm{c}} \end{aligned}$$

where, the curly brackets in the above equation represent normal ordering [1] of the operators within the brackets and the symbol of *contraction* is a special symbol. Two operators, under this symbol are said to be *contracted* if their respective creation and annihilation operators *contract* with each other, always in pairs of one creation and one annihilation operator, in all possible ways. Substituting the above in Eq.3.9 and projecting from LHS by singly and doubly excited determinantal states,

$$\left\langle \Phi_a^r \middle| \left\{ \left(\overbrace{H_N T}\right)_{\mathrm{c}} \right\} \middle| \Phi_0 \right\rangle = 0 \quad (3.12)$$

$$\left\langle \Phi_{ab}^{rs} \middle| \left\{ \left(\overbrace{H_N T}\right)_{\mathrm{c}} \right\} \middle| \Phi_0 \right\rangle = 0 \quad (3.13)$$

Expanding $\left(\overbrace{H_N T}\right)_{\mathrm{c}}$,

$$\left\langle \Phi_a^r \middle| \left\{ \overbrace{H_N T} + \overbrace{H_N T\, T} + \overbrace{\overbrace{H_N T\, T}\, T} + \overbrace{\overbrace{\overbrace{H_N T\, T}\, T}\, T} \right\} \middle| \Phi_0 \right\rangle = -\left\langle \Phi_a^r \middle| H_N \middle| \Phi_0 \right\rangle$$

$$\left\langle \Phi_{ab}^{rs} \middle| \left\{ \overbrace{H_N T} + \overbrace{H_N T\, T} + \overbrace{\overbrace{H_N T\, T}\, T} + \overbrace{\overbrace{\overbrace{H_N T\, T}\, T}\, T} \right\} \middle| \Phi_0 \right\rangle = -\left\langle \Phi_{ab}^{rs} \middle| H_N \middle| \Phi_0 \right\rangle \quad (3.14)$$

Note that the maximum number os T operators contributing to the contraction in the above equation is four. This is because the operator H_N has a maximu level of excitation equal to 2. Since we use the approximation $T = T_1 + T_2$, Eq.3.14 can be recast as

$$\left\langle \Phi_a^r \middle| \left\{ (\overbrace{H_N(T)} T_1 + \overbrace{H_N(T)} T_2) \right\} \middle| \Phi_0 \right\rangle = -\left\langle \Phi_a^r \middle| H_N \middle| \Phi_0 \right\rangle$$

$$\left\langle \Phi_{ab}^{rs} \middle| \left\{ (\overbrace{H_N(T)} T_1 + \overbrace{H_N(T)} T_2) \right\} \middle| \Phi_0 \right\rangle = -\left\langle \Phi_{ab}^{rs} \middle| H_N \middle| \Phi_0 \right\rangle \quad (3.15)$$

[1] Two operators A and B in second quantisation form are said to be normal ordered if the creation operator associated with a core ($a^\dagger_{\mathrm{core}}$) or the annihilation operator associated with the virtual ($a_{virtual}$) appears on the right side of the rest of the operators in the product AB.

The above equations can be written in the form,

$$H_{11}(T)T_1 + H_{12}(T)T_2 = -H_{10} \tag{3.16}$$

$$H_{21}(T)T_1 + H_{22}(T)T_2 = -H_{20} \tag{3.17}$$

where the terms on the RHS are independent of T and the Hamiltonian matrix elements are dependent on T. Combining the above equations,

$$\mathbf{A}(\mathbf{T})T = \mathbf{C} \tag{3.18}$$

where $\mathbf{A}$ is dependent on T and $\mathbf{C}$ is independent of T. This is a non-linear matrix equation which should be solved in a self-consistent way to obtain the unperturbed cluster amplitudes.

3.1.2 H_{EDM} perturbed CC equations

Consider the H_{EDM} perturbed Schroedinger equation for the atomic Hamiltonian H.

$$\left(H_{\mathrm{pert}}\right)\left|\Psi\right\rangle = \left(E\right)\left|\Psi\right\rangle \tag{3.19}$$

where $H_{\mathrm{pert}} = H + \lambda H_{EDM}$ and $|\Psi\rangle = e^T|\Phi_0\rangle = e^{T^{(0)}+\lambda T^{(1)}}|\Phi_0\rangle$. Since terms of one order in λ are taken, this gives,

$$H_{\mathrm{pert}}e^{T^{(0)}}\left(1+\lambda T^{(1)}\right)\left|\Phi_0\right\rangle = Ee^{T^{(0)}}\left(1+\lambda T^{(1)}\right)\left|\Phi_0\right\rangle$$

Substituting $H_{\mathrm{pert}} = H + \lambda H_{EDM}$,

$$= \left(H+\lambda H_{EDM}\right)e^{T^{(0)}}\left(1+\lambda T^{(1)}\right)\left|\Phi_0\right\rangle = Ee^{T^{(0)}}\left(1+\lambda T^{(1)}\right)\left|\Phi_0\right\rangle$$

Comparing λ^0 and λ^1 terms on both sides,

$$\left(He^{T^{(0)}}\right)\left|\Phi_0\right\rangle = Ee^{T^{(0)}}\left|\Phi_0\right\rangle \tag{3.20}$$

and

$$\left(He^{T^{(0)}}T^{(1)} + H_{EDM}e^{T^{(0)}}\right)\Big|\Phi_0\Big\rangle = Ee^{T^{(0)}}T^{(1)}\Big|\Phi_0\Big\rangle \tag{3.21}$$

Multiplying Eq.3.20 by $T^{(1)}$,

$$T^{(1)}He^{T^{(0)}}\Big|\Phi_0\Big\rangle = ET^{(1)}e^{T^{(0)}}\Big|\Phi_0\Big\rangle \tag{3.22}$$

Using the normal-ordered form of $H = H_N + E_{DF}$, Eq.3.21 becomes,

$$\left(H_Ne^{T^{(0)}}T^{(1)} + H_{EDM}e^{T^{(0)}}\right)\Big|\Phi_0\Big\rangle = \left(\Delta E_{corr}e^{T^{(0)}}T^{(1)}\right)\Big|\Phi_0\Big\rangle \tag{3.23}$$

since $T^{(0)}$ and $T^{(1)}$ commute. Now operate Eq.3.23 by $e^{-T^{(0)}}$,

$$\left(\overline{H}_NT^{(1)} + \overline{H}_{EDM}\right)\Big|\Phi_o\Big\rangle = \Delta E_{\rm corr}T^{(1)}\Big|\Phi_o\Big\rangle \tag{3.24}$$

Operating by $e^{-T^{(0)}}$ on Eq.3.20 and converting H into normal form,

$$\overline{H}_N\Big|\Phi_0\Big\rangle = \Delta E_{\rm corr}\Big|\Phi_0\Big\rangle \tag{3.25}$$

subtracting Eq.3.24 from Eq.3.25,

$$\left[\overline{H}_N, T^{(1)}\right]\Big|\Phi_0\Big\rangle = -\overline{H}_{EDM}\Big|\Phi_0\Big\rangle \tag{3.26}$$

where $\overline{O} = e^{-T^{(0)}}\hat{O}e^{T(0)}$ where $\hat{O}$ is any operator. The equation for the coupled-cluster perturbed singles and doubles can be derived from the basic equation, Eq.3.26 by projecting on both sides of the equation with singly and doubly excited determinantal states.

$$\begin{aligned}
\left\langle\Phi_a^r\right|\left[\overline{H}_N, T^{(1)}\right]\Big|\Phi_0\Big\rangle &= -\left\langle\Phi_a^r\right|\overline{H}_{EDM}\Big|\Phi_0\Big\rangle \\
\left\langle\Phi_{ab}^{rs}\right|\left[\overline{H}_N, T^{(1)}\right]\Big|\Phi_0\Big\rangle &= -\left\langle\Phi_{ab}^{rs}\right|\overline{H}_{EDM}\Big|\Phi_0\Big\rangle
\end{aligned} \tag{3.27}$$

which are equivalent to

$$\begin{aligned}
\left\langle\Phi_a^r\right|\left\{\overline{H_NT}^{(1)}\right\}\Big|\Phi_0\Big\rangle &= -\left\langle\Phi_a^r\right|\overline{H}_{EDM}\Big|\Phi_0\Big\rangle \\
\left\langle\Phi_{ab}^{rs}\right|\left\{\overline{H_NT}^{(1)}\right\}\Big|\Phi_0\Big\rangle &= -\left\langle\Phi_{ab}^{rs}\right|\overline{H}_{EDM}\Big|\Phi_0\Big\rangle
\end{aligned} \tag{3.28}$$

Expanding $T^{(1)}$ above, these equations can be cast in the form of a system of linear matrix equations,

$$\begin{aligned} H_{11}T_1^{(1)} + H_{12}T_2^{(1)} &= -H_{10} - H_{10}T_1^{(0)} - H_{10}T_2^{(0)} \\ H_{21}T_1^{(1)} + H_{22}T_2^{(1)} &= -H_{20} - H_{20}T_1^{(0)} - H_{20}T_2^{(0)} \end{aligned} \tag{3.29}$$

which can be expressed in the form $\mathbf{A}T^{(1)} = \mathbf{C}$, where the matrices $\mathbf{A}$ and $\mathbf{C}$ are $T^{(1)}$ - independent. These equations are termed as coupled-cluster EDM (CCEDM) equations in this thesis and are classified into four blocks, T1-T1, T1-T2, T2-T1 and T2-T2, where T1-T1 and T1-T2 contain the diagrams contributing to the $T^{(1)}$ equation through singles and doubles respectively, and T2-T1 and T2-T2 contain the diagrams contributing to the $T^{(2)}$ equation through singles and doubles respectively. The diagrams contributing to the CCEDM equations with zero orders in $T^{(0)}$ are shown in Fig.3.3, 3.5, 3.4, 3.6, 3.7, 3.8. The diagrammatic representation of the operators is shown in Fig.3.2.

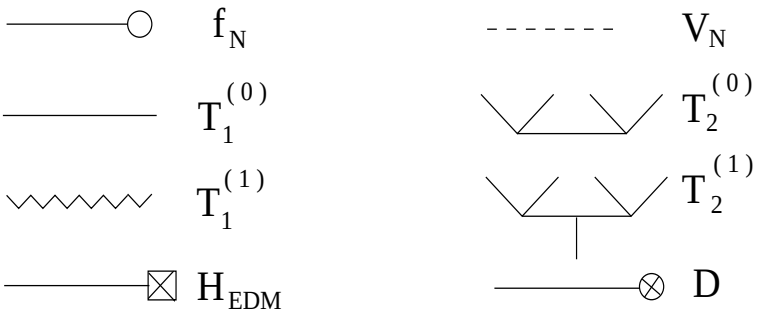

Figure 3.2: Notation. f_N and V_N denote the one- and two- electron parts of H_N respectively.

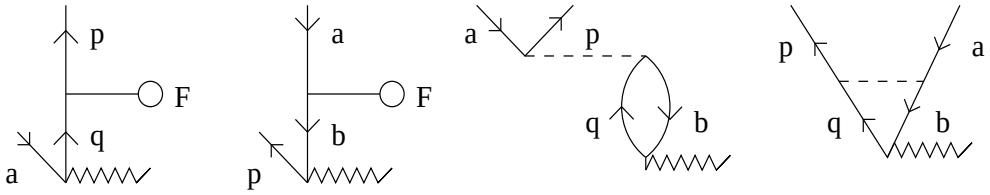

Figure 3.3: Diagrams contributing to T1-T1 block.

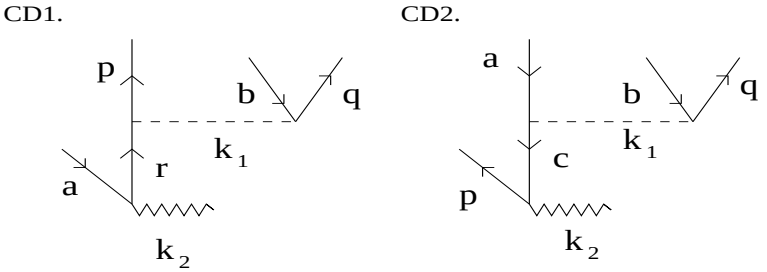

Figure 3.4: Diagrams contributing to T2-T1 block

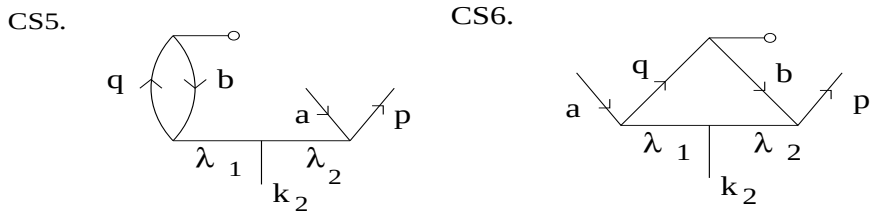

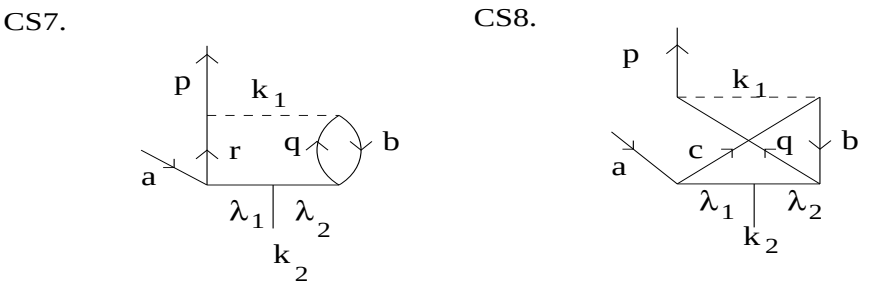

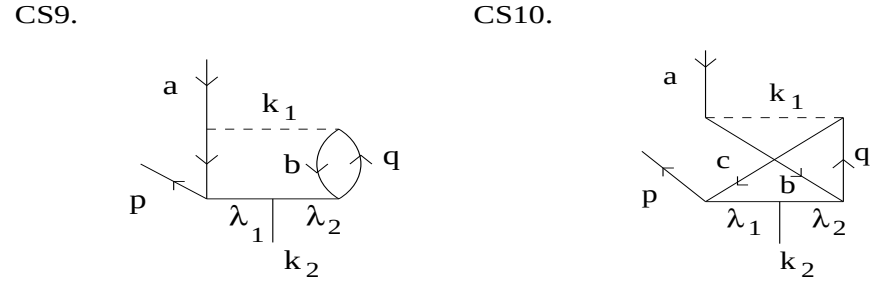

Figure 3.5: Diagrams contributing to T1-T2 block

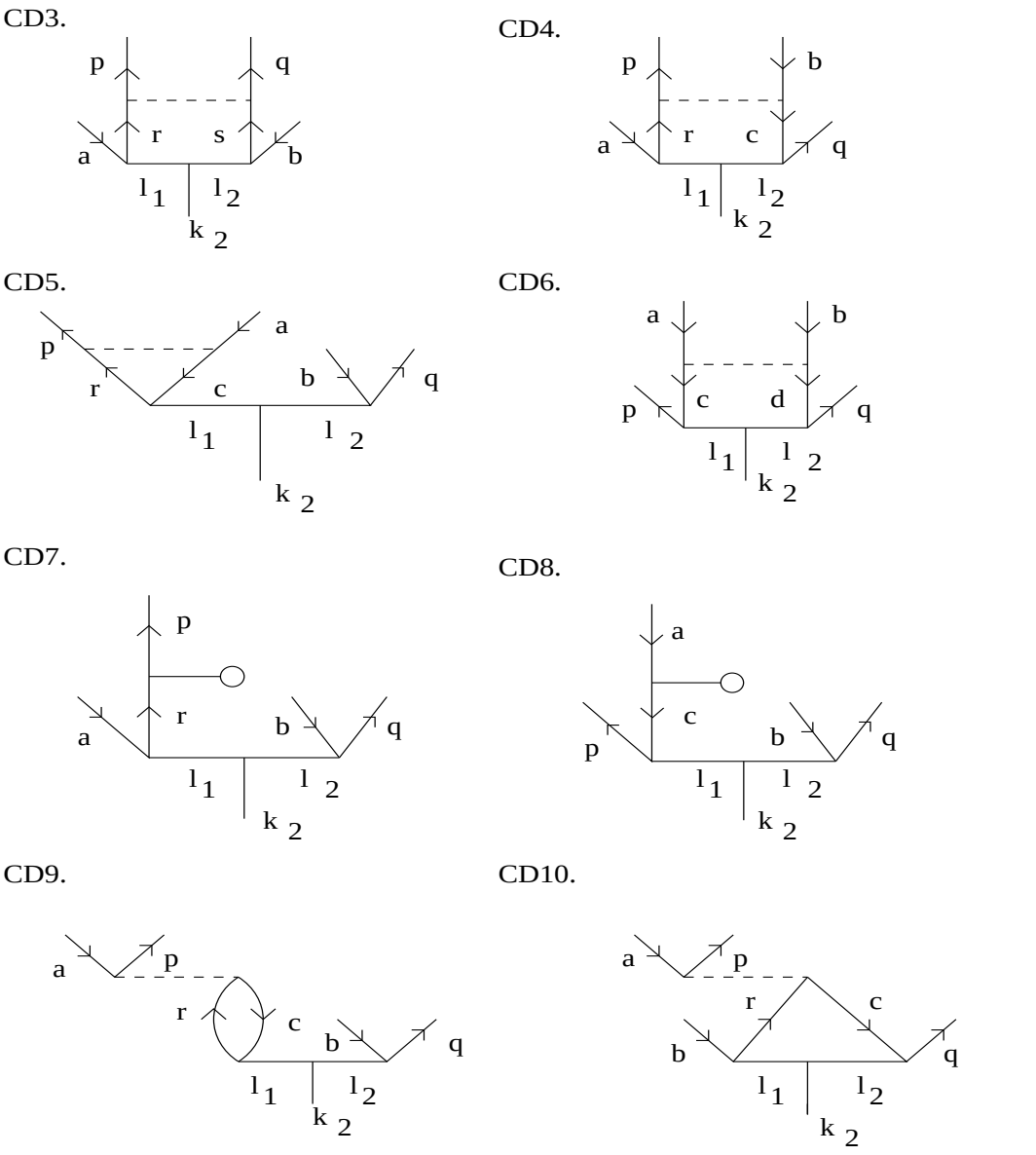

Figure 3.6: Diagrams contributing to T2-T2 block

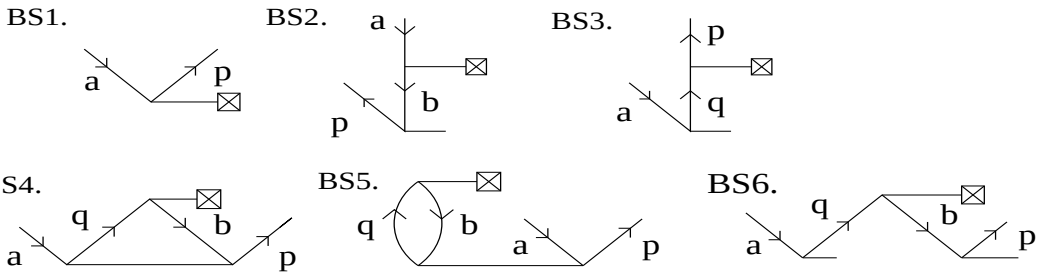

Figure 3.7: Diagrams contributing to the RHS of the singles CCEDM equation.

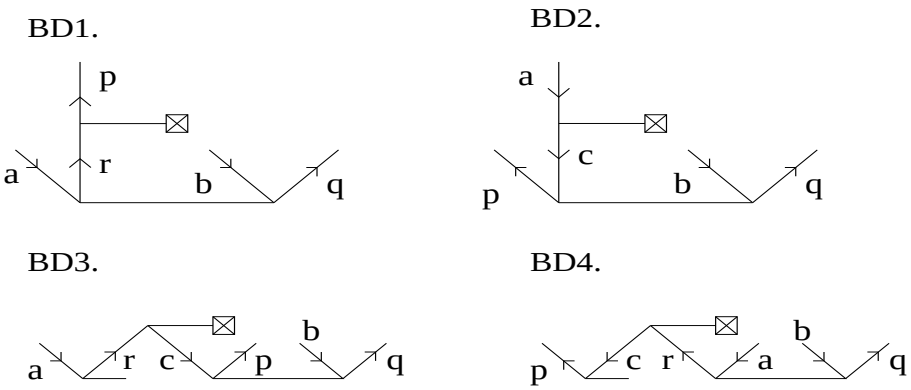

Figure 3.8: The diagrams contributing to the RHS of the doubles CCEDM equation.

3.1.3 Non-Linear CC equations

Consider the H_{EDM} perturbed singles and doubles cluster amplitudes equation (the prime denotes that the reference state and the excited slater determinants are opposite in parity due to the parity odd perturbation)

$$\begin{aligned}\left\langle \Phi_a^{r\prime}\middle|\left\{\overline{H_N T^{(1)}}\right\}\middle|\Phi_0\right\rangle &= -\left\langle \Phi_a^{r\prime}\middle|\left\{\overline{H}_{EDM}\right\}\middle|\Phi_0\right\rangle \\ \left\langle \Phi_{ab}^{rs\prime}\middle|\left\{\overline{H_N T^{(1)}}\right\}\middle|\Phi_0\right\rangle &= -\left\langle \Phi_{ab}^{rs\prime}\middle|\left\{\overline{H}_{EDM}\right\}\middle|\Phi_0\right\rangle \end{aligned} \tag{3.30}$$

Expanding $\overline{H}_N$,

$$\left\langle \Phi_a^{r\prime}\middle|\left\{ H_N + \overline{H_N T^{(0)}} + \frac{1}{2!}\overline{H_N T^{(0)} T^{(0)}} + \frac{1}{3!}\overline{H_N T^{(0)} T^{(0)} T^{(0)}} \right\} T^{(1)}\middle|\Phi_0\right\rangle$$

$$= -\left\langle \Phi_a^{r\prime}\middle|\left\{\overline{H}_{EDM}\right\}\middle|\Phi_0\right\rangle \tag{3.31}$$

This equation can be written as

$$\left\langle \Phi_a^{r\prime}\middle|\left\{ H_N + \overline{H_N T^{(0)}} + \frac{1}{2!}\overline{H_N T^{(0)} T^{(0)}} + \frac{1}{3!}\overline{H_N T^{(0)} T^{(0)} T^{(0)}} \right\} T_1^{(1)}\right.$$

$$\left. + \left\{ H_N + \overline{H_N T^{(0)}} + \frac{1}{2!}\overline{H_N T^{(0)} T^{(0)}} + \frac{1}{3!}\overline{H_N T^{(0)} T^{(0)} T^{(0)}} \right\} T_2^{(1)}\middle|\Phi_0\right\rangle = -\left\langle \Phi_a^{r\prime}\middle|\left\{\overline{H}_{EDM}\right\}\middle|\Phi_0\right\rangle$$

Similarly the double excitations satisfy the equation

$$\left\langle \Phi_{ab}^{rs\prime}\middle|\left\{ H_N + \overline{H_N T^{(0)}} + \frac{1}{2!}\overline{H_N T^{(0)} T^{(0)}} + \frac{1}{3!}\overline{H_N T^{(0)} T^{(0)} T^{(0)}} \right\} T_1^{(1)}\right. \tag{3.32}$$

$$\left. + \left\{ H_N + \overline{H_N T^{(0)}} + \frac{1}{2!}\overline{H_N T^{(0)} T^{(0)}} + \frac{1}{3!}\overline{H_N T^{(0)} T^{(0)} T^{(0)}} \right\} T_2^{(1)}\middle|\Phi_0\right\rangle = -\left\langle \Phi_{ab}^{rs\prime}\middle|\left\{\overline{H}_{EDM}\right\}\middle|\Phi_0\right\rangle$$

writing the equation for singles in terms of matrix elements,

$$\mathbf{A}_{11}(T^{(0)})T_1^{(1)} + \mathbf{A}_{12}(T^{(0)})T_2^{(1)} = -(H_{EDM})_0^1 \tag{3.33}$$

where

$$\mathbf{A}_{11}(T^{(0)})T_1^{(1)} = \left\langle \Phi_a^{r\prime} \middle| \left\{ H_N + \overbrace{H_N T^{(0)}} + \frac{1}{2!}\overbrace{\overbrace{H_N T^{(0)} T^{(0)}}} + \frac{1}{3!}\overbrace{\overbrace{\overbrace{H_N T^{(0)} T^{(0)} T^{(0)}}}} \right\} T_1^{(1)} \middle| \Phi_0 \right\rangle,$$

$$\mathbf{A}_{12}(T^{(0)})T_2^{(1)} = \left\langle \Phi_a^{r\prime} \middle| \left\{ H_N + \overbrace{H_N T^{(0)}} + \frac{1}{2!}\overbrace{\overbrace{H_N T^{(0)} T^{(0)}}} + \frac{1}{3!}\overbrace{\overbrace{\overbrace{H_N T^{(0)} T^{(0)} T^{(0)}}}} \right\} T_2^{(1)} \middle| \Phi_0 \right\rangle$$

Similarly for the double-excitations,

$$\mathbf{A}_{21}(T^{(0)})T_2^{(1)} + \mathbf{A}_{22}(T^{(0)})T_1^{(1)} = -(H_{EDM})_0^2 \tag{3.34}$$

where the matrices $\mathbf{A}_{21}(T^{(0)})$ and $\mathbf{A}_{22}(T^{(0)})$ are the coefficients of $T_1^{(1)}$ and $T_2^{(1)}$ operators in the doubles Eq.3.32 respectively. The Eq.3.33, Eq.3.34 are non-linear in $T^{(0)}$, but linear in $T^{(1)}$ and can be combined as

$$\begin{bmatrix} A_{11} & A_{12} \\ A_{21} & A_{22} \end{bmatrix} \begin{bmatrix} T_1^{(1)} \\ T_2^{(1)} \end{bmatrix} = \begin{bmatrix} B_1 \\ B_2 \end{bmatrix}$$

where

$$B_1 = -(H_{EDM})_0^1$$

and

$$B_2 = -(H_{EDM})_0^2$$

These equations can be recast as,

$$\mathbf{A}(T^{(0)})T^{(1)} = \mathbf{B} \tag{3.35}$$

which can be solved iteratively, to get the perturbed cluster amplitudes, where the $T^{(0)}$ amplitudes are known. Splitting the matrix $\mathbf{A}(T^{(0)})$ in the above equation into diagonal and off-diagonal parts,

$$\mathbf{A}_{\text{diag}}(T^{(0)})T^{(1)} + \mathbf{A}_{\text{offdiag}}(T^{(0)})T^{(1)} = \mathbf{B}$$

gives an equation of the form

$$T^{(1)} = \frac{1}{\mathbf{A}_{\text{diag}}(T)}\left[\mathbf{B} - \mathbf{A}_{\text{offdiag}}(T)T^{(1)}\right] \tag{3.36}$$

This equation has is solved self-consistently for the unknown $T^{(1)}$ amplitudes.

3.1.4 Selection rules for cluster operators

The tensor-pseudotensor electron-nucleus interaction Hamiltonian has the form 2.1,

$$H_{e-N}^{EDM,T} = \frac{iG_F C_T}{\sqrt{2}} \sum_i \boldsymbol{\sigma_N} \cdot \boldsymbol{\gamma_i} \rho_N(r) \tag{3.37}$$

The operator in the electron space is a vector of rank 1. The perturbed cluster amplitudes are associated with the electron space, which can be noted from the second quantization representation of the cluster operators. The rank of the interaction Hamiltonian must be incorporated into the cluster amplitudes and the diagrams representing them. Consider the diagrammatic representation of $T_1^{(1)}$ shown in Fig.3.9(a) . In terms of the multipole components

$$T_1{}^{(1)} = \sum_q (T_1{}^{(1)})_q^1 \tag{3.38}$$

Algebraically, $T_1^{(1)}$ can be written as

$$T_1^{(1)} = \sum_{a,p} a_p^\dagger a_a t_a^p \tag{3.39}$$

where, p is a particle, hence represented by an out-going line, and a is a hole represented by an incoming line, and t_a^p is the corresponding cluster amplitude. The rank of $T^{(1)}$ is $k_2 = 1$.

The vertex formed by the orbital lines (a, p, k_2) in the $T_1^{(1)}$ diagram, satisfies the triangular condition [2],

$$|J_a - 1| \leq J_p \leq J_a + 1,$$

[2] as dictated by the Wigner Eckart theorem for the matrix element of $T_1^{(1)}$

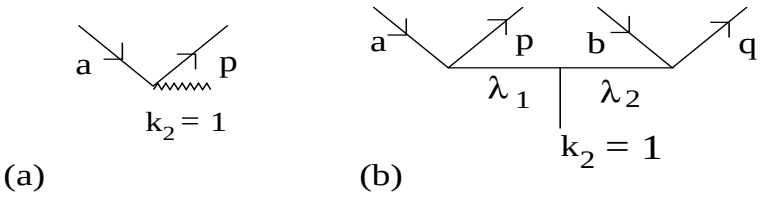

Figure 3.9: Diagram representing $T^{(1)}$ - (a) $T_1^{(1)}$ (b) $T_2^{(1)}$

and the magnetic quantum numbers satisfy,

$$m_a + m_p + q = 0,$$

where the J_i's and m_i's represent the total angular momenta and their projections respectively. The operator $T^{(1)}$ is odd under parity therefore,

$$(-1)^{l_a + l_p} = -1$$

where l is the orbital angular momentum. Consider the diagram representing $T_2^{(1)}$ operator. The vertices formed by the orbital indices (a, p, λ_1), (b, q, λ_2) and $(\lambda_1, \lambda_2, k_2)$ satisfy the triangular conditions

$$|J_a - J_p| \leq \lambda_1 \leq J_a + J_p$$

$$|J_b - J_q| \leq \lambda_2 \leq J_b + J_q$$

$$|\lambda_1 - \lambda_2| \leq k_2 \leq |\lambda_1 + \lambda_2|$$

and the vertices satisfy,

$$(-1)^{l_a + l_p} = (-)\,(-1)^{l_b + l_q}$$

Note that the $T^{(0)}$ operator preserves parity and hence for $T_2^{(0)}$ we have,

$$(-1)^{l_a + l_p} = (-1)^{l_b + l_q}$$

which is the same condition satisfied by the residual Coulomb operator diagram.

3.2 Calculation of Atomic Electric Dipole Moment

The EDM of the atom in an exact state $|\Psi'\rangle$ is

$$D_a = \frac{\left\langle \Psi' \middle| D \middle| \Psi' \right\rangle}{\left\langle \Psi' \middle| \Psi' \right\rangle} \tag{3.40}$$

where D is the induced dipole operator and $|\Psi'\rangle$ is given by,

$$\left| \Psi' \right\rangle = \left| \Psi_0 \right\rangle + \lambda \left| \Psi_0^{(1)} \right\rangle$$

where $|\Psi_0\rangle$ is the unperturbed state, λ is the perturbation parameter and $|\Psi_0^{(1)}\rangle$ is the first order correction to the unperturbed state due to the EDM perturbation. The total wave function is written in terms of the cluster operators as

$$\left| \Psi' \right\rangle = e^{T^{(0)} + \lambda T^{(1)}} \left| \Phi_0 \right\rangle$$

where $|\Phi_0\rangle$ is the reference state. Retaining only the terms of order λ,

$$\left| \Psi' \right\rangle = e^{T^{(0)}} \left(1 + T^{(1)}\right) \left| \Phi_0 \right\rangle$$

Substituting the above expression for $|\Psi'\rangle$ in Eqn.3.40 and simplifying, we obtain the expression for EDM [3],

$$D_a = \frac{\left\langle \Phi_0 \middle| \left[\overline{D} \overline{T^{(1)}} + \overline{T^{(1)}}^{\dagger} \overline{D} \right] \middle| \Phi_0 \right\rangle}{\left\langle \Psi_0 \middle| \Psi_0 \right\rangle} \tag{3.41}$$

where $\overline{D} = e^{T^{(0)}\,\dagger} D e^{T^{(0)}}$, using the fact that $T^{(1)}$ and $\overline{D}$ are odd and $T^{(0)}$ is even under parity, the bra and the ket vectors have same parity and $|\Psi_0\rangle = e^{T^{(0)}} |\Phi_0\rangle$. The $T^{(1)}$ operators are the $H_{\rm EDM}$ perturbed cluster amplitudes. To simplify calculations, expand $\overline{D}$ in the form

$$\overline{D} = \left(1 + T^{(0)\,\dagger} + \frac{T^{(0)\,\dagger}}{2!} + \cdots\right) D\, e^{T^{(0)}}$$

[3]The symbol of contraction appears using $\overline{D} T^{(1)} = \left\{ \overline{D} \overline{T^{(1)}} \right\} + \left\{ \overline{D} T^{(1)} \right\}$ and the expectation value of normal ordered operator is zero

This can be written as

$$\overline{D} = De^{T^{(0)}} + \sum_{n=1}^{\infty} \frac{1}{n!} \left(T^{(0)^\dagger}\right)^n \; De^{T^{(0)}} \tag{3.42}$$

(**This was originally formulated by Dr. Angom Dilip Kumar Singh, Physical Research Laboratory, Ahmedabad, India, in the year 2005**).

The diagrams representing the induced dipole operators are shown in Fig.3.10.

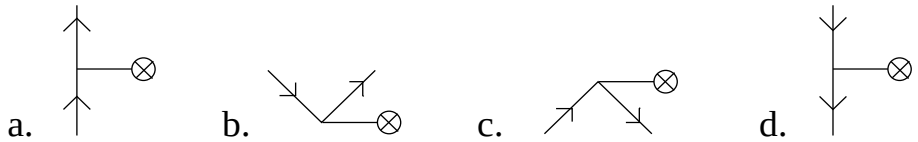

Figure 3.10: Diagrams representing induced dipole operator

The Campbell-Baker-Housdorf expansion cannot be applied to the effective dipole operator $\overline{D}$. In the above expression, the one-body nature of the dipole operator D restricts the maximum possible contractions with $T^{(0)}$ to two. Define

$$\left|\Phi_1\right\rangle = T^{(1)}\left|\Phi_0\right\rangle = \left(T_1^{(1)} + T_2^{(1)}\right)\left|\Phi_0\right\rangle,$$

then

$$D_a = \frac{\left\langle\Phi_1\left|\overline{D}\right|\Phi_0\right\rangle + \left\langle\Phi_0\left|\overline{D}\right|\Phi_1\right\rangle}{\left\langle\Psi_0\middle|\Psi_0\right\rangle} = 2\frac{\left\langle\Phi_1\left|\overline{D}\right|\Phi_0\right\rangle}{\left\langle\Psi_0\middle|\Psi_0\right\rangle} \tag{3.43}$$

The last step follows as the two terms are complex conjugates of each other and give equal contributions. Substituting the expanded form of $\overline{D}$

$$\begin{aligned} D_a &= 2\left\langle\Phi_1\middle|\left[De^{T^{(0)}} + \sum_{n=1}^{\infty}\frac{1}{n!}\left(T^{(0)^\dagger}\right)^n De^{T^{(0)}}\right]\middle|\Phi_0\right\rangle \Big/ \left\langle\Psi_0\middle|\Psi_0\right\rangle \\ &= 2\left[\left\langle\Phi_1\middle|De^{T^{(0)}}\middle|\Phi_0\right\rangle + \left\langle\Phi_1\middle|\sum_{n=1}^{\infty}\frac{1}{n!}\left(T^{(0)^\dagger}\right)^n De^{T^{(0)}}\middle|\Phi_0\right\rangle\right] \Big/ \left\langle\Psi_0\middle|\Psi_0\right\rangle \end{aligned} \tag{3.44}$$

This expression of D_a reduces the complexity of the infinite order summation as not all $T^{(0)^\dagger}$ operators contribute. In this scheme, the zeroth order D_a is terms without $T^{(0)^\dagger}$ operator, first order D_a is terms having one order of $T^{(0)^\dagger}$, and so on. The unlinked terms of the numerator cancel with the denominator and only linked terms contribute in the numerator.

3.2.1 Zeroth order EDM

Consider the numerator of the zeroth order contribution

$$D_a^0 = \left\langle \Phi_1 \middle| De^{T^{(0)}} \middle| \Phi_0 \right\rangle$$

Expanding $\langle \Phi_1 |$

$$\left\langle \Phi_1 \middle| De^{T^{(0)}} \middle| \Phi_0 \right\rangle = \underbrace{\left\langle \Phi_0 \middle| T_1^{(1)\dagger} De^{T^{(0)}} \middle| \Phi_0 \right\rangle}_{Z1} + \underbrace{\left\langle \Phi_0 | T_2^{(1)\dagger} De^{T^{(0)}} \middle| \Phi_0 \right\rangle}_{Z2}. \tag{3.45}$$

The level of excitation (l.o.e) is defined as the excitation number, assigned to a diagram based on the number of excitations versus the number of de-excitations, the orbitals are participating in. Hence, the operators, T_1 and T_2 have l.o.e = 1 and 2 respectively. Then, $T_1^\dagger$ and $T_2^\dagger$ have l.o.e equal to -1 and -2 respectively. Since the operators $T_1^{(1)}$ and $T_2^{(1)}$ have fixed levels of excitation of $+1$ and $+2$ respectively. This restricts the possible terms contributing to the dressed dipole operator in Eq.3.45. In other words, the term Z1 is non-zero only when the coefficient $\left(De^{T^{(0)}}\right)_1$ has l.o.e = 1 (indicated by the subscript). Similarly, for non-zero Z2 contribution $\left(De^{T^{(0)}}\right)_2$ must have a l.o.e = 2. Hence the terms finally contributing to Zeroth order can be read off as,

$$\left(De^{T^{(0)}}\right)_1 = \frac{1}{2!}DT_1^{(0)^2} + DT_2^{(0)} + DT_1^{(0)} + D \tag{3.46}$$

$$\left(De^{T^{(0)}}\right)_2 = \frac{1}{3!}DT_1^{(0)^3} + DT_1^{(0)}T_2^{(0)} + \frac{1}{2!}DT_1^{(0)^2} + DT_2^{(0)} + DT_1^{(0)} \tag{3.47}$$

The diagrams of $(De^{T^{(0)}})_1$ and $(De^{T^{(0)}})_2$ are shown in Fig.3.11 and Fig.3.12 respectively. The linked diagrams of $(De^{T^{(0)}})_1$ are connected, but for $(De^{T^{(0)}})_{n\geq 2}$, disconnected diagrams also contribute.

The diagrams in Fig.3.11 are identical to the diagrams contributing to the RHS of the singles CCEDM equations with the single particle operator $H_{\rm EDM}$ replaced by D (see Fig.3.7).

In Fig.3.12, among the $(De^{T^{(0)}})_2$ diagrams, (a), (c), (g) and (j) are connected and the remaining are disconnected, that is

$$(De^{T^{(0)}})_2 = \left(De^{T^{(0)}}\right)_2^{\rm conn} + \left(De^{T^{(0)}}\right)_2^{\rm discon}, \tag{3.48}$$

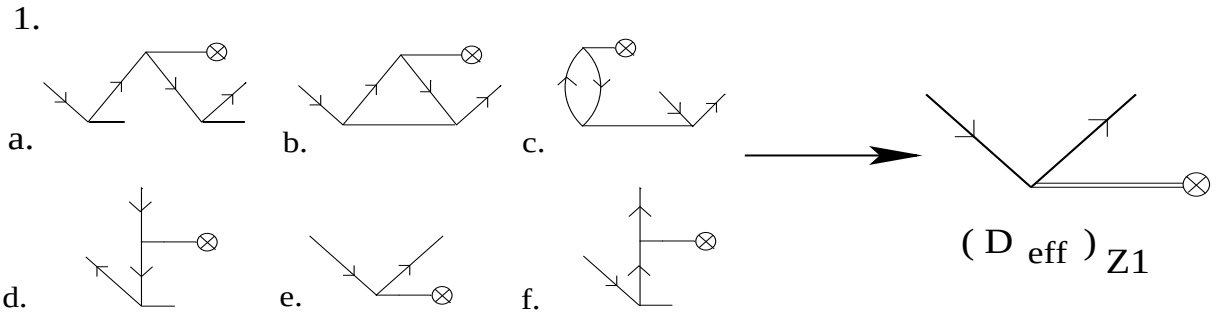

Figure 3.11: Diagrams contributing to $\left(De^{T^{(0)}}\right)_1$. The diagram named $(D_{eff})_{Z1}$ is the effective operator obtained by summing the diagrams (a,b,c,d,e,f). All diagrams are connected.

where the first and second terms represented the connected and disconnected terms. The connected terms resemble the diagrams contributing to the doubles on the RHS of the CCEDM equation, again with the $H_{\rm EDM}$ operator replaced by D (see Fig.3.8). The topology of the diagrams shows that diagrams of $\left(De^{T^{(0)}}\right)_2$ arise from $\left(De^{T^{(0)}}\right)_1 \times T_1^{(0)}$ and $\left(De^{T^{(0)}}\right)_2^{\rm conn}$ diagrams. That is

$$\left(De^{T^{(0)}}\right)_2^{\rm discon} = \left(De^{T^{(0)}}\right)_1 \times T_1^{(0)} \tag{3.49}$$

All the diagrams having same number of free lines and components are grouped together to obtain effective diagrams shown in Fig.3.13(II). The diagrams contributing to EDM Eq.3.40 are shown in Fig.3.14 and are obtained from the contraction of the effective dressed induced dipole operator with the perturbed cluster operator.

3.2.2 First order EDM

Next, consider the $n = 1$ term in Eq.3.44, it is the first order in $T^{(0)\dagger}$

$$\begin{aligned}\left\langle \Phi_1 \middle| T^{(0)\dagger} De^{T^{(0)}} \middle| \Phi_0 \right\rangle &= \left\langle \Phi_0 \middle| \left[T_1^{(1)\dagger} + T_2^{(1)\dagger}\right] T^{(0)\dagger} De^{T^{(0)}} \middle| \Phi_0 \right\rangle \\ &= \left\langle \Phi_0 \middle| \underbrace{T_1^{(1)\dagger} T^{(0)\dagger} De^{T^{(0)}}}_{F1} \middle| \Phi_0 \right\rangle + \left\langle \Phi_0 \middle| \underbrace{T_2^{(1)\dagger} T^{(0)\dagger} De^{T^{(0)}}}_{F2} \middle| \Phi_0 \right\rangle\end{aligned}$$

We now determine the terms contributing to F1 and F2, expanding $T^{(0)\dagger}$ in F1

$$\left\langle \Phi_0 \middle| T_1^{(1)\dagger} T^{(0)\dagger} De^{T^{(0)}} \middle| \Phi_0 \right\rangle = \underbrace{\left\langle \Phi_0 \middle| T_1^{(1)\dagger} \left(T_1^{(0)\dagger} De^{T^{(0)}}\right)_1 \middle| \Phi_0 \right\rangle}_{F1(A)} + \underbrace{\left\langle \Phi_0 \middle| T_1^{(1)\dagger} \left(T_2^{(0)\dagger} De^{T^{(0)}}\right)_1 \middle| \Phi_0 \right\rangle}_{F1(B)}$$

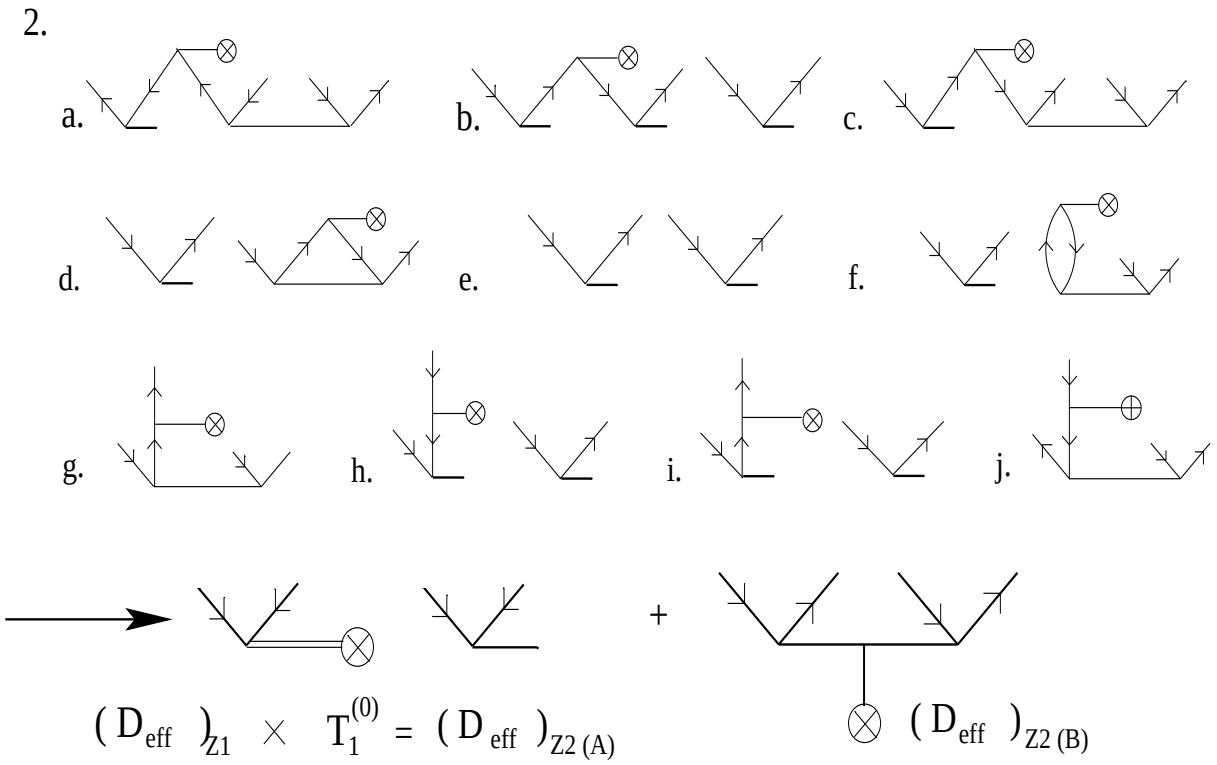

Figure 3.12: Diagrams contributing to $\left(De^{T^{(0)}}\right)_2$.

Further, expanding $De^{T^{(0)}}$ in the first term

$$\begin{aligned}\left(T_1^{(0)\dagger} De^{T^{(0)}}\right)_1 &= T_1^{(0)\dagger}\left(De^{T^{(0)}}\right)_2 \\ &= T_1^{(0)\dagger}\left[\frac{1}{3!}DT_1^{(0)3} + DT_1^{(0)}T_2^{(0)} + \frac{1}{2!}DT_1^{(0)2} + DT_2^{(0)} + DT_1^{(0)}\right]_2 \\ &= T_1^{(0)\dagger}\left[\left(De^{T^{(0)}}\right)_2^{\text{conn}} + (De^{T^{(0)}})_1 \times T_1^{(0)}\right] \qquad (3.50)\end{aligned}$$

As discussed in the zeroth order case, the $(De^{T^{(0)}})_2$ diagrams arise from $(De^{T^{(0)}})_1 \times T_1^{(0)}$ and the actual $(De^{T^{(0)}})_2^{\text{conn}}$ diagrams. We saw that the effective diagrams listed in Fig.3.13 are sum of all the diagrams arising from $(De^{T^{(0)}})_1 \times T_1^{(0)}$ and $(De^{T^{(0)}})_2$. Hence, the effective diagrams of $(T_1^{(0)\dagger} De^{T^{(0)}})_1$ are contraction of the effective diagrams in Fig.3.13 and $T_1^{(0)\dagger}$, these are shown in Fig.3.15. To calculate the contribution from

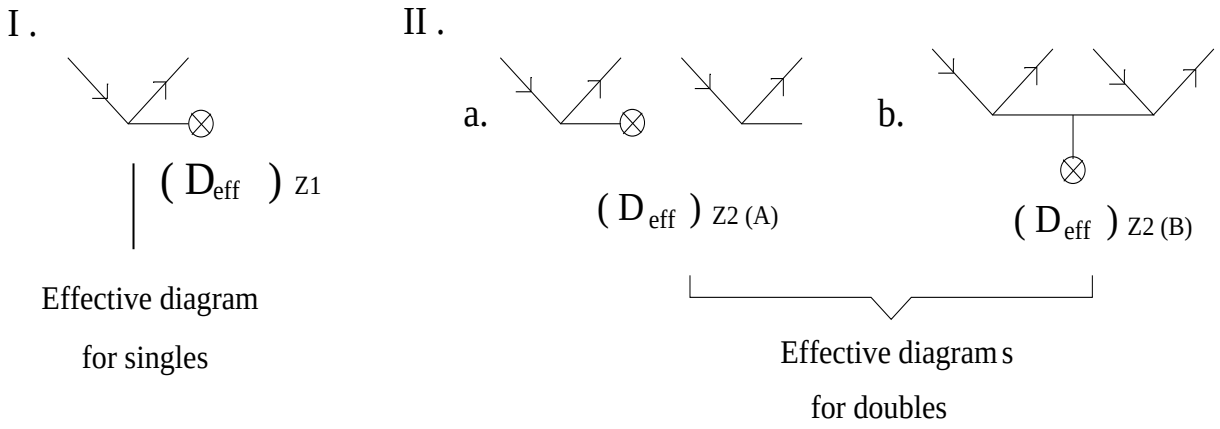

Figure 3.13: Effective diagrams for singles and doubles for zeroth order

the F1(B), we require

$$\begin{aligned}\left(De^{T^{(0)}}\right)_3 &= \left[\frac{1}{4!}DT_1^{(0)4} + \frac{1}{2!}DT_2^{(0)2} + \frac{1}{2!}DT_1^{(0)2}T_2^{(0)} + \frac{1}{3!}DT_1^{(0)3} + \right. \\ &\quad \left. DT_1^{(0)}T_2^{(0)} + \frac{1}{2!}DT_1^{(0)2} + DT_2^{(0)}\right]_3 \qquad (3.51) \\ &= \left(De^{T^{(0)}}\right)_3^{\rm conn} + \left(De^{T^{(0)}}\right)_2^{\rm conn} \times T_1^{(0)} + \left(De^{T^{(0)}}\right)_1 \left[\frac{1}{2!}T_1^{(0)2} + T_2^{(0)}\right] \qquad (3.52)\end{aligned}$$

Similar to the previous cases, $(De^{T^{(0)}})_3$ is the sum of $(De^{T^{(0)}})_1 \times T_1^{(0)^2}$, $(De^{T^{(0)}})_1 \times T_2^{(0)}$ and $(De^{T^{(0)}})_2^{\rm conn} \times T_1^{(0)}$. In the present calculation, we do not include the $(De^{T^{(0)}})_3^{\rm conn}$, which are true three body diagrams. That is, we define

$$\left(De^{T^{(0)}}\right)_3 = \left(De^{T^{(0)}}\right)_2^{\rm conn} \times T_1^{(0)} + \left(De^{T^{(0)}}\right)_1 \left[\frac{1}{2!}T_1^{(0)2} + T_2^{(0)}\right]. \qquad (3.53)$$

The diagrams in Fig.3.16 represent the sum of all the diagrams arising from these terms. The effective diagrams at first order can be obtained by the action of $T_2^{(0)\dagger}$ on the diagrams listed in Fig.3.16, then

$$\left(T_2^{(0)\dagger}De^{T^{(0)}}\right)_1 = T_2^{(0)\dagger}\left[\left(De^{T^{(0)}}\right)_2^{\rm conn} \times T_1^{(0)} + \left(De^{T^{(0)}}\right)_1 \left(\frac{1}{2!}T_1^{(0)2} + T_2^{(0)}\right)\right]. \qquad (3.54)$$

The contribution to EDM are then the contraction of these terms with $T_1^{(1)\dagger}$. These terms are topologically equivalent to the non-linear EDM cluster amplitude diagrams for singles arising from the (particle-hole , particle hole) form of the Coulomb operator,

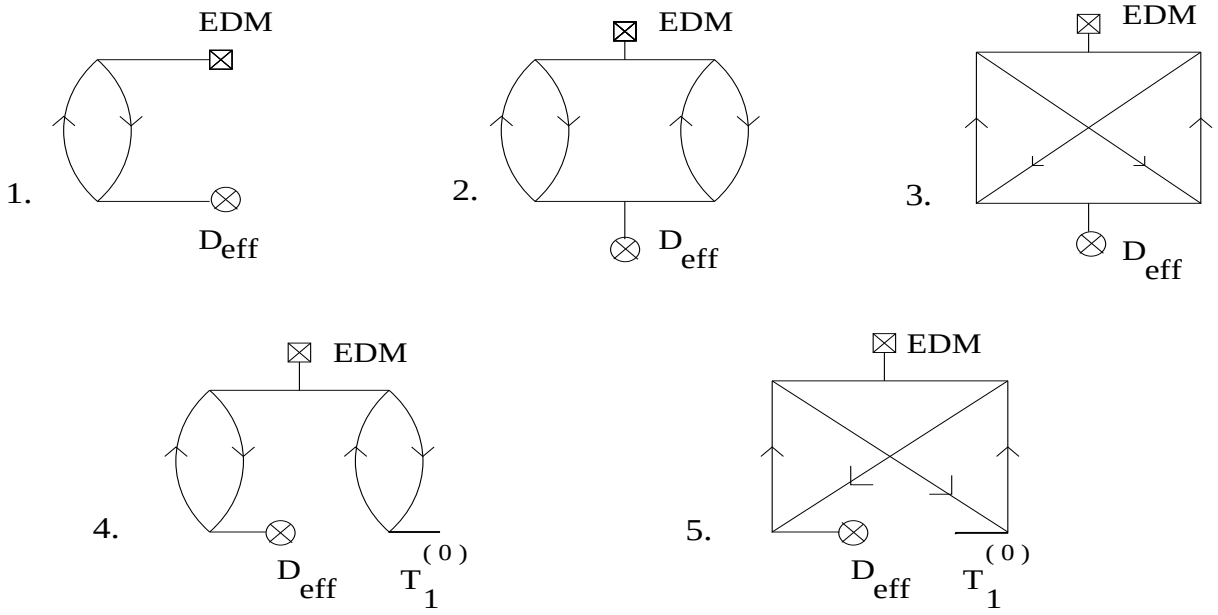

Figure 3.14: Diagrams contributing to EDM from the effective diagrams at zeroth order

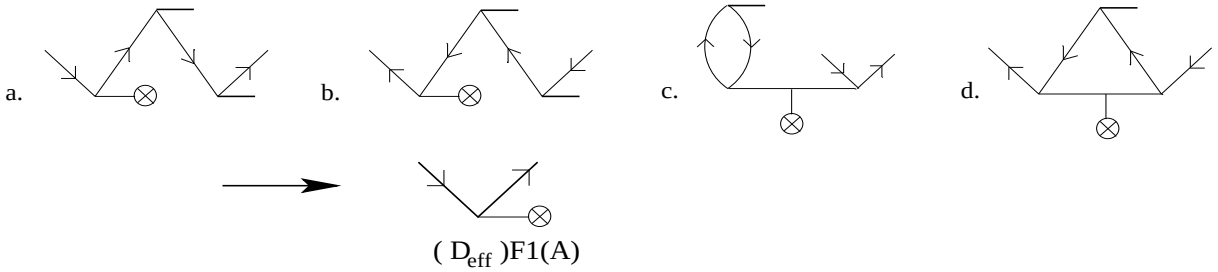

Figure 3.15: Effective diagrams at first order contributing to F1(A)

where $T_1^{(1)}$ replaces the dipole operator, D. Adding Eq. (3.50) and Eq.(3.54), define an effective operator of $\overline{D}$ as

$$\overline{D}_1^1 = \left(T_1^{(0)\dagger} D e^{T^{(0)}}\right)_1 + \left(T_2^{(0)\dagger} D e^{T^{(0)}}\right)_1, \tag{3.55}$$

where the subscript represents the one-body character of the operator and superscript indicates the order of $T^{(0)\dagger}$.

Similar to F1, expanding F2

$$\left\langle \Phi_0 \middle| T_2^{(1)\dagger} T^{(0)\dagger} D e^{T^{(0)}} \middle| \Phi_0 \right\rangle = \underbrace{\left\langle \Phi_0 \middle| T_2^{(1)\dagger} \left(T_1^{(0)\dagger} D e^{T^{(0)}}\right)_2 \middle| \Phi_0 \right\rangle}_{F2(A)} + \underbrace{\left\langle \Phi_0 \middle| T_2^{(1)\dagger} \left(T_2^{(0)\dagger} D e^{T^{(0)}}\right)_2 \middle| \Phi_0 \right\rangle}_{F2(B)} \tag{3.56}$$

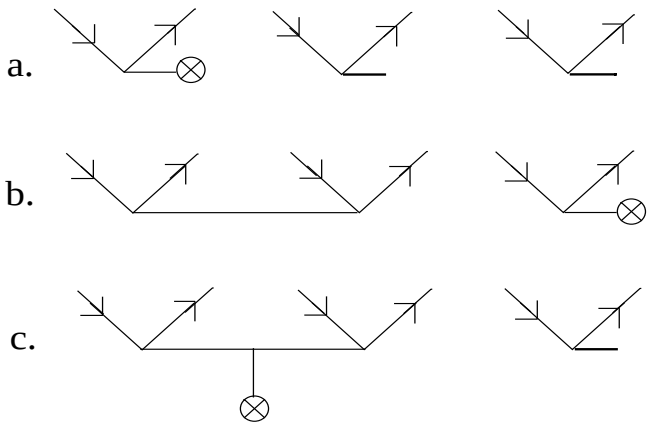

Figure 3.16: Open diagrams at first order for the term $(De^{T^{(0)}})_3$. Multiplication of $T_2^{(0)^\dagger}$ with these diagrams gives the effective diagrams contributing to F1(B)

Consider F2(A), expanding the term within the parenthesis

$$\left\langle \Phi_0 \middle| T_2^{(1)^\dagger} \left(T_1^{(0)^\dagger} De^{T^{(0)}} \right)_2 \middle| \Phi_0 \right\rangle = \left\langle \Phi_0 \middle| T_2^{(1)^\dagger} T_1^{(0)^\dagger} \left(De^{T^{(0)}} \right)_3 \middle| \Phi_0 \right\rangle. \tag{3.57}$$

From the definition of $(De^{T^{(0)}})_3$ in Eq. (3.53)

$$= \left\langle \Phi_0 \middle| T_2^{(1)^\dagger} T_1^{(0)^\dagger} \left[\left(De^{T^{(0)}} \right)_2^{\text{conn}} \times T_1^{(0)} + \left(De^{T^{(0)}} \right)_1 \left(\frac{1}{2!} T_1^{(0)^2} + T_2^{(0)} \right) \right] \middle| \Phi_0 \right\rangle. \tag{3.58}$$

As mentioned earlier, the open diagrams contributing to $(De^{T^{(0)}})_3$ are listed in Fig.3.16. The $\overline{D}$ diagrams are then the contraction of $T_1^{(0)^\dagger}$ with $(De^{T^{(0)}})_3$, these are shown in Fig.3.17. Fig.3.18 shows the effective F2(A) diagrams.

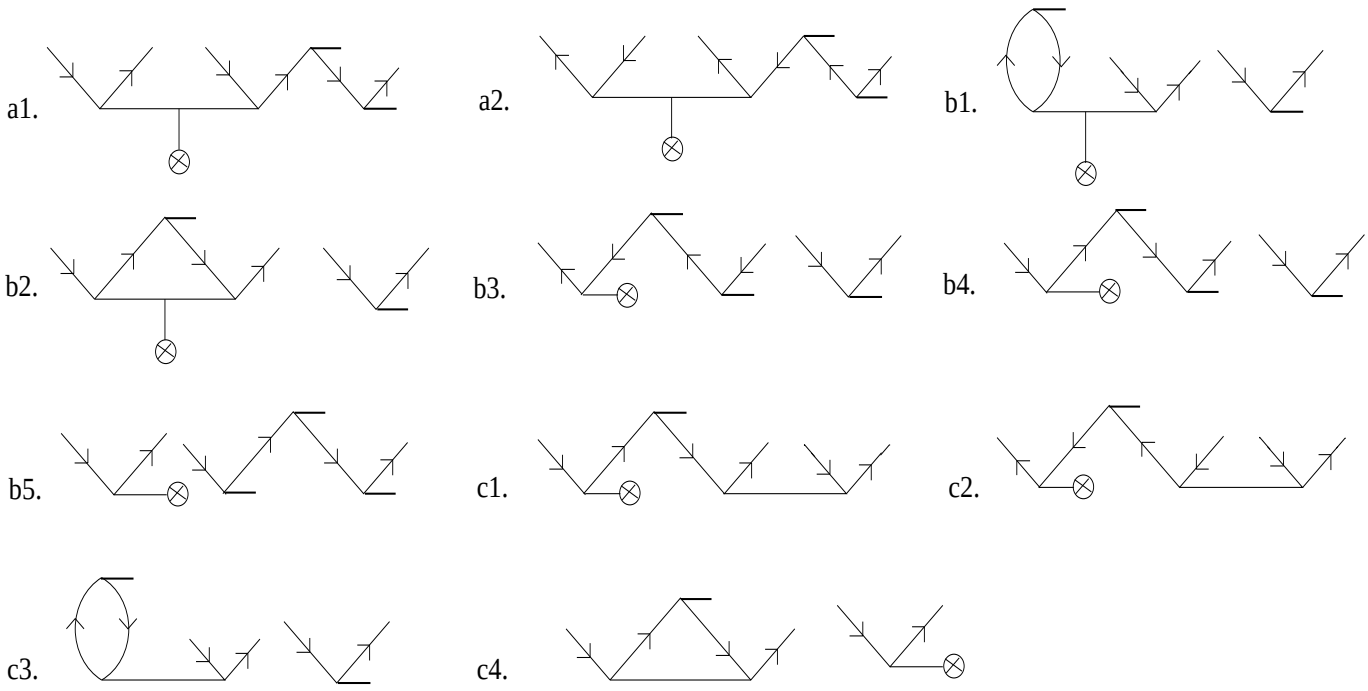

Figure 3.17: Diagrams contributing to effective diagrams at first order for F2(A) - $T_1^{(0)\dagger}(De^{T^{(0)}})_3$

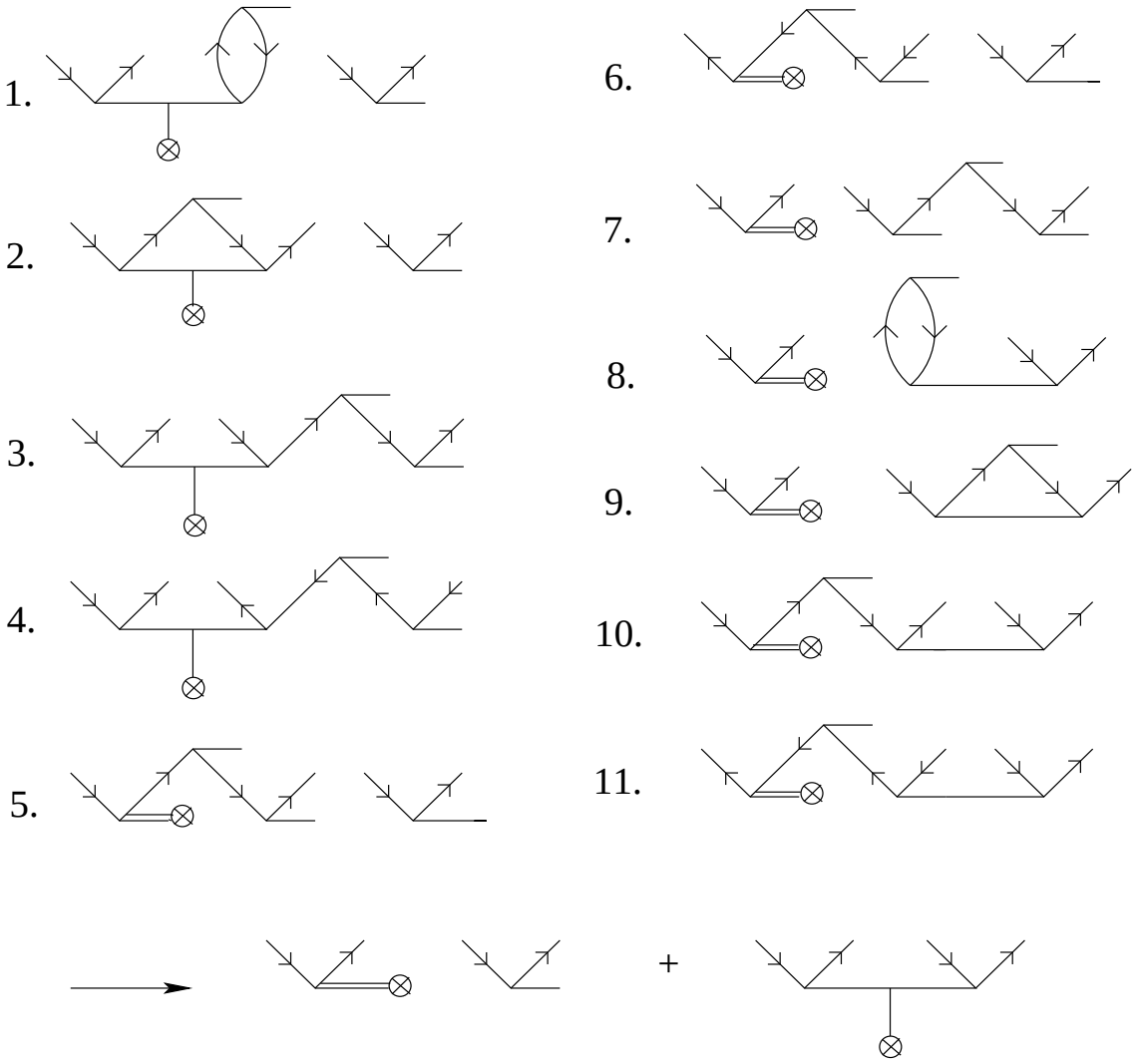

Figure 3.18: Effective diagrams at first order for F2(A) - $T_1^{(0)\dagger}(De^{T^{(0)}})_3$

Fig.3.19 shows the effective diagrams arising from summing the diagrams listed in 3.17. Now, consider the F2(B),

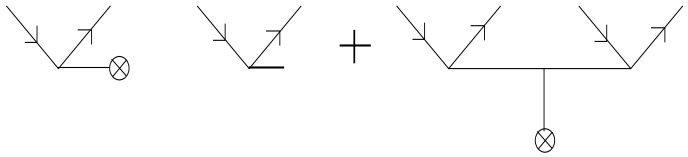

Figure 3.19: Effective diagrams at first order for F2(A) - $T_1^{(0)^\dagger}(De^{T^{(0)}})_3$

$$\left\langle \Phi_0 \middle| T_2^{(1)^\dagger} \left(T_2^{(0)^\dagger} De^{T^{(0)}} \right)_2 \middle| \Phi_0 \right\rangle = \left\langle \Phi_0 \middle| T_2^{(1)^\dagger} T_2^{(0)^\dagger} \left(De^{T^{(0)}} \right)_4 \middle| \Phi_0 \right\rangle. \tag{3.59}$$

Similar to $(De^{t^{(0)}})_3$, we can define

$$\left(De^{T^{(0)}} \right)_4 = \left(De^{T^{(0)}} \right)_2^{\text{conn}} \left[\frac{1}{2!} T_1^{(0)^2} + T_2^{(0)} \right] + \left(De^{T^{(0)}} \right)_1 \left[\frac{1}{3!} T_1^{(0)^3} + T_2^{(0)} T_1^{(0)} \right]. \tag{3.60}$$

We can define effective $\overline{D}$ diagrams of $(T_1^{(0)^\dagger} De^{T^{(0)}})_2$ and $(T_2^{(0)^\dagger} De^{T^{(0)}})_2$. However, unlike $\overline{D}_1^1$ these terms have connected as well as disconnected diagrams

$$\overline{D}_2^1 = \overline{D}_2^{1\text{conn}} + \overline{D}_2^{1\text{discon}} = \left(T_1^{(0)^\dagger} De^{T^{(0)}} \right)_2 + \left(T_2^{(0)^\dagger} De^{T^{(0)}} \right)_2, \tag{3.61}$$

where $\overline{D}_2^{1\text{conn}}$ and $\overline{D}_2^{1\text{discon}}$ are the connected and disconnected contributions.

The EDM contribution from second order $T^{(0)^\dagger}$ can be calculated from $\overline{D}_1^2$ and $\overline{D}_2^2$. Substituting $n = 2$ in Eq.3.42, we get the second order contributin to EDM from the terms,

$$\overline{D}^2 = \frac{T^{(0)^{\dagger 2}}}{2!} De^{T^{(0)}}$$

$$= \left(\frac{T_1^{(0)^{\dagger 2}}}{2!} + \frac{T_2^{(0)^{\dagger 2}}}{2!} + \frac{2}{2!} T_1^{(0)^\dagger} T_2^{(0)^\dagger} \right) De^{T^{(0)}}$$

where $T^{(0)} = T_1^{(0)} + T_2^{(0)}$. Diagrammatically, the effective diagrams of F2(B) are obtained by the multiplication of $T_2^{(0)}$ by diagrams of $\left(De^{T^{(0)}} \right)_4$ as shown in Fig.3.20. The resultant diagrams have the same topology as the diagrams arising from the terms $\left(V_N T_1^{(0)} T_1^{(0)} T_2^{(1)} \right)$, $\left(V_N T_2^{(0)} T_2^{(1)} \right)$, $\left(V_N T_1^{(0)} T_1^{(0)} T_1^{(0)} T_1^{(1)} \right)$, $\left(V_N T_1^{(0)} T_2^{(0)} T_1^{(1)} \right)$, where the residual Coulomb operator has a PH-PH form and is hence replaced by the operator $T_2^{(0)^\dagger}$.

Action of $T_2^{(0)\dagger}$ on

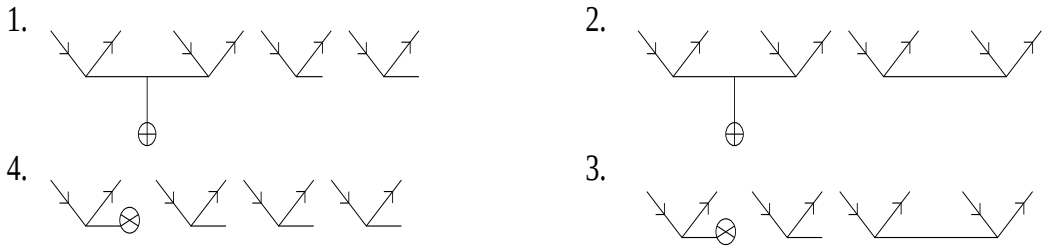

Figure 3.20: Effective diagrams at first order for F2(B) - $T_2^{(0)\dagger}(De^{T^{(0)}})_4$. The diagrams labelled 1 to 4 in the above diagram, when multiplied by $T_2^{(0)\dagger}$, give rise to the effective diagrams of F2(B).

3.3 Comparison of CPHF and Coupled-cluster theories

3.3.0.1 CPHF equations

In this section, we give an outline of CPHF equations and explain how the diagrams arising from the CPHF theory can be related to the diagrams present in coupled-cluster theory. The results of the numerical comparison are presented in Chapter.6. Consider the Hartree-Fock equation Eq.3.6,

$$\left(h^0 + g^0 - \epsilon_a^0\right)\left|\psi_a^0\right\rangle = 0 \tag{3.62}$$

The introduction of CP-violating interaction, $h_{\rm EDM}$, as a perturbation, modifies the Hamiltonian and wavefunctions

$$\left|\psi_a^0\right\rangle \rightarrow \left|\psi_a^0\right\rangle + \lambda\left|\psi_a^1\right\rangle, \quad \text{and} \quad h^0 \rightarrow h^0 + \lambda h_{\rm EDM}$$

where λ is the perturbation parameter and $|\psi_a^1\rangle$ is the first order correction to wavefunction. There is no first order energy correction as the perturbation Hamiltonian $h_{\rm EDM}$ is

parity odd. Then we get the perturbed Hartree-Fock equation

$$\left(h^0+\lambda h_{\rm EDM}\right)\left(\left|\psi_a^0\right\rangle+\lambda\left|\psi_a^1\right\rangle\right)+\sum_{b=1}^{N_{\rm occ}}\left[\left\langle\psi_b^0+\lambda\psi_b^1\right|v\left|\psi_b^0+\lambda\psi_b^1\right\rangle\left|\psi_a^0+\lambda\psi_a^1\right\rangle\right]$$
$$-\sum_{b=1}^{N_{\rm occ}}\left[\left\langle\psi_b^0+\lambda\psi_b^1\right|v\left|\psi_a^0+\lambda\psi_a^1\right\rangle\left|\psi_b^0+\lambda\psi_b^1\right\rangle\right]-\epsilon_a^0\left|\psi_a^0+\lambda\psi_a^1\right\rangle=0 \tag{3.63}$$

Selecting only the terms linear in λ,

$$\left(h^0\left|\psi_a^1\right\rangle+h_{\rm EDM}\left|\psi_a^0\right\rangle\right)+\sum_{b=1}^{N_{\rm occ}}\left\langle\psi_b^0\right|v\left|\psi_b^1\right\rangle\left|\psi_a^0\right\rangle+\left\langle\psi_b^1\right|v\left|\psi_b^0\right\rangle\left|\psi_a^0\right\rangle+\left\langle\psi_b^0\right|v\left|\psi_b^0\right\rangle\left|\psi_a^1\right\rangle\Big)$$
$$-\Big(\left\langle\psi_b^0\right|v\left|\psi_a^1\right\rangle\left|\psi_b^0\right\rangle+\left\langle\psi_b^1\right|v\left|\psi_a^0\right\rangle\left|\psi_b^0\right\rangle+\left\langle\psi_b^0\right|v\left|\psi_a^0\right\rangle\left|\psi_b^1\right\rangle\Big)-\epsilon_a^0\left|\psi_a^1\right\rangle=0 \tag{3.64}$$

Rearranging

$$\left(h^0+g^0-\epsilon_a^0\right)\left|\psi_a^1\right\rangle=\left(-h_{\rm EDM}-g^1\right)\left|\psi_a^0\right\rangle \tag{3.65}$$

where the perturbed two-particle operator

$$g^1\left|\psi_a^0\right\rangle=\sum_{b=1}^{N_{occ}}\left[\left\langle\psi_b^0\right|v\left|\psi_b^1\right\rangle\left|\psi_a^0\right\rangle-\left\langle\psi_b^0\right|v\left|\psi_a^0\right\rangle\left|\psi_b^1\right\rangle+\left\langle\psi_b^1\right|v\left|\psi_b^0\right\rangle\left|\psi_a^0\right\rangle-\left\langle\psi_b^1\right|v\left|\psi_a^0\right\rangle\left|\psi_b^0\right\rangle\right] \tag{3.66}$$

The Eq.(3.65) is the CPHF equation. Expanding the perturbed orbitals as a linear combination of the opposite parity unperturbed orbitals

$$\left|\psi_a^1\right\rangle=\sum_p C_{pa}\left|\psi_p^0\right\rangle$$

where C_{pa} are the mixing coefficients, then

$$\sum_p\left(h^0+g^0-\epsilon_a^0\right)C_{pa}\left|\psi_p^0\right\rangle=\left(-h_{\rm EDM}-g^1\right)\left|\psi_a^0\right\rangle$$

Projecting the above equation by $\langle\psi_m^0|$,

$$\left(\epsilon_p^0-\epsilon_a^0\right)C_{pa}=\left\langle\psi_p^0\right|\left(-h_{\rm EDM}-g^1\right)\left|\psi_a^0\right\rangle$$

Similarly, expanding $|\psi_b^1\rangle = \sum_q C_{qb}|\psi_q^0\rangle$ in g', the mixing coefficients are solutions of the linear alegebraic equations

$$C_{pa}\left(\epsilon_p^0 - \epsilon_a^0\right) + \sum_{bq}\left[\tilde{V}_{pqab}C_{qb}^* + \tilde{V}_{pbaq}C_{qb}\right] + \left\langle p\middle|h_{\rm EDM}\middle|a\right\rangle = 0 \tag{3.67}$$

where $\tilde{V}_{pqab} = \Big(\langle pq|v|ab\rangle - \langle pq|v|ba\rangle\Big)$ and $\tilde{V}_{pbaq} = \Big(\langle pb\,|v|\,aq\rangle - \langle pb\,|v|\,qa\rangle\Big)$.

The wavefunctions $|\psi_p^0\rangle$, $|\psi_a^0\rangle$, $|\psi_b^0\rangle$ and $|\psi_q^0\rangle$ are represented by the orbital indices (p, a, b, q) respectively and hereafter we follow this notation for the single particle orbitals. The zeroth order contribution to the coefficients is

$$C_{pa}^{(0,1)} = -\frac{\left\langle p\middle|h_{\rm EDM}\middle|a\right\rangle}{\left(\epsilon_p^0 - \epsilon_a^0\right)} \tag{3.68}$$

The superscripts on the coefficient denotes the order of the residual Coulomb interaction and that of the h_{EDM} perturbation respectively. The diagrammatic representation of this term is given in Fig.3.21(a).

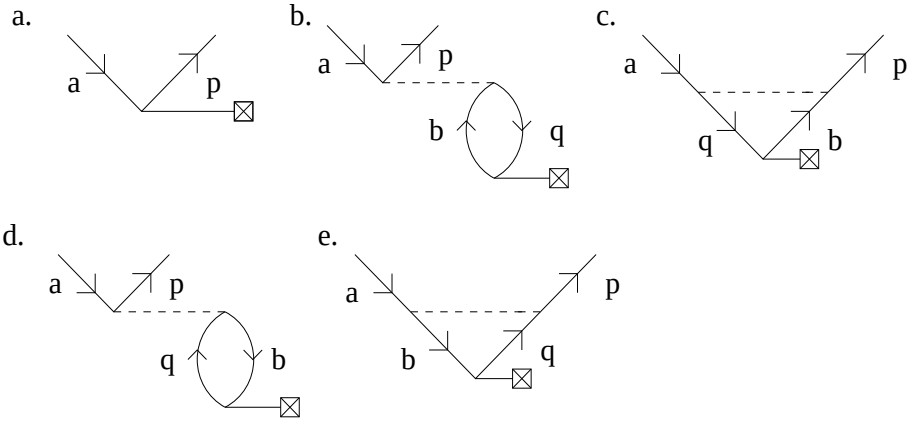

Figure 3.21: CPHF diagrams at zero and one order residual Coulomb interaction. The diagrams (d,e) are called *normal* CPHF diagrams and (b,c) are the *pseudo* CPHF diagrams. The dotted line is the residual Coulomb interaction and the line attached with ⊠ is the EDM interaction.

The Eq.3.67 is expressed in the form of a linear matrix equation,

$$\sum_{qb} A_{pa\ qb}C_{qb} = -B_{pa} \tag{3.69}$$

where $A_{pa\ qb} = \tilde{V}_{pqab} + \tilde{V}_{pbaq} + \left(\epsilon_p^0 - \epsilon_a^0\right)\delta_{pq}\delta_{ab}$ and $B_{pa} = \langle p|h_{\rm EDM}|a\rangle$. This equation is solved iteratively starting with the initial guess for the mixing coefficients given by Eq.3.68. The coefficients of the kth iteration are obtained from,

$$C_{pa}^{(k,1)} = -\frac{B_{pa}}{\epsilon_p^0 - \epsilon_a^0} - \sum_{bq}\left[\left(\tilde{V}_{pqab}\right)\frac{C_{qb}^{(k-1,1)^*}}{\epsilon_p^0 - \epsilon_a^0} + \left(\tilde{V}_{pbaq}\right)\frac{C_{qb}^{(k-1,1)}}{\epsilon_p^0 - \epsilon_a^0}\right] \tag{3.70}$$

With one order in residual Coulomb interaction, we get,

$$C_{pa}^{(1,1)} = -\frac{B_{pa}}{\epsilon_p^0 - \epsilon_a^0} - \sum_{bq}\left[\left(\tilde{V}_{pqab}\right)\frac{C_{qb}^{(0,1)^*}}{\epsilon_p^0 - \epsilon_a^0} + \left(\tilde{V}_{pbaq}\right)\frac{C_{qb}^{(0,1)}}{\epsilon_p^0 - \epsilon_a^0}\right] \tag{3.71}$$

The diagrams arising from the above equation are shown in Fig.3.21.

Substituting the expression of $C_{qb}^{(0,1)}$

$$C_{pa}^{(1,1)} = -\frac{B_{pa}}{\epsilon_p^0 - \epsilon_a^0} - \sum_{bq}\left[\left(\tilde{V}_{pqab}\right)\frac{(B_{qb})^\dagger}{(\epsilon_b^0 - \epsilon_q^0)(\epsilon_p^0 - \epsilon_a^0)} + \left(\tilde{V}_{pbaq}\right)\frac{B_{qb}}{(\epsilon_b^0 - \epsilon_q^0)(\epsilon_p^0 - \epsilon_a^0)}\right] \tag{3.72}$$

The contribution of the *normal* CPHF diagrams for one order in residual Coulomb interaction is,

$$\left(C_{pa}^{(1,1)}\right)_{\rm normal} = -\sum_{bq}\left[\left(\tilde{V}_{pbaq}\right)\frac{B_{qb}}{(\epsilon_b^0 - \epsilon_q^0)(\epsilon_p^0 - \epsilon_a^0)}\right] \tag{3.73}$$

This expression is used later to compare with similar expression arising in CCEDM. Consider the two pseudo diagrams of CPHF. Writing only the pseudo diagrams,

$$\left(C_{pa}^{(1,1)}\right)_{\rm pseudo} = -\sum_{bq}\left[\left(\tilde{V}_{pqab}\right)\frac{(B_{qb})^\dagger}{(\epsilon_b^0 - \epsilon_q^0)(\epsilon_p^0 - \epsilon_a^0)} + \right] \tag{3.74}$$

These terms are diagrammatically represented by Fig.3.21(b,c). This point is discussed in detail later in the paper.

3.3.0.2 CCEDM equations

Consider the EDM perturbed singles and doubles cluster amplitude equations (CCEDM),

$$\left\langle \Phi_a^{p\prime} \middle| \left[\overline{H_N T^{(1)}} \right] \middle| \Phi_0 \right\rangle = -\left\langle \Phi_a^{p\prime} \middle| \overline{H}_{EDM} \middle| \Phi_0 \right\rangle \tag{3.75}$$

$$\left\langle \Phi_{ab}^{pq\prime} \middle| \left[\overline{H_N T^{(1)}} \right] \middle| \Phi_0 \right\rangle = -\left\langle \Phi_{ab}^{pq\prime} \middle| \overline{H}_{EDM} \middle| \Phi_0 \right\rangle \tag{3.76}$$

Consider the CCEDM equation for singles by setting $\overline{H}_N = H_N$ and $\overline{H}_{EDM} = H_{EDM}$ and ignore the doubles for the present.

$$\left\langle \Phi_a^{p\prime} \middle| \overline{H_N T_1^{(1)}} \middle| \Phi_0 \right\rangle = -\left\langle \Phi_a^{p} \middle| H_{EDM} \middle| \Phi_0 \right\rangle \tag{3.77}$$

using $\left[\overline{H_N T^{(1)}} \right] = \left\{ \overline{H_N T^{(1)}} \right\}$. Introducing a complete set of singly excited states,

$$\sum_{bq} \left\langle \Phi_a^{p\prime} \middle| H_N \middle| \Phi_b^{q\prime} \right\rangle \left\langle \Phi_b^{q\prime} \middle| T_1^{(1)} \middle| \Phi_0 \right\rangle = -\left\langle \Phi_a^{p} \middle| H_{EDM} \middle| \Phi_0 \right\rangle \tag{3.78}$$

we get

$$\sum_{bq} \left(H_N\right)_{ap,bq} \left(T_1^{(1)}\right)_{bq} = -\left(H_{EDM}\right)_{ap} \tag{3.79}$$

where $\left(H_N\right)_{ap,bq} = V_{pb,aq} - V_{pb,qa} + f_{pq} - f_{ba}$ considering only the terms of H_N which have a CPHF counterpart. The operator, $H_N = f_N + V_N$, where f_N and V_N are the normal ordered one- and two-body operators respectively. The one-body terms contribute to the single particle orbital energies. In terms of single-particle wavefunctions, the CCEDM equation becomes

$$\sum_{bq} \left[\left\langle pb \middle| V \middle| aq \right\rangle - \left\langle pb \middle| V \middle| qa \right\rangle - \left\langle a \middle| f \middle| b \right\rangle + \left\langle p \middle| f \middle| q \right\rangle \right] \times \left\langle q \middle| t^{(1)} \middle| b \right\rangle = \left\langle p \middle| -h_{EDM} \middle| a \right\rangle$$

$$\Rightarrow \sum_{bq} \left[\tilde{V}_{pb,aq}\, t_b^{q(1)} \right] + \left(\epsilon_p - \epsilon_a \right) t_a^{p(1)} = \left\langle p \middle| -h_{EDM} \middle| a \right\rangle$$

The perturbed cluster amplitudes are hence given by,

$$t_a^{p(1)} = \left(-B_{ap} - \sum_{bq} \tilde{V}_{pb,aq} t_b^{q(1)} \right) \Big/ \left(\epsilon_p - \epsilon_a \right) \tag{3.80}$$

Where the matrix B_{ap} is given by,

$$B_{ap} = \left\langle p \middle| h_{EDM} \middle| a \right\rangle$$

Expressing the above equation in an iterative form,

$$t_a^{p(k,1)} = \left(-B_{ap} - \sum_{bq} \tilde{V}_{pb,aq} t_b^{q(k-1,1)} \right) \Big/ \left(\epsilon_p - \epsilon_a \right) \tag{3.81}$$

The perturbed cluster amplitudes are solutions of the Eq.3.81, where the initial guess is given by,

$$t_a^{p(0,1)} = \frac{-\left\langle p \middle| h_{EDM} \middle| a \right\rangle}{\left(\epsilon_p - \epsilon_a \right)}$$

For one order in residual Coulomb interaction, $k = 1$ and get,

$$t_a^{p(1,1)} = \left(-B_{ap} - \sum_{bq} \tilde{V}_{pb,aq} t_b^{q(0,1)} \right) \Big/ \left(\epsilon_p - \epsilon_a \right) \tag{3.82}$$

Substituting for $t_b^{q(0,1)}$, we get,

$$t_a^{p(1,1)} = \frac{\left\langle p \middle| -h_{EDM} \middle| a \right\rangle}{\left(\epsilon_p - \epsilon_a \right)} - \sum_{bq} \left(\left\langle pb \middle| V \middle| aq \right\rangle - \left\langle pb \middle| V \middle| qa \right\rangle \right) \frac{\left\langle q \middle| -h_{EDM} \middle| b \right\rangle}{\left(\epsilon_q - \epsilon_b \right) \left(\epsilon_p - \epsilon_a \right)} \tag{3.83}$$

The second term of the above equation is exactly equivalent to the equation for the CPHF mixing coefficient, Eq.3.73. The diagrammatic representation of the terms in Eq.3.73 are shown in Fig.3.21 (d-e). This establishes the equivalence of *normal* CPHF diagrams and the corresponding diagrams arising in the coupled-cluster theory. A detailed comparison of the mixing coefficients of CPHF and the cluster amplitudes from coupled-cluster theory is performed and is demonstrated numerically for atomic mercury results are summarized in Chapter.6. Now consider the contribution of the atomic EDM in terms of the CPHF mixing coefficients,

$$EDM = \sum_{ap} \left\langle \psi_a^0 \middle| D \middle| \psi_p^0 \right\rangle C_{pa}^{(\infty,1)} + C_{pa}{}^{*(\infty,1)} \left\langle \psi_p^0 \middle| D \middle| \psi_a^0 \right\rangle$$

The zeroth order contribution to EDM is,

$$EDM = 2 \sum_{ap} \frac{\left\langle \psi_a^0 \middle| D \middle| \psi_p^0 \right\rangle \left\langle \psi_p^0 \middle| H_{\rm EDM} \middle| \psi_a^0 \right\rangle}{\left(\epsilon_a^0 - \epsilon_p^0 \right)}$$

since $C_{pa}^* = C_{pa}$. The diagrams contributing to atomic EDM in CPHF theory are shown in Fig.3.22. The atomic EDM in terms of the cluster operators is

$$EDM = \left\langle \Phi_0 \middle| T^{(1)^\dagger} \overline{D} + \overline{D} T^{(1)} \middle| \Phi_0 \right\rangle \tag{3.84}$$

where $\overline{D} = e^{T^{(0)^\dagger}} D e^{T^{(0)}}$. The same diagrams in coupled-cluster theory (Fig.3.23(III)) arise from the term $D\left(T_1^{(1)}\right)_{eff}$ at the level of the final EDM matrix element. The effective operator $\left(T_1^{(1)}\right)_{eff}$ results from the contraction of singles cluster amplitude operator $(T_1{}^{(1)^\dagger})$ and the residual Coulomb interaction.

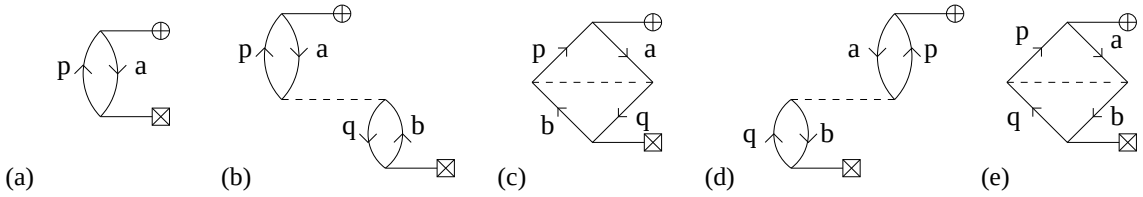

Figure 3.22: CPHF diagrams contributing to EDM

As shown in Fig.3.23, the CPHF diagrams of the kind shown in 3.22 (b,c) are obtained by summing the two MBPT diagrams Fig.3.23(I(a,b) & II(a,b)). These diagrams seem to be arising from the terms $\left(D(T_1^{(1)})_{\rm eff} + T_1^{(1)^\dagger} D T_2^{(0)}\right)$ where $(T_1^{(1)})_{\rm eff}$ is the effective diagram arising from the contraction of the cluster amplitude $T_1^{(1)^\dagger}$ and the residual coulomb interaction. The diagrams listed under (III) are directly present in the coupled-cluster theory, but (I) and (II) can be shown to be present only indirectly.

As shown in Fig.3.23, the CPHF diagrams at one order residual Coulomb interaction can arise by summing two coupled-cluster diagrams corresponding to the terms $\left(D(T_1^{(1)})_{\rm eff} + T_1^{(1)^\dagger} D T_2^{(0)}\right)$ where $(T_1^{(1)})_{\rm eff}$ is the effective diagram arising from the contraction of the cluster amplitude $T_1^{(1)^\dagger}$ and the residual coulomb interaction. The diagrams listed under (III) are directly present in the coupled-cluster theory. The CPHF

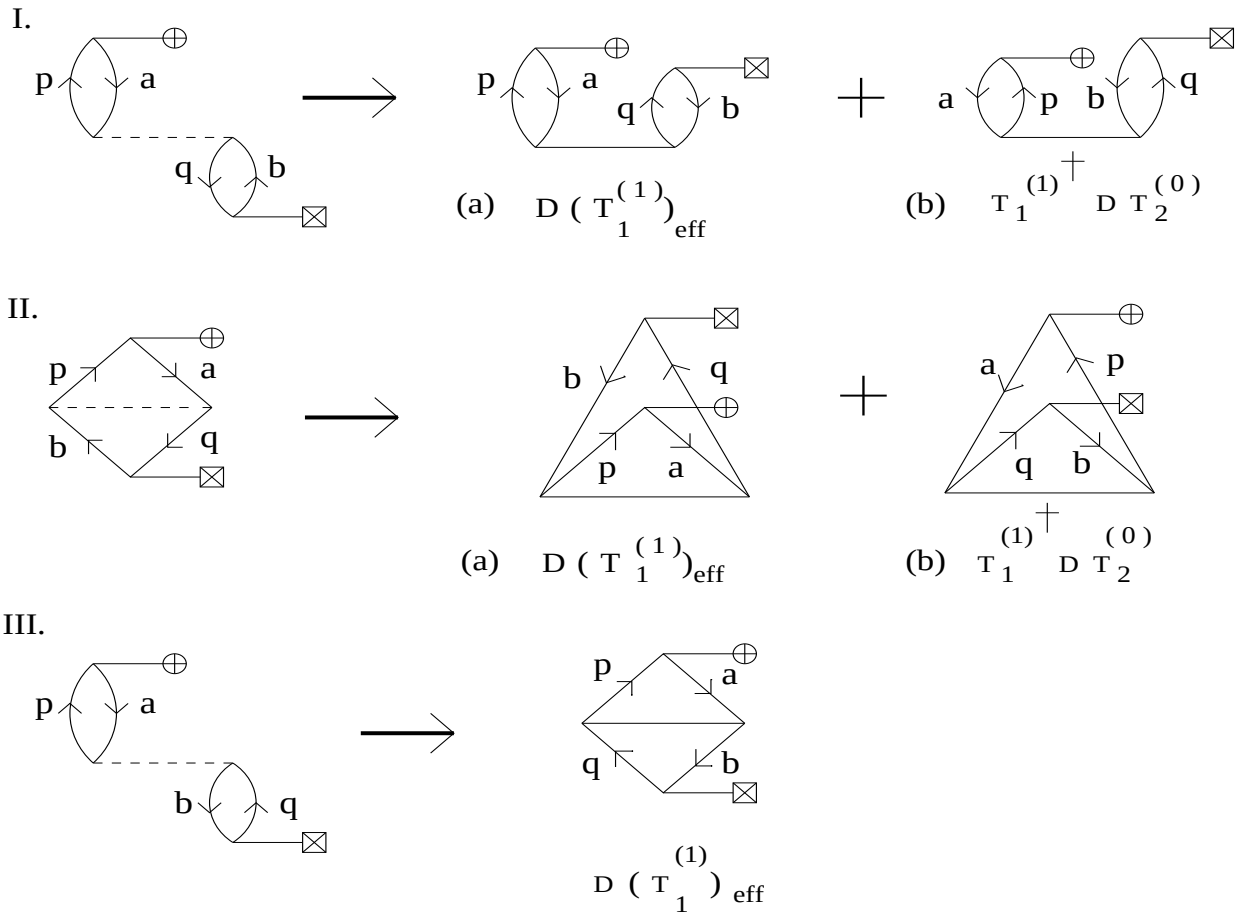

Figure 3.23: Diagrams contributing to EDM - Solid interaction lines in I(a)&(b), II(a)&(b) and III(a)&(b) represent the Coulomb interaction treated to all orders. The operator $T_{1\,\text{eff}}^{(1)}$ is a result of the contraction $T_2^{(0)}T_1^{(1)\dagger}$, which, when contracted with the induced dipole operator (D), gives the diagram contributing to D_a. Here, the diagrams (I) and (II) are the pseudo diagrams of CPHF. We try to pick out the corresponding terms in coupled- cluster theory.

coefficients computed during the first iteration of the CPHF equation contain one order residual Coulomb iteraction. The EDM computed using these coefficients can be compared with the coupled-cluster terms as indicated above.

3.4 Comparison of Coupled-cluster theory with Configuration Interaction

Before we move on the the calculation of atomic EDMs using CCT, we make a theoretical comparison between the Coupled-cluster, the Configuration Interaction (CI) and the Many-body perturbation methods. The exact atomic wave function in coupled-cluster theory is expressed as

$$|\Psi_{CC}\rangle = \Omega|\Phi_0\rangle = e^T|\Phi_0\rangle$$

where Ω is the wave operator, $|\Phi_0\rangle$ is the reference state and T is the hole-particle excitation operator and $|\Psi_{CC}\rangle$ is the exact atomic state. In the present discussion let $T = T_1 = \sum_{a,p} a_p^\dagger a_a t_a^p$. This gives

$$|\Psi_{CC}\rangle = \left[1 + T_1 + \frac{T_1^2}{2!} + ...\right]|\Phi_0\rangle \tag{3.85}$$

and

$$T_1|\Phi_0\rangle = \sum_{a,p} a_p^\dagger a_a|\Phi_0\rangle.t_a^p = \sum_{a,p}|\Phi_a^p\rangle t_a^p$$

t_a^p is the probability amplitude for the excitation from 'a' to 'p'. Consider the CI wavefunction,

$$|\Psi_{CI}\rangle = C_0|\Phi_0\rangle + \sum_s C_s|\Phi_s\rangle + C_d\sum_d|\Phi_d\rangle + ... \tag{3.86}$$

where $|\Phi_0\rangle$, $|\Phi_s\rangle$ (set of all single excitations), $|\Phi_d\rangle$ (set of all double excitations)... form a complete set of basis vectors in Hilbert space. Comparing Eq.3.85 and Eq.3.86,

$$T_1|\Phi_0\rangle = \sum_{a,p}|\Phi_a^p\rangle t_a^p = \sum_s C_s|\Phi_s\rangle$$

Hence, T_1 is equivalent to the set of all the single excitations as given by the CI wavefunction. From Eq.3.85 and Eq.3.86 it can also be noted that for double excitations, it is necessary to include them explicitly in the CI wavefunction, but the CC wavefunction can give the same through T_1^2 term at a lower level of truncation of the exponential. The $|\Phi_s\rangle$ of the CI is identical to $|\Phi_a^p\rangle$ of CCT. Now consider the wavefunction as described

in the many-body perturbation theory in terms of the unperturbed state,

$$|\Psi\rangle = |\Phi_0\rangle + |\Phi_0^1\rangle + |\Phi_0^2\rangle + ... \tag{3.87}$$

where $|\Phi_0\rangle$ is the unperturbed wavefunction and others are the higher order corrections to $|\Phi_0\rangle$. We have,

$$|\Phi_0^1\rangle = \sum_{I\neq 0} |\Phi_I\rangle \frac{\langle\Phi_I|H'|\Phi_0\rangle}{E_0 - E_I}$$

$|\Phi_0^1\rangle$ can be expanded in terms of the complete set,

$$|\Phi_0^1\rangle = \sum_s C_s^1 |\Phi_s\rangle + \sum_d C_d^1 |\Phi_d\rangle + ...$$

Similarly,

$$|\Phi_0^2\rangle = \sum_s C_s^2 |\Phi_s\rangle + \sum_d C_d^2 |\Phi_d\rangle + ...$$

where for $|\Phi_0^1\rangle$, 'I' stands for all the single excited intermediate states. The exact wavefunction $|\Psi\rangle$ can now be written as

$$|\Psi\rangle = |\Phi_0\rangle + \sum_s \left[C_s^1 + C_s^2 + ...\right] |\Phi_s\rangle + \sum_d \left[C_d^1 + C_d^2 + ...\right] |\Phi_d\rangle + ... \tag{3.88}$$

$|\Phi_0^1\rangle$ has one order residual coulomb interaction(perturbation), $|\Phi_0^2\rangle$ has two orders, and so on. This implies that there are infinite no. of residual coulomb interactions giving rise to a single excitation, infinite Couplomb interactions giving rise to double excitations and so on, where C_s^1, C_s^2 etc represent 1 order in Coulomb with 1 intermediate state(I), 2 orders in Coulomb with 2 intermediate states (I,J) respectively. Comparing Eq.3.85 and Eq.3.88, we get

$$T_1|\Phi_0\rangle = \sum_s \left[C_s^1 + C_s^2 + ...\right] |\Phi_s\rangle \tag{3.89}$$

which indicates that T_1 contains infinite orders of Coulomb interaction corresponding to all possible single excitations. The above T_1 refers to the unperturbed cluster operator $T_1^{(0)}$. The H_{EDM} perturbed operator $T_1^{(1)}$ contains, in addition to infinite orders in Coulomb perturbation, one order in H_{EDM}. The above equations also demostrate that

under a given approximation of singles and doubles, the summation over the corresponding mixing coefficients is equivalent to treating the perturbation to all orders. Hence, an all order calculation of the cluster amplitudes t_a^p and t_{ab}^{pq} is equivalent to calculation of the mixing coefficients to all orders using many-body perturbation theory.

3.5 Size consistency and Size extensivity

Size consistency : A method is 'size consistent' if the corresponding energy of two well-separated (in the limit of infinite separation) subsystems A and B is equal to $(E_A + E_B)$, the sum of the energies of the two systems computed independently.

Consder a CI wavefunction $|\Psi_{CI}\rangle$, which is expanded in terms of a linear excitation operator, unlike the CC wavefunction,

$$|\Psi_{CI}\rangle = (1 + C)\,|\Phi_0\rangle$$

where C is a linear combination of various excitation operators,

$$C = C_s + C_d + C_t + \cdots$$

which can be represented in a second quantized form as,

$$C = \sum_{i,a} c_i^a\; a_a^\dagger\, a_i \;+\; \frac{1}{4}\sum_{ij,ab} c_{ij}^{ab}\; a_a^\dagger a_b^\dagger a_i a_j + ... \tag{3.90}$$

Truncation of the operator C to singles and double excitations (CISD) leads to a wavefunction with exactly same number of amplitudes c_i^a and c_{ij}^{ab}, as that needed for the CCSD, t_i^a and t_{ij}^{ab}. However, the CCSD theory implicitly includes the higher excitations like triples, quadruples, through the inclusion of higher powers of T which arise inherently due to the CC exponential ansatz. Both the full CI and full CC produce exact wavefunctions. Consider the structure of the CC and CI wavefunctions for a system involving two non-interacting and infinitely separated components, A and B. It is possible to disssociate the cluster operators for the two components, assuming that the orbitals

used to define T and C are localized on each of the two components,

$$T = T_A + T_B \text{ and } C = C_A + C_B$$

Hence,

$$|\Psi_{CC}\rangle = e^T |\Phi_0\rangle = e^{T_A} e^{T_B} |\Phi_0\rangle$$

Under the localized orbital description, the reference determinant $|\Phi_0\rangle$ is factorizable into independent determinants of each fragment, the total CC wavefunction can be written as a product of CC wavefunctions of each fragment. The resulting energies would then be a sum of energies of each of the fragments and is would be the same as that computed for the system as a whole. In other words,

$$E_{CC} = E^A_{CC} + E^B_{CC}$$

This property is known as size extensivity. Since for CI, multiplicative separability is not possible,

$$|\Psi_{CI}\rangle = (1 + C) |\Phi_0\rangle = (1 + C_A + C_B) |\Phi_0\rangle$$

the sum of the energies of the separate fragments is not equal to the energy of the system computed as a whole,

$$E_{CI} \neq E^A_{CI} + E^B_{CI}$$

If CI is non-trucated, then it is possible to write the full CI wavefunction as a product of wavefunctions for separate fragments by transforming the linear operator into an exponential. For a Hydrogen molecule, there are only two electrons to be correlated and hence CCSD and CISD are exact for this system. But the CCSD gives correct total energy and CISD doesn't due to the inseparability of the CI wavefunction.

Size extensivity : A method is said to be 'size extensive', if the energy calculated thereby scales linearly with the number of particles. The SCF and the CC methods are both 'size extensive'. Size consistency applies only to non-interacting molecular fragments, but size extensivity is a more general mathematical concept that applies to any point on the potential energy surface. We now show that exponential ansatz guarantees size extensivity, whereas truncated CI does not.

Consider the structure of the CI Shroedinger equation,

$$H_N\Big(1 + C_1 + C_2 + ...\Big)\Big|\Phi_0\Big\rangle = \Big(E_{CI} - E_0\Big)\Big(1 + C_1 + C_2 + ...\Big)\Big|\Phi_0\Big\rangle$$

where H_N is the normal ordered Hamiltonian and intermediate normalization[4] is assumed. Projecting by reference state from the left,

$$(E_{CI} - E_0) = \langle\Phi_0|H_N\left(C_1 + C_2\right)|\Phi_0\rangle$$

where CI expansion is truncated using Slater rules. By the application of Wick's theorem, this equation can be written in the algebraic form as,

$$(E_{CI} - E_0) = \sum_{i,a} f_{ia}c_i^a + \frac{1}{4}\sum_{ij,ab}\langle ij|v|ab\rangle c_{ij}^{ab}$$

For HF choice of the single particle orbitals, the first term is zero due to Brillouin's theorem. Assuming a localized orbital basis, for a given orbital $|\phi_i\rangle$, the two-electron integral will be zero, unless the orbitals $|\phi_j\rangle$,$|\phi_a\rangle$ and $|\phi_b\rangle$ are reasonably close to $|\phi_i\rangle$ due to the relatively short range nature of the inter-electronic potential.

Full CI is a size extensive and size consistent theory, but most truncated CI methods are neither.

[4] $\langle < \Phi_0|\Psi\rangle >= 1$, where $|\Psi\rangle >$ is the exact state.

Chapter 4

Implementation of CCEDM

In this chapter some of important issues in the implementation of the CCEDM program are discussed. The program is written in FORTRAN-77. Refer to Appendix C for the basic program skeleton. The number of diagrams contributing to CCEDM Eq.3.28 are $n_{\text{total}} = 154$ with $n_{\text{sing}} = 42$ and $n_{dbl} = 102$ where n_{sing} and n_{dbl} are the number of diagrams contributing through the singles and the doubles CCEDM equations respectively and 10 diagrams arise from the RHS from singles and doubles. The program is composed of 54 subroutines. Deatils of diagrams, the angular factors, description of the program etc. can be obtained from [27].

4.1 Conventions and Symbols

The matrix elements present in the coupled cluster equations are calculated by separating them into the radial and the angular parts. The angular part is manually calculated by representing each diagram by a corresponding angular momentum diagram. The closed part of an angular momentum diagram is evaluated using the JLV theorems [28]. The radial integrals are programmed and calculated with the existing integration subroutines. The convention used for the angular factor calculation is shown in Fig.4.1. In addition to these rules, the arrow on the incoming free hole line is removed and the sign at the vertex formed by the three multipoles of the $T_2^{(1)}$ operator, (see Fig. 3.9) (λ_1, λ_2, K_2) is given a '+' sign by our convention. For the complete details of the angular factor calculations, see [27].

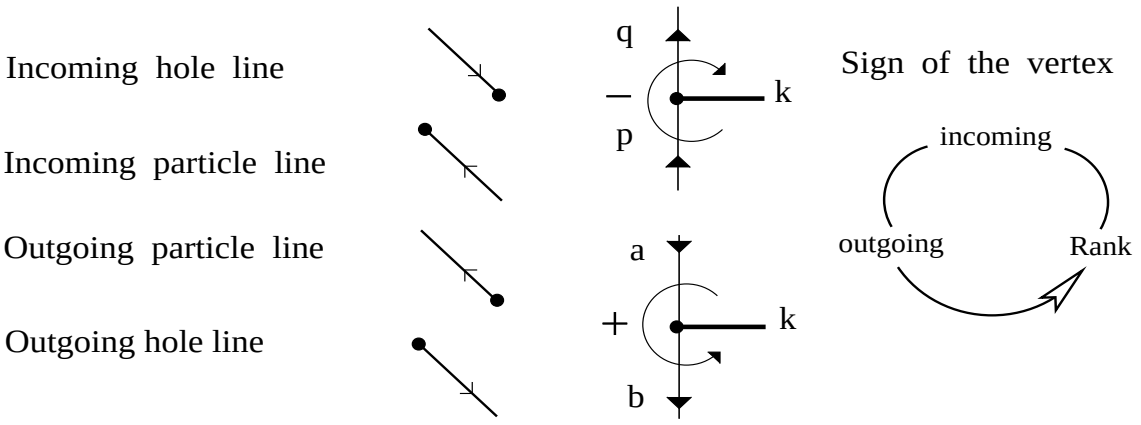

Figure 4.1: Notation for orbital lines

4.2 Implementation of the iterative scheme

The CCEDM equations are,

$$\begin{aligned}
\left\langle \Phi_a^r \middle| \left\{ \overline{H_N T^{(1)}} \right\} \middle| \Phi_0 \right\rangle &= -\left\langle \Phi_a^r \middle| \overline{H}_{EDM} \middle| \Phi_0 \right\rangle \\
\left\langle \Phi_{ab}^{rs} \middle| \left\{ \overline{H_N T^{(1)}} \right\} \middle| \Phi_0 \right\rangle &= -\left\langle \Phi_{ab}^{rs} \middle| \overline{H}_{EDM} \middle| \Phi_0 \right\rangle
\end{aligned} \tag{4.1}$$

Introducing a complete set of orbitals and expanding $T^{(1)} = T_1^{(1)} + T_2^{(1)}$,

$$\begin{aligned}
\sum_I \left\langle \Phi_a^r \middle| \overline{H}_N \middle| \Phi_I \right\rangle \left\langle \Phi_I \middle| T_1^{(1)} \middle| \Phi_0 \right\rangle + \sum_J \left\langle \Phi_a^r \middle| \overline{H}_N \middle| \Phi_J \right\rangle \left\langle \Phi_J \middle| T_2^{(1)} \middle| \Phi_0 \right\rangle &= -\left\langle \Phi_a^r \middle| \overline{H}_{EDM} \middle| \Phi_0 \right\rangle \\
\sum_I \left\langle \Phi_{ab}^{rs} \middle| \overline{H}_N \middle| \Phi_I \right\rangle \left\langle \Phi_I \middle| T_1^{(1)} \middle| \Phi_0 \right\rangle + \sum_J \left\langle \Phi_{ab}^{rs} \middle| \overline{H}_N \middle| \Phi_J \right\rangle \left\langle \Phi_J \middle| T_2^{(1)} \middle| \Phi_0 \right\rangle &= -\left\langle \Phi_{ab}^{rs} \middle| \overline{H}_{EDM} \middle| \Phi_0 \right\rangle
\end{aligned}$$

which can be written in the form of a set of matrix linear equations,

$$\overline{A}_1 T_1^{(1)} + \overline{A}_2 T_2^{(1)} = \overline{B}_1 \tag{4.2}$$

$$\overline{A}_3 T_1^{(1)} + \overline{A}_4 T_2^{(1)} = \overline{B}_2 \tag{4.3}$$

where $\overline{A}_i$ are identified as the dressed Coulomb Hamiltonian which is a rectangular matrix and $\overline{B}_i$, the dressed EDM Hamiltonian operator, and the cluster amplitude matrix $T_1^{(1)}$ is a column vector. The first Eqn.4.2 is solved for $T_1^{(1)}$, with an initial guess for $T_2^{(1)}$, and is used in 4.3 to obtain a new set of $T_2^{(1)}$. The $T_2^{(1)}$ amplitudes are then used in Eqn.4.2

to obtain a new set of $T_1^{(1)}$ amplitudes. This procedure is repeated until convergence is achieved for both $T_1^{(1)}$ and $T_2^{(1)}$ amplitudes. In other words, we have,

$$T_1^{(1,k)} = \frac{\left(B_1 - A_2 T_2^{(1,k-1)}\right)}{A_1}$$
$$T_2^{(1,k)} = \frac{\left(B_2 - A_3 T_2^{(1,k)}\right)}{A_4}$$

where $k = 1, 2, 3, ...$ is the iteration count.

Usage of fresh iterates each time could help speed up the convergence of CCEDM equations.

4.3 Complementary and Equivalent diagrams

Complementary diagrams arise due to the contraction of an asymmetric operator eg., $T_2^{(1)}$ and a symmetric operator eg., V_N, $T_2^{(0)}$. The asymmetricity of $T_2^{(1)}$ arises due to the opposite vertex parity at it's two vertices which gives rise to two distinct diagrams from one contraction with any symmetrix operator. While it is necessary to calculate the contributions from complementary diagrams, it is important to avoid repetition of such diagrams which are generated whenever the complementary diagrams are topologically equivalent to normal diagrams. One example of the diagram for which the actual and it's complementary are not the same is shown in Fig.B.2 (CD4). The cluster amplitudes diagrams are calculated in the subroutines, named after the form of the two-body Coulomb operator they arise from and called in the *driver* routine. The complementary diagrams are calculated by calling the routines of the cluster amplitudes twice, where the first and the second call to the routine differs in the arguments of the routine. The arguments, which are the actual orbital indices, corresponding to the open lines are flipped leaving the internal orbital indices (which hence are summed) fixed. As an example consider the diagrams CD4 of Fig.B.2. The 'normal' and the 'complementary' calls are :

```
call dpphh(ia, ip, ib, iq, ir, ic, l1, l2, .....)  (Normal)
```

```
call dpphh(ib, iq, ia, ip, ir, ic, l2, l1, .....)  (Complementary)
```

It is important to note that the parity of the vertices (a, p, λ_1) is *fixed* to be odd and that of (b, q, λ_2) to be even. The calculation of complementary diagrams this way can give rise to equivalent diagrams when the *normal* and the *complementary* diagrams are not distinct. Equivalent diagrams in unperturbed and perturbed coupled-cluster diagrams originate due to the presence of diagrams of symmetric topology, which results in the repeated calculation of same cluster diagrams. In this thesis, we discuss only the equivalent diagrams arising from CCEDM implementation. These diagrams particularly arise from the contraction of the diagrams of the kind where the Coulomb operator and a cluster amplitude operator are involved ($V_N T_2^{(1)}$). The cluster diagrams arising from the contraction of the four-particle, (two-particle, two-hole) and four-hole forms of the Coulomb operator and the clusterm amplitude $T_2^{(1)}$, generate equivalent diagrams. In the next few sections, we explain in detail, the diagrams that contribute to the double counting of cluster amplitudes in LCCEDM and the numerical factors associated with them to account for it. For the $T_2^{(1)}$ diagrams, the outermost loops correspond to the orbital indices $(a, p, b, q, \lambda_1, \lambda_2)$. Due to the parity condition at the two vertices of the $T_2^{(1)}$ diagram, the simultaneous flip of (a, b) and (p, q) is not allowed during the loop execution. But, the flip of (a, b) or (p, q) is possible. In the following sections, we consider these issues separately for the cluster diagrams arising from the (four-particle), (four-hole), (two-particle, two-hole), (three-particle, one-hole) form of the Coulomb operator and deduce the factors associated with them. For the cluster diagrams arising from the (four-particle) and (four-hole) form of the Coulomb operator, calculation of the equivalent diagrams means the calculation of the diagram obtained by the mirror reflection of the original diagram.

4.3.1 Four particle form of Coulomb operator

Consider the diagram shown in Fig.4.2. The *normal* and the *complementary* diagrams are equivalent for the cluster diagram with the bare Coulomb operator, but not for the diagram with the dressed Coulomb operator, which contributes through LCCEDM.

Therefore, the complementary diagrams need to be calculated with a factor (1/2) for the diagram Fig.4.2 (I).

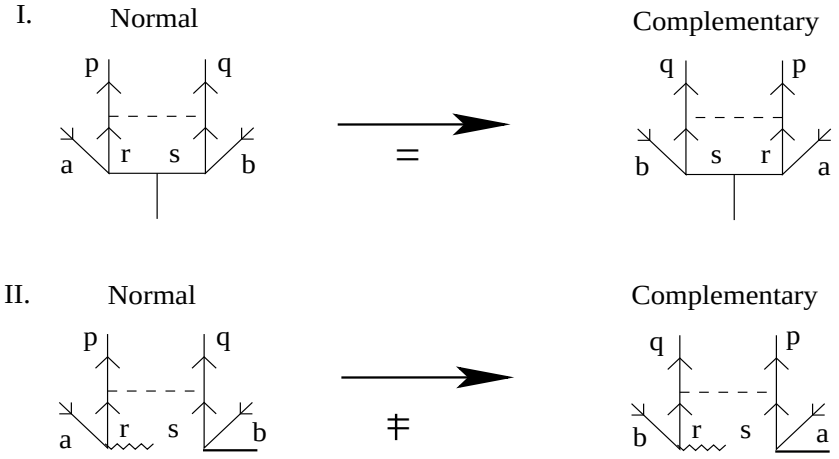

Figure 4.2: Equivalent diagrams - Diagram (I) shows the contraction between the bare-Coulomb and $T_2^{(1)}$ operators and Diagram (II), the dressed Coulomb ($H_N T_1^{(0)}$) and $T_1^{(1)}$ operator.

Exactly the same arguments given above are valid for the cluster diagrams arising from the (four-hole) form of the Coulomb operator. Hence, these diagrams are calculated along with the complementary diagrams, including a numerical factor (1/2) for the cluster diagram arising from the bare Coulomb operator and no factor associated with the cluster diagrams arising from the dressed Coulomb operator.

4.3.2 Two-particle, two-hole form of Coulomb operator

The cluster diagrams arising from the (two-particle, two-hole) form of the Coulomb operator contributing to LCCEDM is shown in Fig.4.3. Note that there are no equivalent diagrams as the normal and complementary diagrams are distinct.

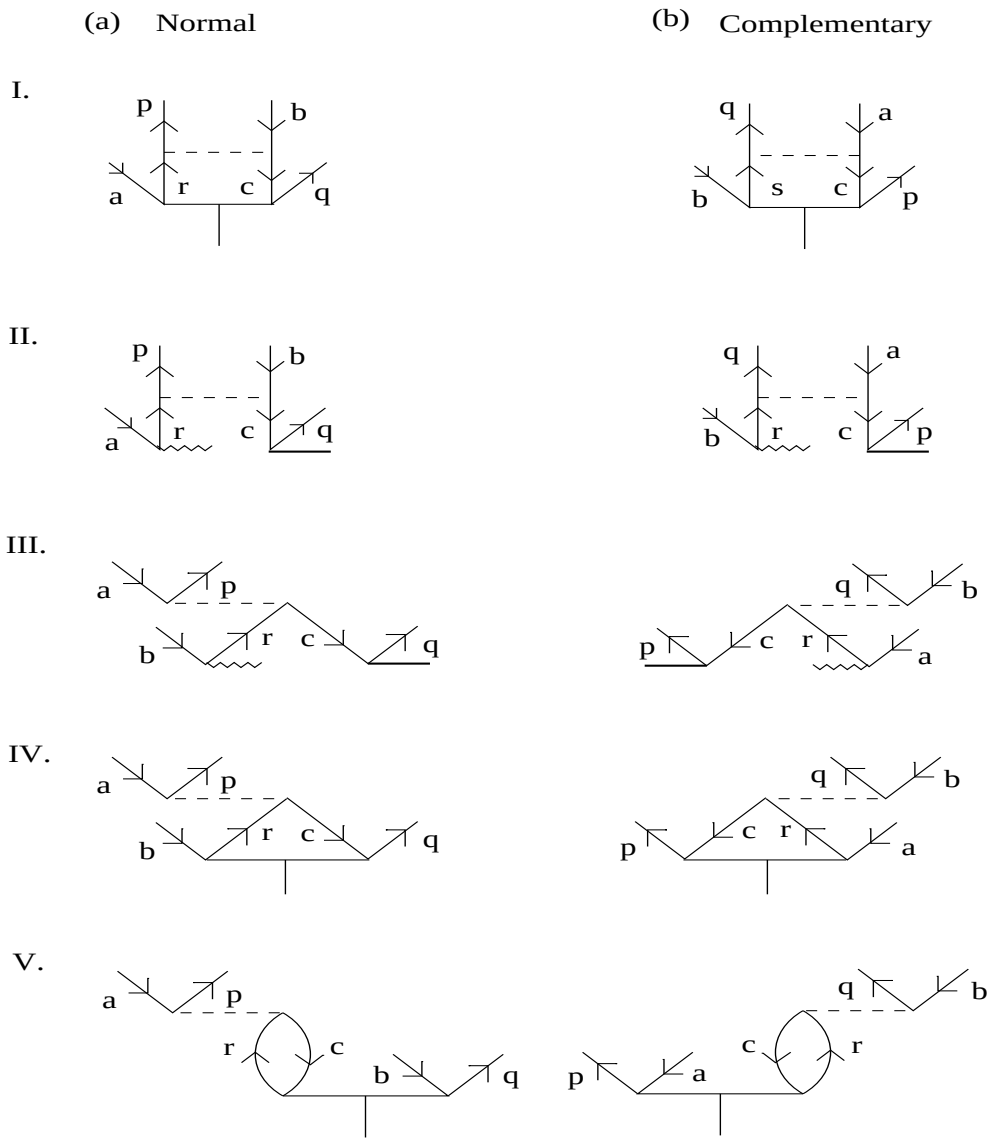

Figure 4.3: The *normal* and *complementary* diagrams are all distinct and hence there are no numerical factor associated with these diagrams.

4.3.3 Three-particle (three-hole) - one-hole (one-particle) form of the Coulomb operator

The cluster diagrams arising from the (three-particle, one-hole) and (one-particle, three-hole) form of the Coulomb operator are shown in Fig.4.4. The *complementary* diagrams

are distinct from the *normal* diagrams and hence there is no numerical factor associated with the diagrams.

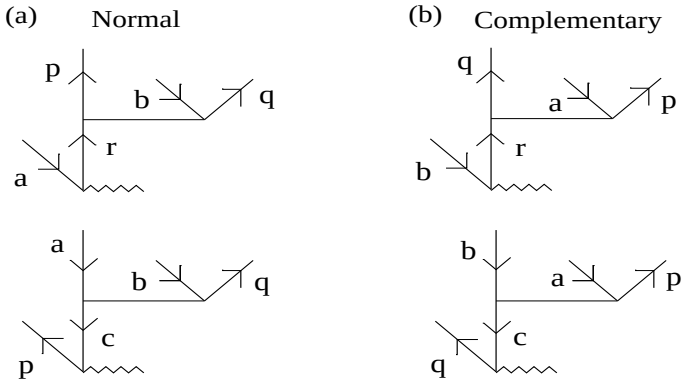

Figure 4.4: The *normal* and *complementary* diagrams are all distinct and hence there are no numerical factor associated with these diagrams.

4.4 Intermediate Storage Scheme

Consider a diagram contributing to CCEDM equations shown in Fig.$C.8(a)$. This diagram contains four particle and four holelines. To calculate this diagram, the total number of operations required is $= n_h^4 \times n_p^4$. For a reasonable basis, with number of occupied (holes) and unoccupied (particles) orbitals given by $n_h = 22$ and $n_p = 40$, the number of operations would be $\approx 6 \times 10^{11}$. Such diagrams demand a large amount of computational time. Using the Intermediate Storage scheme, it is possible to reduce the number of computations, **by calculating a portion of such diagrams which are common to a set of actual amplitude diagrams**. The diagram in Fig.$C.8(a)$ is termed as an 'EDM-IMS' diagram, where the the operators formed by the portion, $\overline{V_N T_2^{(1)}}$ and $\overline{V_N T_1^{(1)} T_1^{(0)}}$ are calculated and stored to give an EDM-IMS diagram as shown in Fig.$C.8(b)$. The number of operations now become $= n_h^2 \times n_p^3 + n_h^2 \times n_p^3 = 2n_h^2 \times n_p^3 = 6 \times 10^7$ which is reduced by a factor $(1/2)n_h^2 n_p = 10^4$. The CCEDM diagrams arising from the (2-particle, 2-hole) form of the Coulomb operator have been classified into EDM-IMS and Coulomb-IMS diagrams based on the topology of the diagram and the number of orbital lines con-

nected to $T_2^{(0)}$ and $T_2^{(1)}$ respectively. The IMS diagrams are calculated only once and are used for further calculation of the complete cluster amplitude diagrams arising from the particular kind of IMS diagrams. At present, this scheme has been implemented only for the (2-particle, 2-hole), but in general can be used for the diagrams involving orbital lines as large as 6 - 8 because such diagrams consume a large amount of CPU time due to the execution of loops corresponding to the orbital lines. The Fig.4.5 shows the cluster diagrams calculated using EDM IMS diagrams. The diagrams contributing to EDM-IMS diagrams are shown in Fig.4.6, 4.7 and those contributing to the Coulomb IMS are shown in Figs.4.8. These diagrams are of (hole - hole) or (particle - particle) form. The actual cluster amplitudes are then obtained by the contraction of the effective IMS diagrams with the corresponding cluster operator diagrams - the $T_2^{(1)}$ diagram for Coulomb IMS and $T_2^{(0)}$ for EDM IMS diagrams. The possible cluster diagrams in terms of the IMS diagrams are shown in Fig.4.9. For details on the cluster diagrams calculated using Coulomb IMS diagrams, refer to the documentation [27]. The pseudo code can be found in Appendix C.

From the topology of the EDM IMS diagrams it is interesting to note that the rotation of the free lines of the Coulomb vertices generates a diagram which is topologically identical to the cluster diagrams arising from the singles CCEDM equations. This is a very useful observation which enabled us to use our program where the singles cluster amplitude diagrams are calculated (in particular, the cluster diagrams arising from the (3 particle - 1 hole) and (3 hole- 1 particle) form of Coulomb diagrams).

The EDM IMS diagrams are only a one-body kind, whereas the Coulomb IMS diagrams are both One- and two - body kind. The two-body Coulomb IMS diagrams are shown in Fig.4.10. The angular factors of the IMS diagrams can be obtained from [27].

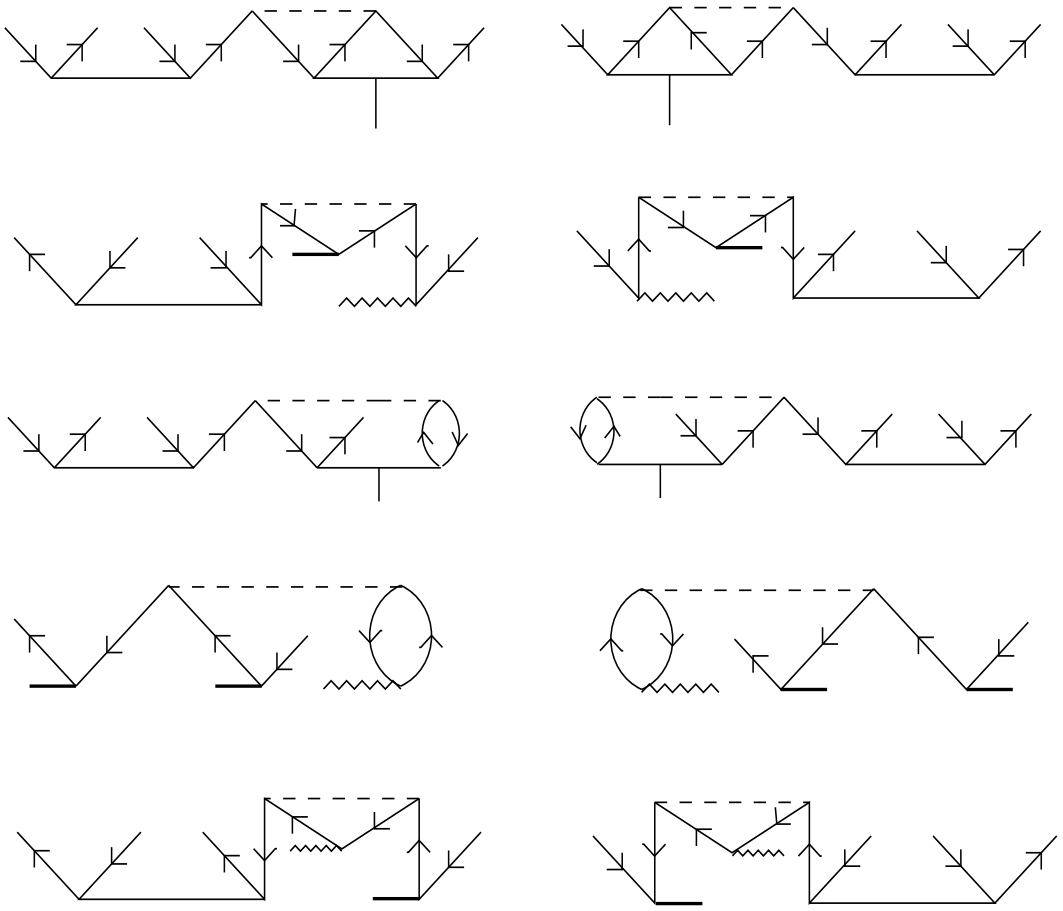

Figure 4.5: EDM IMS diagrams - They arise from the terms $\widehat{V_N T_2^{(1)}}$ and $\widehat{V_N T_1^{(0)} T_1^{(1)}}$.

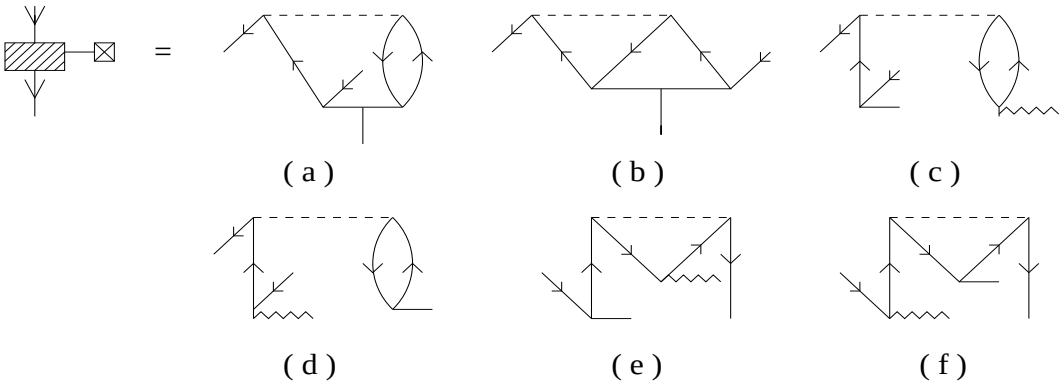

Figure 4.6: H_{EDM} perturbed hole-hole one-body IMS diagrams.

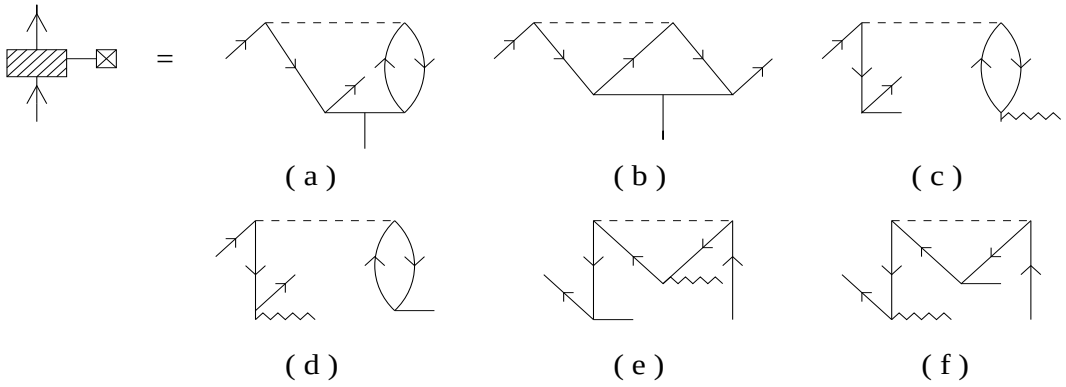

Figure 4.7: $H_{\rm EDM}$ perturbed particle-particle one-body IMS diagrams.

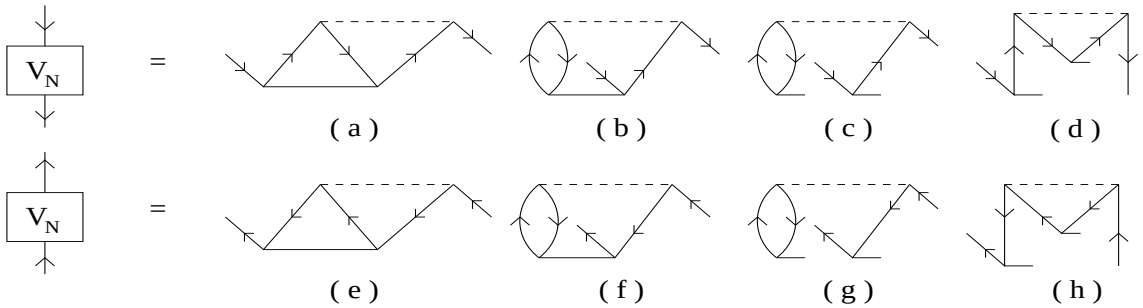

Figure 4.8: One-body V_N effective diagrams

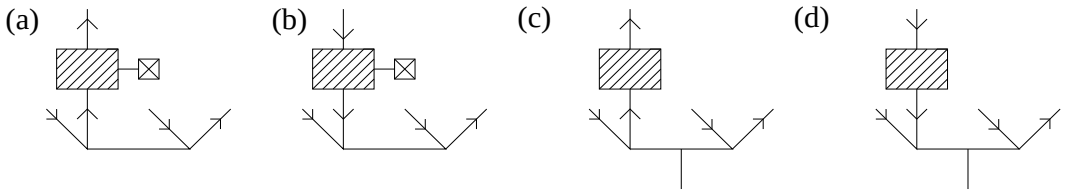

Figure 4.9: (a)& (b) - Cluster diagrams arising from hole-hole and particle-particle $H_{\rm EDM}$ perturbed IMS diagrams, (c)& (d) - cluster diagrams arising from hole-hole and particle-particle Coulomb IMS diagrams.

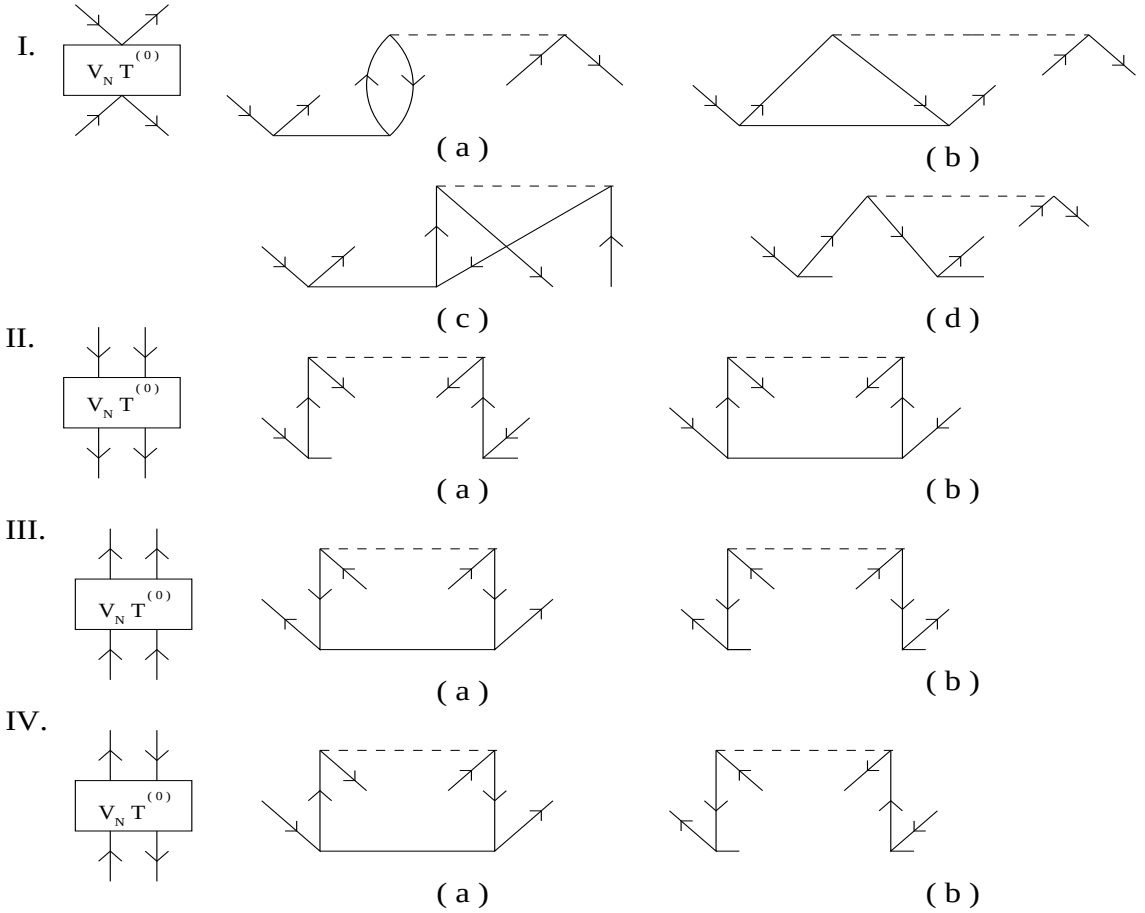

Figure 4.10: Two-body V_N effective diagrams - ph-hp(I), hh-hh(II), pp-pp(III), ph-ph(IV)

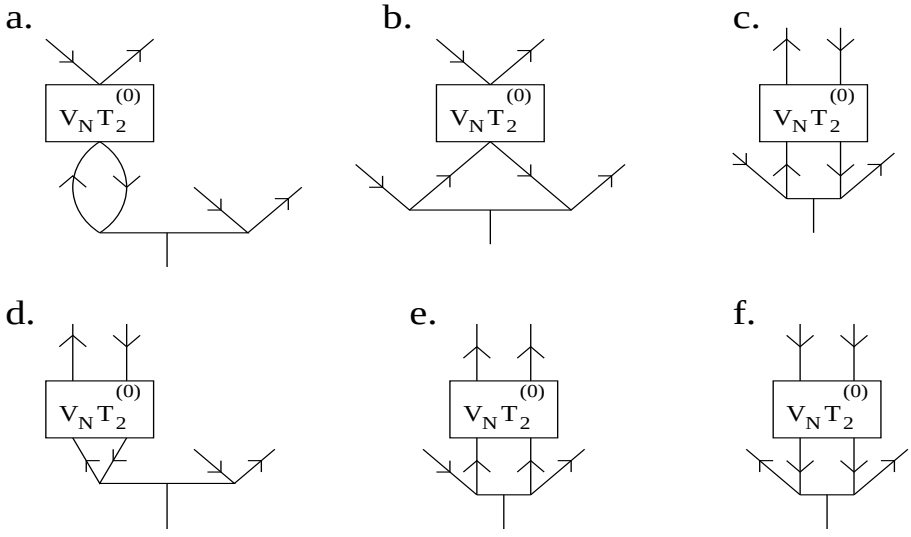

Figure 4.11: Cluster diagrams arising from the two-body Coulomb IMS diagrams - contraction of IMS diagrams with $T_2^{(1)}$.

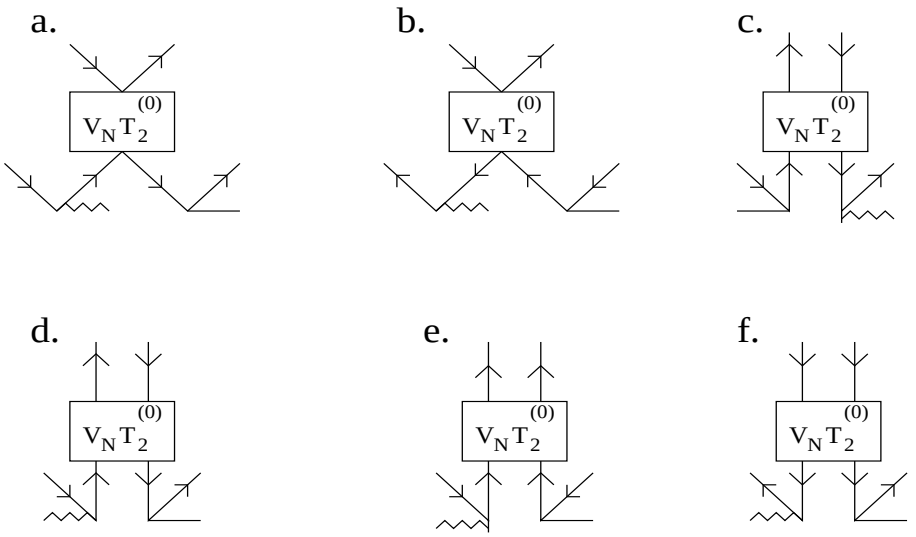

Figure 4.12: Cluster diagrams arising from the two-body Coulomb IMS diagrams - contraction of IMS diagrams with $T_1^{(0)} T_1^{(1)}$.

4.5 Calculation of Atomic EDM

Chapter 5

Application of CC theory to polarizability

5.1 Static polarizability

The concept of polarizability arises from the effects of electric field on matter. In the presence of an external electric field, a nuetral atom gets polarized, where the positive and negative charge clouds shift from their original positions and reach an equilibrium. This gives rise to an induced dipole moment on the atom $\mathbf{D}_{\text{ind}}$ which points in the same direction as $\mathbf{E}$ and proportional to it : $\mathbf{D}_{\text{ind}} = \alpha\mathbf{E}$. The constant of proportionality α is called the atomic polarizability. When the external field is time dependent, it is known as the dynamic polarizability. We now derive a quantum mechanical way of identifying the polarizability as arising from treating the induced dipole operator as the perturbation to first order. (derivation of α done later).

Consider the expression for the static atomic polarizability,

$$\alpha = 2\sum_I \frac{\left\langle \Psi_a^{(0)} \middle| \vec{D}_{\text{ind}} \middle| \Psi_I^{(0)} \right\rangle \left\langle \Psi_I^{(0)} \middle| \vec{D}_{\text{ind}} \middle| \Psi_a^{(0)} \right\rangle}{\left(E_a^{(0)} - E_I^{(0)} \right)} \tag{5.1}$$

Let

$$\left| \Psi_a^{(1)} \right\rangle = \sum_I \left| \Psi_I^{(0)} \right\rangle \frac{\left\langle \Psi_I^{(0)} \middle| \vec{D}_{\text{ind}} \middle| \Psi_a^{(0)} \right\rangle}{\left(E_a^{(0)} - E_I^{(0)} \right)} \tag{5.2}$$

where $|\Psi^{(0)}\rangle$ and $|\Psi^{(1)}\rangle$ are the unperturbed and perturbed atomic wavefunctions respectively. $E^{(0)}$ are the unperturbed energy eigen values. The unperturbed atomic

Hamiltonian H_0 satisfies the Schroedinger equation,

$$\left(H_0 - E_a^{(0)}\right)\left|\Psi_a^{(0)}\right\rangle = 0$$

In the presence of the interaction H', we have the perturbed Schroedinger equation,

$$\left(H_0 - E_a^{(0)}\right)\left|\Psi_a^{(1)}\right\rangle = -H'\left|\Psi_a^{(0)}\right\rangle \tag{5.3}$$

Assuming H' to be an odd-parity operator, the first order corrections to the energy do not contribute. Act $\left(H_0 - E_a^{(0)}\right)$ on Eq.5.2,

$$\left(H_0 - E_a^{(0)}\right)\left|\Psi_a^{(1)}\right\rangle = \sum_I \left(H_0 - E_a^{(0)}\right)\left|\Psi_I^{(0)}\right\rangle \frac{\left\langle \Psi_I^{(0)}\left|\vec{D}_{\text{ind}}\right|\Psi_a^{(0)}\right\rangle}{\left(E_a^{(0)} - E_I^{(0)}\right)}$$

$$= \sum_I \left|\Psi_I^{(0)}\right\rangle\left\langle \Psi_I^{(0)}\left|\vec{D}_{\text{ind}}\right|\Psi_a^{(0)}\right\rangle$$

since $|\Psi_I^{(0)}\rangle$ is an eigen function of H_0. Since $\vec{D}_{\text{ind}}$ is an odd parity operator, $|\Psi_I^{(0)}\rangle$ must be opposite in parity to $|\Psi_a^{(0)}\rangle$. Using this we have,

$$\left(H_0 - E_a^{(0)}\right)\left|\Psi_a^{(1)}\right\rangle = -\vec{D}_{\text{ind}}\left|\Psi_a^{(0)}\right\rangle \tag{5.4}$$

Comparing Eq.5.4 and Eq.5.3, we identify $\vec{D}_{\text{ind}}$ as the perturbation H'. The sample calculation of polarizability for atomic ^{199}Hg is shown in Section.6.4.3.

5.2 Polarizability of atomic Xe using linear CCEDM

Chapter 6

Analysis of Hg EDM results

The single particle orbitals for all the calculations in the subsequent sections are generated using the Gaussian basis set expansion for the many-body atomic state, whose large and small components are expanded as [29]

$$\begin{aligned} P_{n\kappa}(r) &= \sum_p C^L_{\kappa p}\, g^L_{\kappa p}(r) \\ Q_{n\kappa}(r) &= \sum_p C^S_{\kappa p}\, g^S_{\kappa p}(r) \end{aligned}$$

where the summation over the index p runs over the number basis functions N, $g^L_{\kappa p}(r)$ and $g^S_{\kappa p}(r)$ correspond to the large and small components, whcih are expanded as linear combinations of Gaussian Type Orbitals (GTOs) as

$$g^L_{\kappa p}(r) = N^L_p r^{n_\kappa} e^{-\alpha_p r^2}$$

where $\alpha_p = \alpha_0\, \beta^{p-1}$, where α_0 and β are input parameters and $n_\kappa = 1$ for s, 2 for p and so on and N^L_p is the normalisation factor for the large component. The large and small components are related by

$$g^S_{\kappa p}(r) = N^S_p \left(\frac{d}{dr} + \frac{\kappa}{r} \right) g^L_{\kappa p}(r)$$

where

$$N^S_p = \sqrt{\frac{\alpha_p}{2n_\kappa - 1} \Big[4\left(\kappa^2 + \kappa + n_\kappa\right) - 1 \Big]}$$

6.1 Results for the CCEDM-CPHF comparison

The details of the basis used are as shown in Table.6.1.

Table 6.1: No. of basis functions used to generate the even tempered Dirac-Fock orbitals and the corresponding value of α_0 and β used. The total number of active orbitals are shown in the brackets of 'Active holes'.

	$s_{1/2}$	$p_{1/2}$	$p_{3/2}$	$d_{3/2}$	$d_{5/2}$	$f_{5/2}$	$f_{7/2}$	$g_{7/2}$	$g_{9/2}$
Number of basis	31	32	32	20	20	20	20	10	10
$\alpha_0(\times 10^{-5})$	725	715	715	700	700	695	695	655	655
β	2.725	2.715	2.715	2.700	2.700	2.695	2.695	2.655	2.655
Active holes	6	6	6	4	4	4	4	3	3
Active particles	6	4	4	3	3	1	1	0	0

The calculated $T^{(1)}$ amplitudes are in excellent agreement with the CPHF mixing coefficients to an accuracy of 99%. The zeroth order contribution is $-0.46 \times 10^{-11} C_T \sigma_N$ which compares with the previous calculation of Martensson as $-0.38 \times 10^{-11} C_T \sigma_N$ a.u [7]. We attribute this difference to the type of orbitals used. We have used a Gaussian basis set expansion for generating single particle orbitals, while Martensson et.al.[7] has used the solutions of the differential equation derived from the CPHF equations as the saingle particle orbitals. The variation of D_{Hg} with *normal* diagrams for the chosen basis, with the inclusion of higher angular momentum virtual states shows the following trend with the inclusion of normal diagrams : The Table.6.2 indicates that the higher angular

S.No.	nsym	EDM ($\times 10^{-22}$ e-m)	
		Normal	(Normal+Pseudo)
1	3	-6.30	-5.48
2	5	-6.31	-5.53
3	7	-6.16	-5.81
4	9	-6.16	-5.81

Table 6.2: Variation of $D_{\rm Hg}$ with the inclusion of higher angular momentum virtual states.

momentum states give a positive contribution. The dominant contribution arises from the $6s_{1/2}$-$p_{1/2}$ and $6s_{1/2}$-$p_{3/2}$ intermediate states, whose matrix elements are tabulated in Table.6.3. Total contribution (*normal* + *pseudo*) from $6s_{1/2}$-np $= -225.030$ converting into atomic units, $D_{\rm Hg}$ is $= -1.413 \times 10^{-11} C_T e a_0 \sigma_N$. This compares with the CPHF

Table 6.3: Dominant contributions to $D_{\rm Hg}$(in units of $2\sqrt{(2)}G_F C_T e a_0$) from *normal* and *pseudo* diagrams for np intermediate states.

Occ.	np	$T_{1_{\rm eff}}^{(1)}$		$\overline{D}$		$T_{1_{\rm eff}}^{(1)} \times \overline{D}$	
		Normal	Pseudo	Normal	Pseudo	Normal	Pseudo
$6s_{1/2}$	$2p_{1/2}$	111.753	95.739	0.872	0.835	−32.485	6.033
$6s_{1/2}$	$3p_{1/2}$	-269.402	-233.805	−1.821	−1.734	−163.518	29.396
$6s_{1/2}$	$4p_{1/2}$	270.725	242.544	1.388	1.311	−125.286	20.034
$6s_{1/2}$	$5p_{1/2}$	-198.267	-189.975	−0.344	−0.319	−22.748	2.629
$6s_{1/2}$	$6p_{1/2}$	-106.923	-108.978	0.068	0.059	2.424	-0.276
$6s_{1/2}$	$2p_{3/2}$	20.542	15.054	0.995	0.904	6.814	-2.442
$6s_{1/2}$	$3p_{3/2}$	-54.653	-39.743	−2.372	−2.109	43.218	-16.581
$6s_{1/2}$	$4p_{3/2}$	-58.035	-41.318	−2.311	−1.876	42.779	-18.803
$6s_{1/2}$	$5p_{3/2}$	30.418	20.049	0.771	0.513	7.816	-5.282
Total						−239.655	14.624

value of Martensson's result $-1.8 \times 10^{-11} C_T e a_0 \sigma_N$. The discrepancy in the zeroth order results of Martensson's and our calculation is also present at the all all-order level and can be attributed to the numerical differences arising primarily from the generation of single particle orbitals. From the present study, it is evident that the contribution from pseudo diagrams though important is 6 % of the normal diagram contribution and opposite in phase. An increase in the number of virtual orbitals, results in deviation from the values listed in Table.6.3. For example, with the basis (1-14)$s_{1/2}$, (2-14)$p_{1/2,3/2}$,(3-12)$d_{3/2,5/2}$, (4-8)$f_{5/2,7/2}$ and (5-9)$g_{7/2,9/2}$, the results are shown in Table.6.4.

S.No.	HF	EDM ($\times 10^{-22}$ e-m)	
		Normal	(Normal+Pseudo)
1	-2.39	-6.31	-6.54

Table 6.4: Variation of the *normal* and *pseudo* diagram contributions with increase in the basis for nsym = 9. Note that pseudo diagram contribution is 3.5 %.

6.2 Calculation of unperturbed cluster amplitudes

In the absence of an external perturbation, e.g., $H_{\rm EDM}$, the perturbed CC equations reduce to the unperturbed CC equations. Hence, the unperturbed cluster amplitudes take the role of the perturbed cluster amplitudes and the CC equation can be solved to obtain the unperturbed cluster amplitudes. This exercise can serve as a good check for the CCEDM code. This can be implemented at two stages, linear and non-linear. In the next section, the calculation of the unperturbed amplitudes from CCEDM equations in the limit $H_{\rm EDM} \rightarrow 0$ at the linear level is discussed.

6.2.0.1 Calculation of unperturbed cluster amplitudes at the linear level

Consider the linearised CC equations,

$$\left\langle \Phi_a^r \middle| \left\{ H_N + \overbrace{H_N T^{(0)}} \right\} \middle| \Phi_0 \right\rangle = 0 \tag{6.1}$$

$$\left\langle \Phi_{ab}^{rs} \middle| \left\{ H_N + \overbrace{H_N T^{(0)}} \right\} \middle| \Phi_0 \right\rangle = 0 \tag{6.2}$$

(For derivation, refer to Section.3.1.1. Note that in the present section, we have renamed T in Eq.3.14 as $T^{(0)}$.) Since we use the approximation $T^{(0)} = T_1^{(0)} + T_2^{(0)}$,

$$\left\langle \Phi_a^r \middle| H_N \middle| \Phi_0 \right\rangle + \left\langle \Phi_a^r \middle| \left\{ \overbrace{H_N T_1^{(0)}} + \overbrace{H_N T_2^{(0)}} \right\} \middle| \Phi_0 \right\rangle = 0 \tag{6.3}$$

$$\left\langle \Phi_{ab}^{rs} \middle| H_N \middle| \Phi_0 \right\rangle + \left\langle \Phi_{ab}^{rs} \middle| \left\{ \overbrace{H_N T_1^{(0)}} + \overbrace{H_N T_2^{(0)}} \right\} \middle| \Phi_0 \right\rangle = 0 \tag{6.4}$$

The above equations can be written in the form,

$$H_{11} T_1^{(0)} + H_{12} T_2^{(0)} = -H_{10} \tag{6.5}$$

$$H_{21} T_1^{(0)} + H_{22} T_2^{(0)} = -H_{20} \tag{6.6}$$

where the RHS of the above equations is independent of $T^{(0)}$. Combining the equations,

$$\mathbf{A} T^{(0)} = \mathbf{C} \tag{6.7}$$

where **A** and **C** are independent of T. This is a linear matrix equation. Consider the CCEDM equation,

$$\left\langle \Phi^* \middle| \left[\overline{H}_N, T^{(1)} \right] \middle| \Phi_0 \right\rangle = -\left\langle \Phi^* \middle| \overline{H}_{\mathrm{EDM}} \middle| \Phi_0 \right\rangle \tag{6.8}$$

where $|\Phi^*\rangle$ is a singly or doubly excited slater determinant. (Refer to Section.3.1.2 for derivation.) The linearised CCEDM equations are obtained by approximating, $\overline{H}_N \approx H_N$ where $T^{(0)}$ takes the place of $T^{(1)}$. This gives, for singles,

$$\left\langle \Phi_a^r \middle| \left[H_N, T^{(1)} \right] \middle| \Phi_0 \right\rangle = -\left\langle \Phi_a^r \middle| \overline{H}_{\mathrm{EDM}} \middle| \Phi_0 \right\rangle \tag{6.9}$$

In the absence of perturbation the RHS of the Eq.6.9, H_{EDM} is replaced by $\bar{H}_{\mathrm{N}}$. Hence the singles equation becomes, becomes,

$$\left\langle \Phi_a^r \middle| \left\{ \overline{H_N T^{(0)}} \right\} \middle| \Phi_0 \right\rangle = -\left\langle \Phi_a^r \middle| \overline{H}_N \middle| \Phi_0 \right\rangle \tag{6.10}$$

In the LHS of the Eq.6.10 equation, the terms of $\{\overline{H_N T^{(0)}}\}$ contributing to the singles and linear in $T^{(0)}$ arise only from the (2-hole, 2-particle)(diagrams CS3, CS4), (3-particle, 1-hole)(diagrams CS7, CS8), (3-hole, 1-particle)(diagrams CS9, CS10) and particle-particle (CS1) and hole-hole (CS2) form of the residual Coulomb operator (See Appendix B Fig.B.2). With the inclusion of only these diagrams listed in the brackets, under a linear approximation and in the absence of H_{EDM} perturbation, Eq.6.10 become mathematically equivalent to the unperturbed CC equations, Eq.6.4.

Similarly, consider from the CCEDM equation for doubles,

$$\left\langle \Phi_{ab}^{rs} \middle| \left[\overline{H}_a^N, T^{(1)} \right] \middle| \Phi_0 \right\rangle = -\left\langle \Phi_{ab}^{rs} \middle| \overline{H}_{\mathrm{EDM}} \middle| \Phi_0 \right\rangle \tag{6.11}$$

Replacing the H_{EDM} terms on the RHS of the Eq.6.11, by $\bar{H}_{\mathrm{N}}$ and taking only the terms linear in $T^{(0)}$ on the LHS,

$$\left\langle \Phi_{ab}^{rs} \middle| \left\{ \overline{H_N T^{(0)}} \right\} \middle| \Phi_0 \right\rangle = -\left\langle \Phi_{ab}^{rs} \middle| \overline{H}_{\mathrm{N}} \middle| \Phi_0 \right\rangle \tag{6.12}$$

The diagrams contributing to the LHS are (4-hole) (diagram CD6), (4-particle) (diagram CD3), (3-particle, 1-hole) (diagrams CD1, CD2), (2-particle, 2-hole) (diagrams CD4, CD5, CD9, CD10) and particle-particle (CS1) and hole-hole (CS2) (See Appendix B Fig.B.2). Consider the Eqs.6.10,Eq.6.12,

$$\begin{aligned} \left\langle \Phi_a^r \middle| \overline{H_N T^{(0)}} \middle| \Phi_0 \right\rangle &= -\left\langle \Phi_a^r \middle| H_{\rm N} \middle| \Phi_0 \right\rangle \\ \left\langle \Phi_{ab}^{rs} \middle| \overline{H_N T^{(0)}} \middle| \Phi_0 \right\rangle &= -\left\langle \Phi_{ab}^{rs} \middle| H_{\rm N} \middle| \Phi_0 \right\rangle \end{aligned} \tag{6.13}$$

These equations are termed as the 'unperturbed' CCEDM equations and can be represented in terms of elements of a matrix as

$$\begin{aligned} H'_{11} T_1^{(0)} + H'_{12} T_2^{(0)} &= H'_{10} \\ H'_{21} T_1^{(0)} + H'_{22} T_2^{(0)} &= H'_{20} \end{aligned} \tag{6.14}$$

These are equivalent to the Coupled-cluster equations Eq.6.6. The term $\langle \Phi_a^r | H_{\rm N} | \Phi_0 \rangle = 0$ on the RHS of Eq. 6.14, due to Brillouin's theorem. The singles equation after substituting $T^{(0)} = T_1^{(0)} + T_2^{(0)}$ becomes,

$$\left\langle \Phi_a^r \middle| \overline{H_N T_1^{(0)}} + \overline{H_N T_2^{(0)}} \middle| \Phi_0 \right\rangle = 0$$

For the initial guess, set the matrix elements of $T_2^{(0)} = 0$ and hence

$$\left\langle \Phi_a^r \middle| \overline{H_N T_1^{(0)}} \middle| \Phi_0 \right\rangle = \sum_I \left\langle \Phi_a^r \middle| H_N \middle| \Phi_I \right\rangle \left\langle \Phi_I \middle| T_1^{(0)} \middle| \Phi_0 \right\rangle = 0$$

For a given value of I, the matrix elements of $T_1^{(0)} = 0$. The initial guess values for the doubles cluster amplitudes are then obtained from the doubles equation,

$$\left\langle \Phi_{ab}^{rs} \middle| \overline{H_N T_2^{(0)}} \middle| \Phi_0 \right\rangle = -\left\langle \Phi_{ab}^{rs} \middle| H_{\rm N} \middle| \Phi_0 \right\rangle \tag{6.15}$$

The matrix elements on the RHS of Eq.6.15 reduce to

$$\left\langle \Phi_{ab}^{rs} \middle| H_N \middle| \Phi_0 \right\rangle = \left\langle rs \middle| v \middle| ab \right\rangle - \left\langle rs \middle| v \middle| ba \right\rangle$$

and the initial guess for $T_2^{(0)}$ becomes,

$$= -\frac{\left[\left\langle rs\middle|v\middle|ab\right\rangle - \left\langle rs\middle|v\middle|ba\right\rangle\right]}{\epsilon_a + \epsilon_b - \epsilon_p - \epsilon_q}$$

The Eqns.6.14 are then solved for the unknown $T^{(0)}$ amplitudes.

6.3 Calculation of correlation energy

The details of the Gaussian basis set calculation are discussed in the next few sections. Table.6.5 shows the details of the number of basis functions used to generate the Gaussian basis set and the active orbitals used in the present calculation. Four sets of calculations are performed with inputs of increasing basis size whose details are given in the next few sections.

Table 6.5: No. of basis functions used to generate the even tempered Dirac-Fock orbitals and the corresponding value of α_0 and β used. The total number of active orbitals are shown in the brackets of 'Active holes'.

	$s_{1/2}$	$p_{1/2}$	$p_{3/2}$	$d_{3/2}$	$d_{5/2}$	$f_{5/2}$	$f_{7/2}$	$g_{7/2}$	$g_{9/2}$
Number of basis	31	32	32	20	20	20	20	10	10
$\alpha_0(\times 10^{-5})$	725	715	715	700	700	695	695	655	655
β	2.725	2.715	2.715	2.700	2.700	2.695	2.695	2.655	2.655
Active holes (36)	2	2	2	2	2	1	1	1	1
Active holes (39)	3	3	3	2	2	1	1	1	1
Active holes (43)	3	3	3	3	3	2	2	1	1
Active holes (45)	3	3	3	3	3	3	3	1	1
Active particles	6	4	4	3	3	1	1	0	0

The correlation energy is calculated using the Eq.3.9,

$$e^{-T}\left(H_N + E_{HF}\right)e^{T}\left|\Phi_0\right\rangle = E\left|\Phi_0\right\rangle$$

Projecting the equation by the reference state,

$$\left\langle\Phi_0\middle|e^{-T}\left(H_N + E_{HF}\right)e^{T}\middle|\Phi_0\right\rangle = E\left\langle\Phi_0\middle|\Phi_0\right\rangle \tag{6.16}$$

Hence,

$$E_{\rm corr} = \left\langle \Phi_0 \middle| \overline{H}_N \middle| \Phi_0 \right\rangle$$

where $E_{\rm corr} = E - E_{\rm HF}$. In linear CCT, the diagrams contributing to the correlation energy are shown in Fig.6.1.

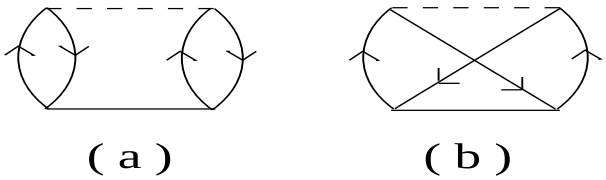

Figure 6.1: Correlation energy diagrams in linear coupled-cluster theory.

The comparison of the correlation energy calculated using the CCEDM program and the linear unperturbed coupled-cluster singles and doubles program in the limit of the perturbation $H_{\rm EDM} \to 0$ is shown in Table.6.6.

Table 6.6: Correlation energies calculated with converged unperturbed cluster amplitudes

Basis	$E_{\rm corr}$ (LCCSD)	$E_{\rm corr}$ (LCCEDM)
36	-2.86 $\times 10^{-3}$	-2.01 $\times 10^{-3}$
39	-2.01 $\times 10^{-2}$	-1.64 $\times 10^{-2}$
43	-2.21 $\times 10^{-2}$	-1.85 $\times 10^{-2}$
45	-2.26 $\times 10^{-2}$	-1.91 $\times 10^{-2}$

6.4 LCCEDM for atomic Hg

The calculation presented in this chapter is for a test basis with only few virtuals orbitals. The results presented here, are hence preliminary. A summary of the results obtained by gradually increasing the basis set is presented towards the end of this ' chapter. The details of the single particle orbitals and other inputs are presented briefly :

The single particle wavefunctions are calculated using GTOs. The input for the present calculation is shown in Table 6.5.

Table 6.7: No. of basis functions used to generate the even tempered Dirac-Fock orbitals and the corresponding value of α_0 and β used. The total number of active orbitals are shown in the brackets of 'Active holes'.

	$s_{1/2}$	$p_{1/2}$	$p_{3/2}$	$d_{3/2}$	$d_{5/2}$	$f_{5/2}$	$f_{7/2}$	$g_{7/2}$	$g_{9/2}$
Number of basis	31	32	32	20	20	20	20	10	10
$\alpha_0(\times 10^{-5})$	725	715	715	700	700	695	695	655	655
β	2.725	2.715	2.715	2.700	2.700	2.695	2.695	2.655	2.655
Active holes (36)	2	2	2	2	2	1	1	1	1
Active holes (39)	3	3	3	2	2	1	1	1	1
Active holes (43)	3	3	3	3	3	2	2	1	1
Active holes (45)	3	3	3	3	3	3	3	1	1
Active particles	6	4	4	3	3	1	1	0	0

In the next step the unperturbed cluster amplitudes ($T^{(0)}$) are generated with the active holes (36) and active particles as shown in Table.6.5. Then, the perturbd cluster amplitudes are calculated using the CCEDM program. The program converged in 7 iterations and the Hartree-Fock contribution is $D_{Hg} = -0.35 \times 10^{-11} C_T \sigma_N a_0$. Following are the terms contributing to the EDM expectation value at the linear level :

$$D_{\text{atom}} = \left\langle \Phi_0 \middle| \overline{D} T^{(1)} + T^{(1)\dagger} \overline{D} \middle| \Phi_0 \right\rangle$$

where

$$\overline{D} = e^{T^{(0)\dagger}} D e^{T^{(0)}}$$

. At the linear level,

$$= \left(1 + T^{(0)}\right)^{\dagger} D \left(1 + T^{(0)}\right)$$

$$= D + DT^{(0)} + T^{(0)\dagger} D = D + DT_1^{(0)} + D + DT_2^{(0)} + T_1^{(0)\dagger} D + T_2^{(0)\dagger} D$$

Now the EDM expectation value becomes,

$$D_{atom} = 2\left\langle \Phi_0 \middle| \left[T_1^{(1)\dagger} D + T_1^{(1)\dagger} D T_1^{(0)} + T_1^{(1)\dagger} D T_2^{(0)} + T_2^{(1)\dagger} D T_2^{(0)} + T_2^{(1)\dagger} D T_1^{(0)} \right] \middle| \Phi_0 \right\rangle \quad (6.17)$$

It must be noted that the operators D and H_{EDM} are both single particle operators and have the same rank ($K_2 = 1$). Also, diagrammatically both the operators have same

representations. Hence the atomic EDM calculated by considering $H_{\rm EDM}$ as a perturbation and subsequently calculating the expectation value of the induced dipole operator between the perturbed states or treating the induced dipole operator as the perturbation and taking the expectation value of the $H_{\rm EDM}$ operator, is identical. This is particularly true for the EDM property as it is an expectation value, unlike for PNC amplitudes, for which it is necessary to preserve the order of perturbation. Computatonally, it is a very efficient way to calculate the EDMs induced by T-PT, NSM and also properties like the polarizability, by using the cluster amplitudes perturbed by the induced dipole operator. Hence, the calculation of the single particle wavefunctions, the unperturbed and the perturbed amplitudes is performed only once.

6.4.1 Results for Hg EDM induced by the $\hat{P}$ and $\hat{T}$ violating T-PT interaction

Contributions from each of the terms in Eq.6.17 is shown in Table.6.8. The final result

Table 6.8: Individual contributions

	Contributions in atomic units
$T_1^{(1)^\dagger} D$	-85.93
$T_1^{(1)^\dagger} D T_1^{(0)}$	-17.98
$T_1^{(1)^\dagger} D T_2^{(0)}$	+2.96
$T_2^{(1)^\dagger} D T_2^{(0)}$	-15.45
$T_2^{(1)^\dagger} D T_1^{(0)}$	+0.019
Total	-116.37

can be translated in units of $e-m$,

$$D_{Hg} = -3.87 \times 10^{-22} C_T e - m$$

6.4.2 Results for Hg EDM induced by the $\hat{P}$ and $\hat{T}$ violating Nuclear Schiff moment

The ^{199}Hg atomic EDM induced by the nuclear Schiff moment is calculated for the same input given in the previous section 6.4.1. The method of generation of the perturbed and the unperturbed cluster amplitudes is the same as described above. The Hartree-Fock contribution is $D_{Hg} = -0.22 \times 10^{-17}$ecm $\frac{S}{efm^3}$. Contributions from each of the above terms is shown in Table.6.9.

Table 6.9: Individual contributions

	Contributions in units of 10^{-17}e cm $\left(\frac{S}{e\ fm^3}\right)$
$T_1^{(1)^\dagger} D$	-0.113
$T_1^{(1)^\dagger} D T_1^{(0)}$	-0.024
$T_1^{(1)^\dagger} D T_2^{(0)}$	0.0039
$T_2^{(1)^\dagger} D T_2^{(0)}$	-0.023
$T_2^{(1)^\dagger} D T_1^{(0)}$	0.252×10^{-4}
Total	-0.156

The final result is,

$$D_{Hg} = -2.08 \times 10^{-16}\text{ecm}\frac{S}{e\ fm^3}$$

6.4.3 Sample Calculation of polarizability

Polarizability of a closed shell atomic system is calculated by replacing the $H_{\rm EDM}$ operator by the induced dipole operator (see Section.5.1). With the same input given in Table.6.5, the individual contributions of terms in Eq.6.17 are given n Table.6.10 :

The experimental value of the polarizability in atomic units [30] is $34.45ea_0^3$ (50 %).

6.4.4 Summary of the results

Table 6.10: Individual contributions

	Contributions in $(-)\, ea_0^3$
$T_1^{(1)^\dagger} D$	-14.16
$T_1^{(1)^\dagger} D T_1^{(0)}$	-0.096
$T_1^{(1)^\dagger} D T_2^{(0)}$	-0.040
$T_2^{(1)^\dagger} D T_2^{(0)}$	0.056
$T_2^{(1)^\dagger} D T_1^{(0)}$	0.006
Total	-14.24

Table 6.11: Summary of the preliminary results. More realistic calculations must involve basis functions as large as 90.

Basis size	In units of $10^{-22} C_T$ e m	In units of 10^{-17} e cm $\frac{S}{e\, fm^3}$	Polarizability in $e\, a_0^3$
36	-3.88	-0.156	14.24
39	-5.69	-0.227	21.11
43	-4.10	-0.158	21.52
45	-7.71	-0.309	21.88

6.5 Implications of the tensor-pseudotensor coupling constant for physics beyond the Standard Model

The Standard Model of particle physics does not accommodate the tensor-pseudo tensor P and T violating electron-nuclear interaction. Any non-zero value of C_T would mean physics beyond the Standard Model. The present limit on $C_T = 0$ is obtained from the comparison of the ratio $R = d_{\text{atom}}/C_T$ using Coupled-perturbed Hartree-Fock theory [7] and the latest experimental result [5]. More details of this theory are presented in Section.3.3. The diagrams arising in the CPHF theory Fig.3.21 form only a subset of the correlation effects shown in Fig.B.2. This comparison gives,

$$C_T = \Big(1.77 \pm 0.82 \pm 0.67\Big) \times 10^{-9} \sigma_N$$

An improved accuracy of the calculation of the quantity R would give an improved estimate of C_T. From the Fig.1.1, the contribution to the closed atomic EDMs induced by the tensor-pseudo tensor electron-nucleus interaction arises from the electron-nucleon interactions which originates from the electron-quark interactions. The interaction involves the nuclear spin σ_N and hence C_T is weighted by the neutron and proton spins :

$$C_T = \left\langle C_{Tp} \sum_p \sigma_p + C_{Tn} \sum_n \sigma_n \right\rangle$$

where σ_p and σ_n are the proton and neutron spins respectively. The nucleus of ^{199}Hg has an unpaired neutron with $I = \frac{1}{2}$. The underlying CP-violation models indirectly predict the coupling constants associated with the electron-quark interactions.

6.6 Implications of the Nuclear Schiff Moment for physics beyond the Standard Model

It has already been explained in earlier sections that the EDM of atomic ^{199}Hg could arise from the P and T violating nuclear interactions. These interactions NSMproduce the . In this chapter we discuss the connection between the NSM with the P and T violating quark interactions.

The contribution to the nuclear Schiff moment (NSM) can arise from

1. The nucleon EDM : The nuclei which consist of unpaired nucleons can induce an EDM due to the EDMs of the lone nucleons.

2. $\hat{P}$ and $\hat{T}$ violating nucleon-nucleon interactions : The presence of CP violation at the quark level can induce nucleon-nucleon interactions which are $\hat{P}$ and $\hat{T}$ violating, in addition to the nucleon EDMs of the form

$$H_{PT} = \frac{G_F}{\sqrt{2}} \eta_{ab} \left(\bar{N}_a i\gamma_5 N_a\right) \left(\bar{N}_b N_b\right). \tag{6.18}$$

In the non-relativistic limit, Eq.6.18, reduces to,

$$H_{PT} = \frac{G_F}{\sqrt{2}} \frac{\eta_{ab}}{2m_p} \sigma_{\mathbf{a}} \cdot \nabla \rho_b$$

This interaction can be written as an interaction of a single valence nucleon N_a and the nuclear core with the density distribution ρ as,

$$H_{nc} = \frac{G_F}{\sqrt{2}} \frac{1}{2m_p} \eta_a \sigma_{\mathbf{a}} \cdot \nabla \rho \tag{6.19}$$

where

$$\eta_i = \left[\eta_{ip} Z + \eta_{in} \left(A - Z\right)\right] / A$$

For ^{129}Xe and ^{199}Hg, the unpaired nucleon is a neutron. The NSM caused by the internal proton excitations is parameterized in terms of the constant η_{np}. It was later understood that the contributions of the internal nucleons to the T-odd nuclear moments is as important as the contribution of external ones. The most accurate measurement of the ^{199}Hg atomic EDM is [5],

$$d_{Hg} = -\left(1.06 \pm 0.49 \pm 0.40\right) \times 10^{-28}\, e - cm \tag{6.20}$$

and the numerical calculations of the ^{199}Hg atomic EDM induced by the nuclear Schiff moment yielded the latest value [10]

$$d_{Hg} = -2.8 \times 10^{-17} \left(\frac{Q}{e\, fm^3}\right) e\ cm \tag{6.21}$$

The NSM, Q is related to the parameter η_{np} by [12],

$$\frac{Q}{e\, fm^3} = -1.4\ \times 10^{-8}\, \eta_{np} \tag{6.22}$$

From Eq.6.21 and 6.22, we get,

$$\begin{aligned} d_{Hg} &= -2.8 \times 10^{-17} \times (-1.4) \times 10^{-8}\, \eta_{np} e\ cm \\ &= 3.92 \times 10^{-25} \eta_{np} e\ cm \end{aligned} \tag{6.23}$$

From 6.20, we obtain,

$$-\left(1.06 \pm 0.49 \pm 0.40\right) \times 10^{-28} = 3.92 \times 10^{-25} \eta_{np} \tag{6.24}$$

Hence,

$$\begin{aligned} \eta_{np} &= -\frac{\big(1.06 \pm 0.49 \pm 0.40\big) \times 10^{-28}}{3.92 \times 10^{-25}} \\ &= -\big(2.7 \pm 1.3 \pm 1.0\big) \times 10^{-4} \end{aligned} \tag{6.25}$$

(see Ref.[10], Table.VIII.)

To estimate the η_{np} parameter, it is assumed that the terms $\big(G_F/\sqrt{2}\big)\,\eta_{np}\bar{N}i\gamma_5 N\;\bar{N}N$ arise from a one pion exchange. The lowest intermediate state contributing to η_{np} is the π^0 meson, which is related to the pion-nucleon coupling constant by,

$$\eta_0 \frac{G_F}{\sqrt{2}} = -\frac{g_{\pi NN}\,\bar{g}_{\pi NN}}{m_\pi^2} \tag{6.26}$$

where, $G_F = 1.17 \times 10^{-11}\,(MeV)^{-2}$ is the Fermi's coupling constant, $m_\pi = 140 MeV$ is the pion mass, $g_{\pi NN} \approx 13.5$ is the usual pion-nucleon coupling constant, and $\bar{g}_{\pi NN}$ is the $\hat{P}$ and $\hat{T}$ violating pion-nucleon coupling constant. For ^{199}Hg, we have,

$$-\,g_{\pi NN}\,\bar{g}_{\pi NN} = \eta_{np} \times \frac{G_F m_\pi^2}{\sqrt{2}} \tag{6.27}$$

where $G_F m_\pi^2 = 2.29 \times 10^{-7}$. Substituting,

$$\begin{aligned} -\,g_{\pi NN}\,\bar{g}_{\pi NN} &= -\big(2.7 \pm 1.3 \pm 1.0\big) \times 10^{-4} \times \frac{2.29 \times 10^{-7}}{\sqrt{2}} \\ \bar{g}_{\pi NN} &= \big(2.7 \pm 1.3 \pm 1.0\big) \times 10^{-11} \times \frac{2.29}{13.5 \times \sqrt{2}} \\ &= \big(2.7 \pm 1.3 \pm 1.0\big) \times 0.11 \times 10^{-11} \\ &= \big(3.0 \pm 1.4 \pm 1.1\big) \times 10^{-12} \end{aligned} \tag{6.28}$$

(see Ref.[10], Table.VIII.)

According to [31], the above value of $\bar{g}_{\pi NN}$ for ^{199}Hg can be used to set limits on the QCD vacuum angle $\theta_{\rm QCD}$ using,

$$\bar{g}_{\pi NN} \approx -0.027\,\theta_{\rm QCD}$$

which gives,

$$\theta_{\rm QCD} = \big(1.1 \pm 0.5 \pm 0.4\big) \times 10^{-10} \tag{6.29}$$

(See [10] Table.VIII).

Apart from the limits on $\theta_{\rm QCD}$, it is possible to set limits on the linear combination of quark chromo EDMs using,

$$\eta_{\rm np} = \frac{1}{4\pi G_F}\,\frac{3g_{\pi \rm pp}m_0^2}{f_\pi m_\pi^2} \times \left(\tilde{d}_d - \tilde{d}_u - 0.012\tilde{d}_s\right)$$

where f_π is the pion decay constant, $g_{\pi \rm pp}$ is the CP conserving coupling constant. Also, the $I = 1$ component of $\bar{g}_{\pi NN}$ is related to the chromo electric EDM of the light quarks[14],

$$\bar{g}^{\rm I=1}_{\pi NN} = 2\left(\tilde{d}_u - \tilde{d}_d\right) \times 10^{14}$$

where the terms on the RHS are all expressed in centimeters. From the limit on $\bar{g}_{\pi NN}$, we obtain the limit for the linear combination of the quark chromo EDMs,

$$\begin{aligned} e\left(\tilde{d}_u - \tilde{d}_d\right) &= \left(3.0 \pm 1.4 \pm 1.1\right) \times 10^{-12} over 2 \times 10^{14} \\ &= \left(1.5 \pm 0.7 \pm 0.6\right) \times 10^{-26}\text{ecm} \end{aligned}$$

(See [10] Table.VIII).

It is also possible to obtain a limit on the neutron and proton EDMs from the ^{199}Hg EDM. The neutron EDM d_N is estimated in terms of the the CP-odd θ terms in the QCD Lagrangian [32],

$$d_N \approx \left(5.2 \times 10^{-16}\text{ecm}\right)\,\theta$$

Using Eq.6.29,

$$d_N = \left(5.2 \times 10^{-16}\text{ecm}\right) \times \left(1.1 \pm 0.5 \pm 0.4\right) \times 10^{-10} \tag{6.30}$$

we get,

$$d_N = \left(5.7 \pm 2.6 \pm 2.1\right) \times 10^{-26}\text{ecm}$$

which can be used to set limit on the proton EDMs [15],

$$Q = s_p\, d_p + s_n\, d_n \tag{6.31}$$

where the NSM Q is presented as the sum of proton and neutron EDMs and $s_p = 0.2 \pm 0.02 fm^2$ and $s_n = 1.895 \pm 0.035 fm^2$. It is possible from the above relations, to get a limit for the proton EDM from ^{199}Hg EDM.

6.7 Conclusions and Future directions

The results shown in Section.6.4 correspond to a linearised Coupled-cluster theory applied to the calculations of closed-shell atomic EDMs. The LCCEDM calculations with larger basis sets are critical for these calculations and are in progress. Also, the inclusion of non-linear terms in the coupled-cluster equations would mean a highly accurate calculation of the P and T violating coupling constants. The high accuracy calculations of the coupling constants are underway and it should be possible to obtain the results of the non-linear CCEDM calculation in very near future considering the present status of the CCEDM program, and the accessibility of the techniques of parallelisation. The stage is now all set for further research on atomic EDMs, given the status of the experimental accuracy, there is a clearly necessity for accurate calculations of R. The inclusion of the non-linear effects would improve the limits set on the coupling constants by the earlier calculations. The accurate calculations of the coupling constants would help in providing important insights into many models of particle physics that predict them.

Appendix A

$\hat{P}$ and $\hat{T}$ violation and electric dipole moments

Implications of $\hat{P}$ and $\hat{T}$ symmetries on intrinsic electric dipole moments

The permanent electric dipole moment(EDM) is defined as the expectation value of the electric dipole operator between non-degenerate atomic states. Let $\mathcal{D}_{int}$ denote the intrinsic or the permanent EDM of a non-degenerate physical system in a state $|\Psi\rangle$. Then, it's EDM is given by,

$$\mathcal{D}_{int} = \langle \Psi \, | D_{ind} | \, \Psi \rangle \tag{A.1}$$

where D_{ind} is the induced dipole operator. Consider the above quantity in a parity transformed corrdinate system,

$$\mathcal{D}_{int} = \langle \Psi' \, | D_{ind} | \, \Psi' \rangle$$

where $| \, \Psi' \rangle \; = \; \hat{P} | \, \Psi \rangle$. Since $\hat{P} = \hat{P}^{\dagger} = \hat{P}^{-1}$, the above can be modified into,

$$\begin{aligned} \mathcal{D}_{\rm int} \;\; &= \;\; \langle \Psi' \, | \big(\, \hat{P} \; \hat{P}^{\dagger} \, \big) D_{\rm ind} \, \big(\hat{P} \; \hat{P}^{\dagger} \, \big) | \, \Psi' \rangle \\ &= \;\; \langle \Psi \, | \hat{P}^{\dagger} \; \hat{P} \, \big(\hat{P}^{\dagger} \; D_{\rm ind} \; \hat{P} \, \big) \; \hat{P}^{\dagger} \; \hat{P} | \Psi \rangle \end{aligned} \tag{A.2}$$

Since, $\big(\hat{P}^{\dagger} \; D_{\rm ind} \; \hat{P} \, \big) = \; - \; D$, we have,

$$\mathcal{D}_{\rm int} = \; - \, \langle \Psi \, | D_{\rm ind} \, | \Psi \rangle \tag{A.3}$$

$$\langle \Psi' \, | D_{ind} | \, \Psi' \rangle = \;\; - \;\; \langle \Psi \, | D_{\rm ind} \, | \Psi \rangle$$

The state $|\Psi\rangle$ is a stationary state and hence if the Hamiltonian determining the system is $\mathcal{H}$, then, $\mathcal{H}|\Psi\rangle = \mathcal{E}|\Psi\rangle$. Assuming the Hamiltonian to be invariant under $\hat{P}$, we have $\hat{P}^{-1}\mathcal{H}\hat{P} = \mathcal{H}$. Hence,

$$\begin{aligned} \left(\hat{P}\mathcal{H}\hat{P}^{-1}\right)\hat{P}|\Psi\rangle &= \mathcal{E}\hat{P}|\Psi\rangle \\ \mathcal{H}|\Psi' &= \mathcal{E}|\Psi'\rangle \end{aligned}$$

This implies, both $|\Psi\rangle$ and $\Psi'\rangle \equiv \hat{P}|\Psi\rangle$ describe stationary states with same eigen value $\mathcal{E}$. If this energy level is non-degenerate, then the two states cannot be independent and hence $\hat{P}|\Psi\rangle = c|\Psi\rangle$, where $c = \pm 1$. From $A.1$ and $A.3$,

$$\begin{aligned} \langle\Psi\ |D_{\text{ind}}\ |\Psi\rangle &= -\ \langle\Psi'\ |D_{ind}|\ \Psi'\rangle \\ &= -\ c^2\ \langle\Psi\ |D_{\text{ind}}\ |\Psi\rangle \\ &= -\ \langle\Psi\ |D_{\text{ind}}\ |\Psi\rangle \end{aligned}$$

In other words,

$$\langle\Psi\ |D_{\text{ind}}\ |\Psi\rangle = 0$$

It is hence proved that

If the Hamiltonian is invariant under a $\hat{P}$ transformation, and if the state is non-degenerate, then there can be no permanent electric dipole moment in that state

Appendix B

Classification of CCEDM diagrams

Diagrammatic representation of Coulomb operator and classification of diagrams with respect to the form of Coulomb operator

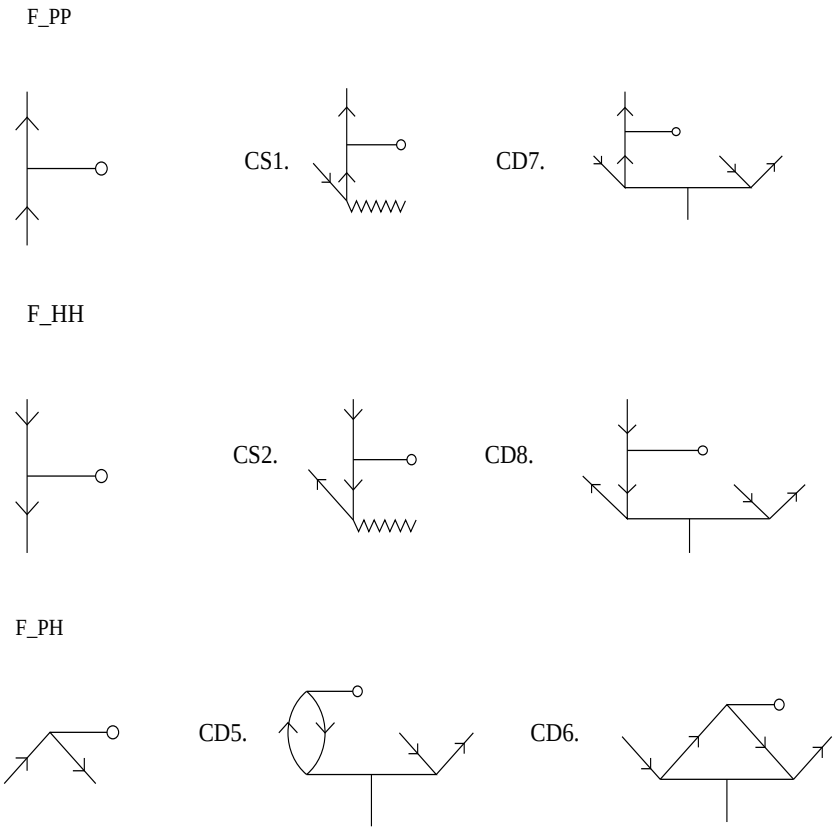

Figure B.1: CCEDM diagrams listed according to the form of V_N.

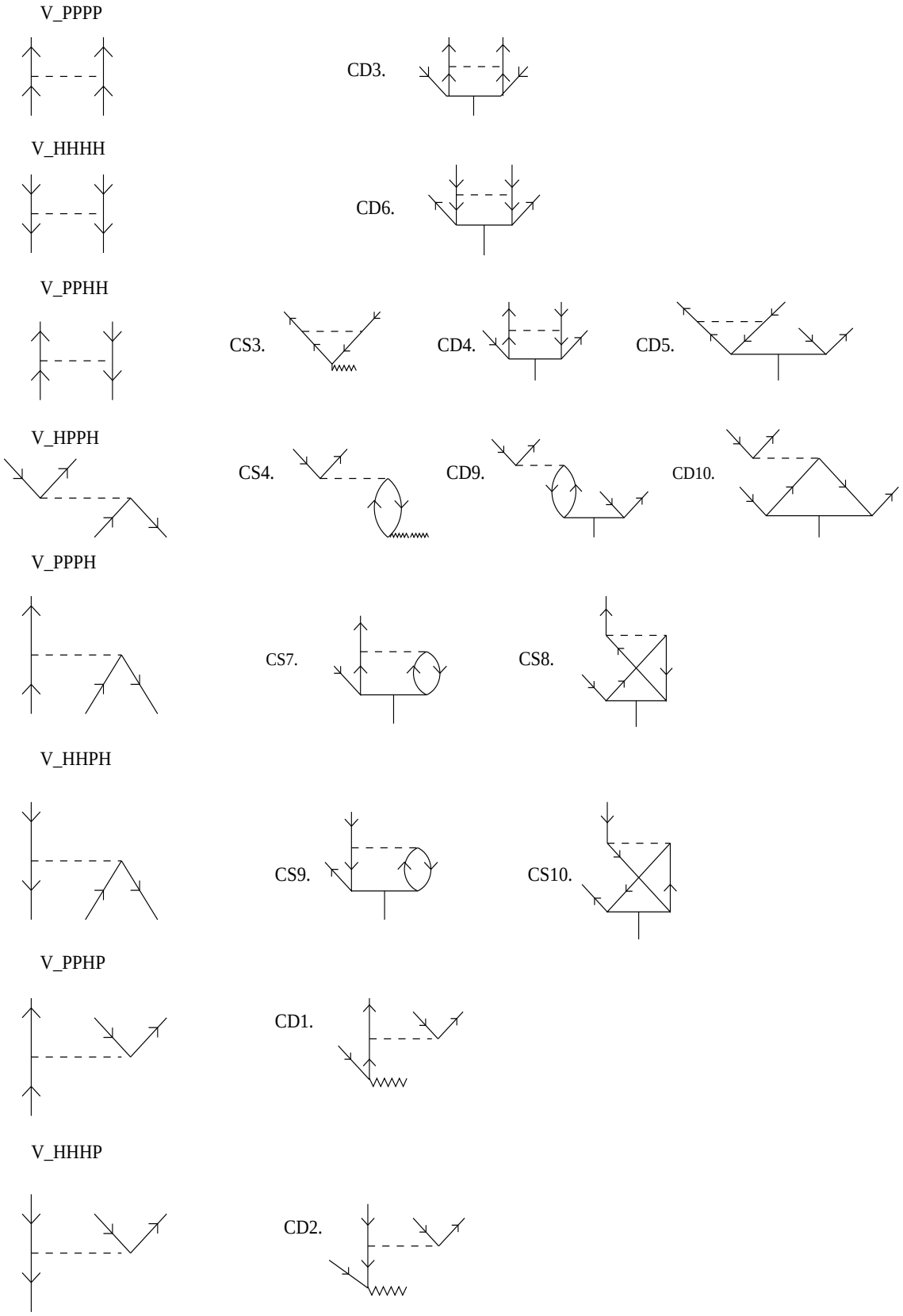

Figure B.2: CCEDM diagrams listed according to the form of V_N - contd.

Appendix C

Technical details of the CCEDM program

Flow chart for the CCEDM program is shown in Fig.$C.1$.
The program consists of routines to calculate various parameter/quantities necessary for setting up the CCEDM equations. The routines important for the actual EDM calculation are described below briefly :[1]

- **Subroutine readinp**: Reads the input containing the number of basis, number of occupied orbitals and the ranks of the EDM and induced dipole operators.
- **Subroutine symm**: This routine sets up the equation indices for retrieving $T^{(0)}$ amplitudes and also the skip information necessary for the locations of the Coulomb integrals.
- **Subroutine symm-edm**: This routine sets up the equation indices for the $T^{(1)}$ amplitudes.
- **Subroutine findlam**: This routine calculates the multipoles (λ_1, λ_2) of the $T_2^{(1)}$ operator, stores them in an array and also defines the locations for storing them.
- **Subroutine coulims**: This routine calculates the bare Coulomb integrals - (4-particle), (4-hole), (2 particle, 2 hole), (3 particle, 1 hole) diagrams and stores them in memory.

[1]For a detailed description of the program refer to the documentation to be put up in our webpage : http://www.iiap.res.in/research/NAPP/main.html

- **Subroutine aimshhph**: This routine calculates the (particle - particle) EDM IMS contributions.
- **Subroutine aimsppph**: This routine calculates the (hole - hole) EDM IMS contributions.
- **Subroutine edmtp**: This routine calculates the T-PT EDM matrix element.
- **Subroutine edmtp**: This routine calculates the induced dipole matrix element.
- **Subroutine schiff**: This routine calculates the EDM matrix element arising from NSM.
- **Subroutine vdriver**: This routine solves the CCEDM equations for the unknown $T^{(1)}$ amplitudes. The method employed to solve them is based on the Gauss-Seidel iterative scheme. Then the amplitudes are saved in a binary file for property calculations.
- **Subroutine vimsloc**: This routine sets up the equation indices for storing the Coulomb integrals $\langle ij|V|kl\rangle$.
- **Subroutine sppph**: This routine calculates the perturbed cluster amplitudes arising from the (3 particle - 1 hole) form of Coulomb diagrams, contributing to singles CCEDM equations (See Fig.B.2).
- **Subroutine shhph**: This routine calculates the perturbed cluster amplitudes arising from the (3 hole - 1 particle) form of Coulomb diagrams, contributing to singles CCEDM equations (See Fig.B.2).
- **Subroutine sphph**: This routine calculates the perturbed cluster amplitudes arising from the (2 hole - 2 particle) form of Coulomb diagrams, contributing to singles CCEDM equations (See Fig.B.2).
- **Subroutine dpphp**: This routine calculates the perturbed cluster amplitudes arising from the (3 particle - 1 hole) form of Coulomb diagrams, contributing to the doubles CCEDM equations (See Fig.B.2).

- **Subroutine dhhhp**: This routine calculates the perturbed cluster amplitudes arising from the (1 particle - 3 hole) form of Coulomb diagrams, contributing to the doubles CCEDM equations (See Fig.B.2).

- **Subroutine dpphh**: This routine calculates the perturbed cluster amplitudes arising from the (2 hole - 2 particle) form of Coulomb diagrams, contributing to the doubles CCEDM equations (See Fig.B.2).

- **Subroutine dpppp**: This routine calculates the perturbed cluster amplitudes arising from the (4 particle) form of Coulomb diagrams, contributing to the doubles CCEDM equations (See Fig.B.2).

- **Subroutine dhhhh**: This routine calculates the perturbed cluster amplitudes arising from the (4 hole) form of Coulomb diagrams, contributing to the doubles CCEDM equations (See Fig.B.2).

- **Subroutine dppph**: This routine calculates the perturbed cluster amplitudes arising from the (3 particle - 1 hole) form of Coulomb diagrams, contributing to the doubles CCEDM equations (See Fig.B.2).

- **Subroutine dhhph**: This routine calculates the perturbed cluster amplitudes arising from the (1 particle - 3 hole) form of Coulomb diagrams, contributing to the doubles CCEDM equations (See Fig.B.2).

- **Subroutine compute-edm**: This routine calculates the EDM expectation value arising from the T-PT and NSM and also the polarizabilities.

- **Subroutine edm-lin**: This routines is particularly written for calculating the contribution to the EDM expectation value from linear CCEDM calculation. In the Appendix 6.4.1, a sample calculation is given, listing the specific terms contributing to the EDM calculation at the linear CC level.

In this Appendix, I describe some of the milestones in the project of the implementation of the CCEDM theory program.

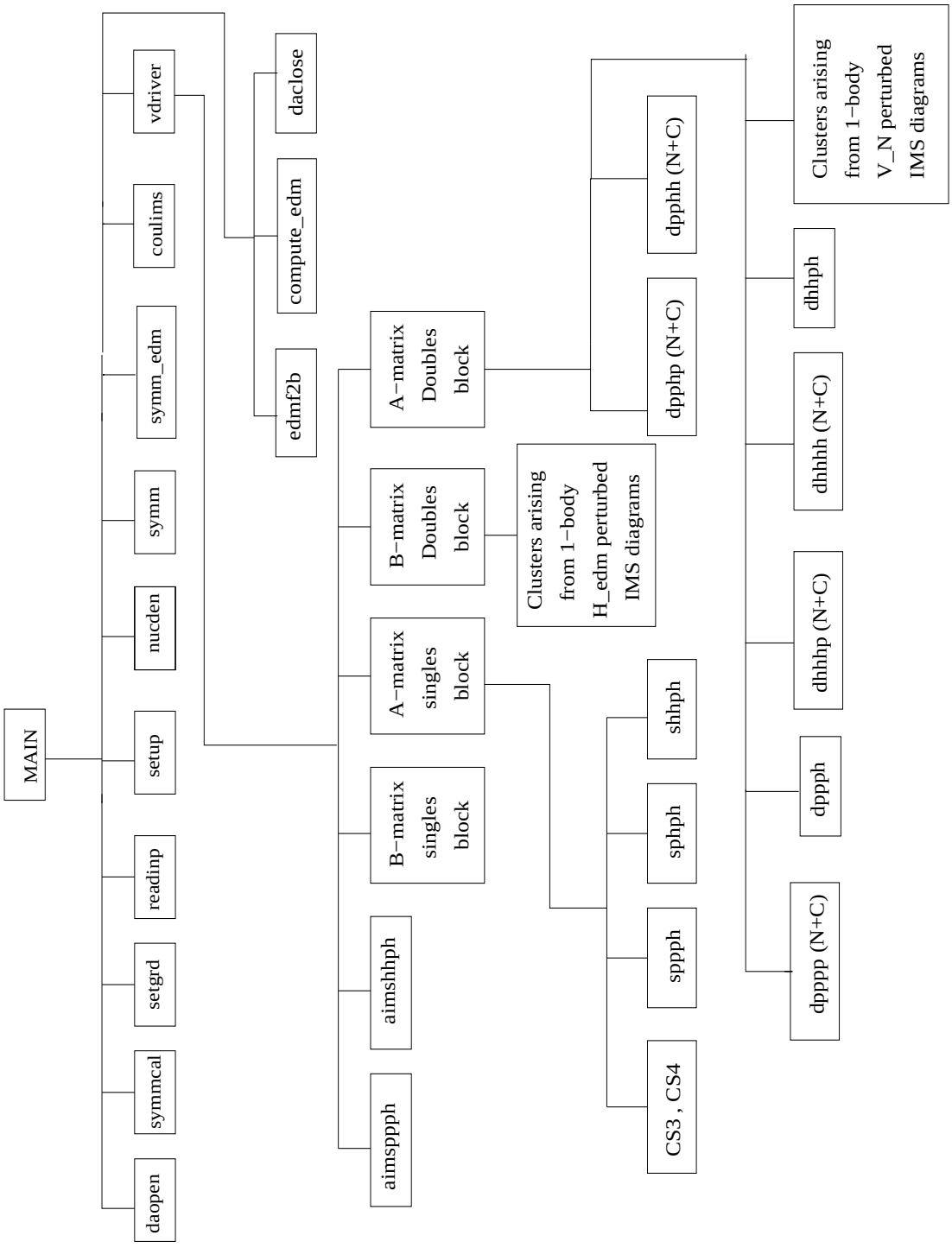

Figure C.1: Flow-chart for the non-linear CCEDM code - The driver routine calls the routines *sppph, sphph, shhph*, where the cluster diagrams arising from PPPH, PHPH, HHPH form of the coulomb operator (V_N) respectively, contributing to singles are calculated. Similarly the routines, *dpphp, dpppph, dpppp, dpppph, dhhhp, dhhhh* are called where the diagrams arising from corresponding form of the coulomb operator contributing to doubles are calculated.The driver routine also calculates the diagrams contributing to the RHS -(B matrix) of the CCEDM equation.

Loop over two holes & two particles

Loop over ' ic '
Loop over ' ir '
Loop over ' id '
Loop over ' is '

Hole−hole H_{EDM} IMS diagrams

Loop over ' ia '

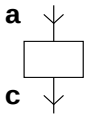

End ' ia '

Particle−particle H_{EDM} IMS diagrams

Loop over ' ip '

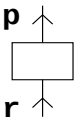

End ' ip '

End ' is '
End ' id '
End ' ir '
End ' ic '

Loop over open lines

Loop over ' ia '
Loop over' ip '

Begin singles

Compute B−matrix diagrams for singles

Loop over ' ib '
Loop over ' iq '

Diagrams CS3 & CS4 − T1−T1 block

Loop over ' ir '

Singles clusters arising from V_PPPH

Loop over ' ic '

Singles clusters arising from V_PHPH

End ' ic '
End ' ir '
Loop over ' ic '

Singles clusters arising from V_HHPH

End ' ic '
End ' iq '
End ' ib '

Compute $T_1^{(1)}$ for iteration

End singles
Begin doubles

Loop over ' ib '
Loop over ' iq '

Compute B−matrix diagrams for doubles

Loop over ' ir '

Doubles clusters arising from V_PPHP

Figure C.2: Loop structure for the driver routine

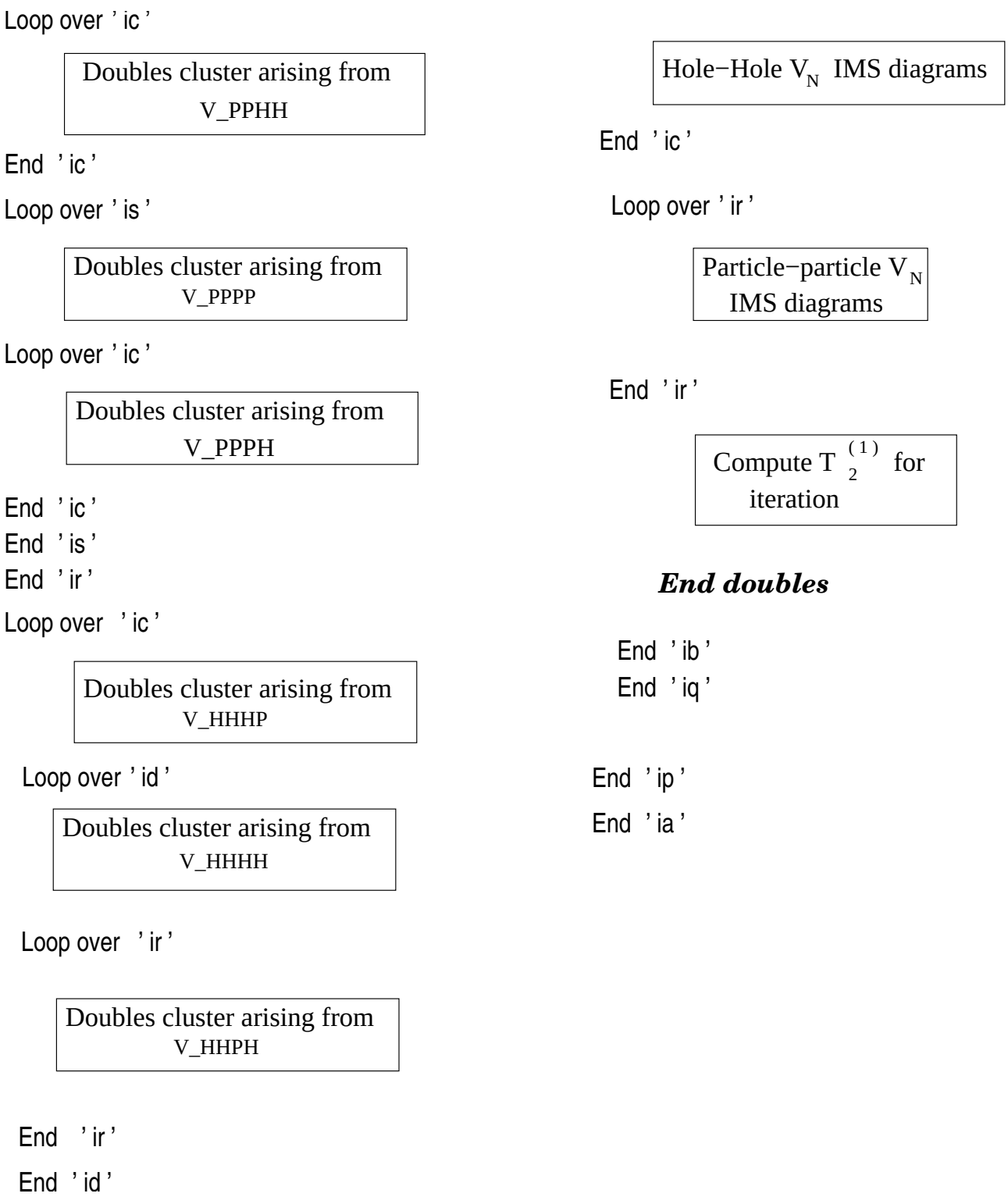

Figure C.3: Loop structure for the driver routine

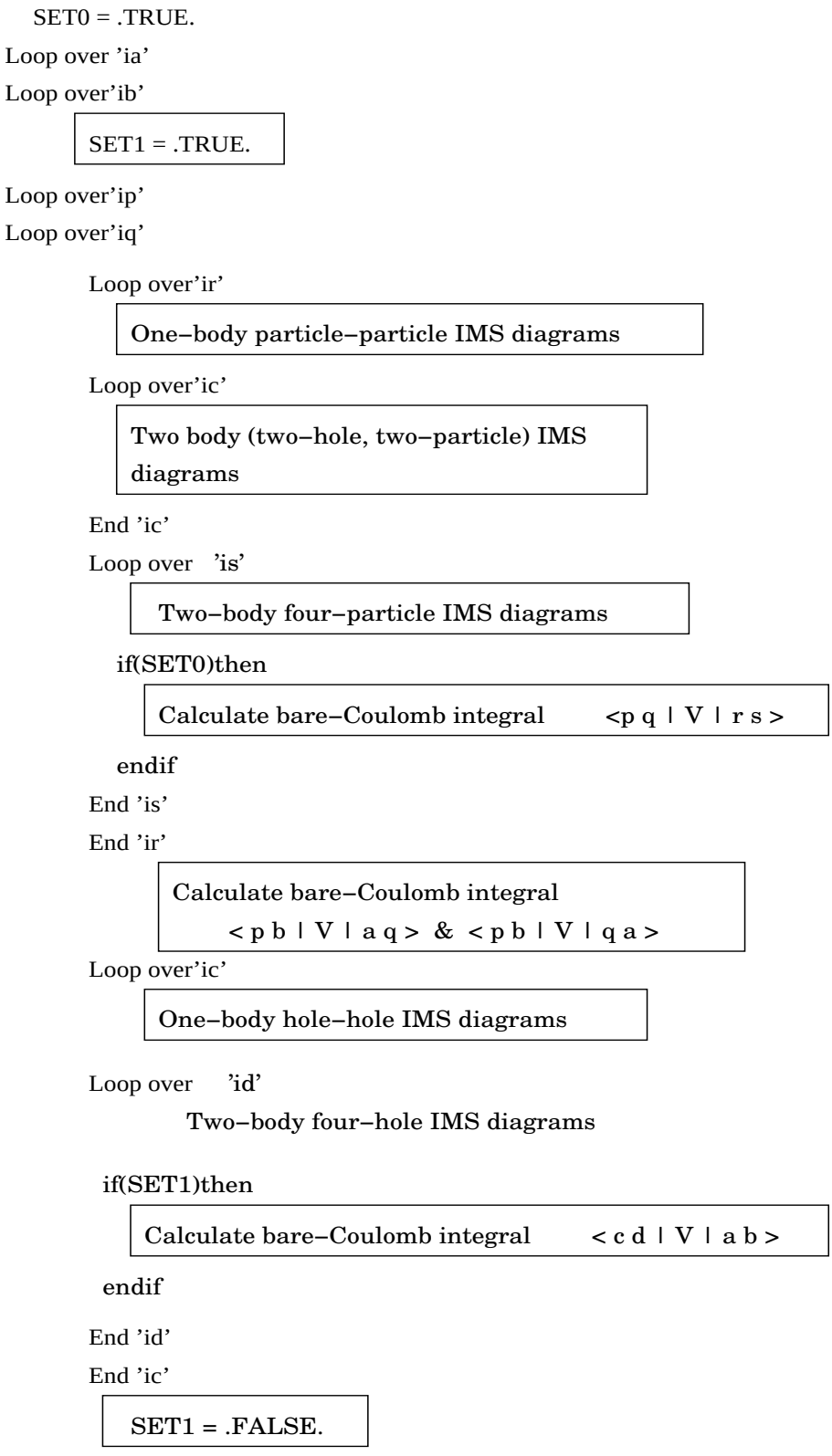

Figure C.4: Loop structure in the routine 'coulims.f' routine

Loop over 'ia'
Loop over 'ip'

Loop over 'ic'
Loop over 'ir'

Loop over 'id'
Loop over 'is'

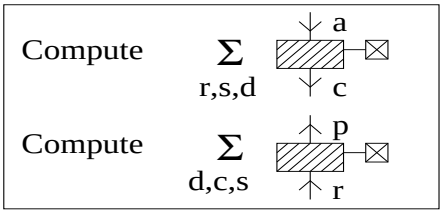

End 'is'
End 'id'

End 'ir'
End 'ic'

End of singles loop

Loop over 'ib'
Loop over 'iq'

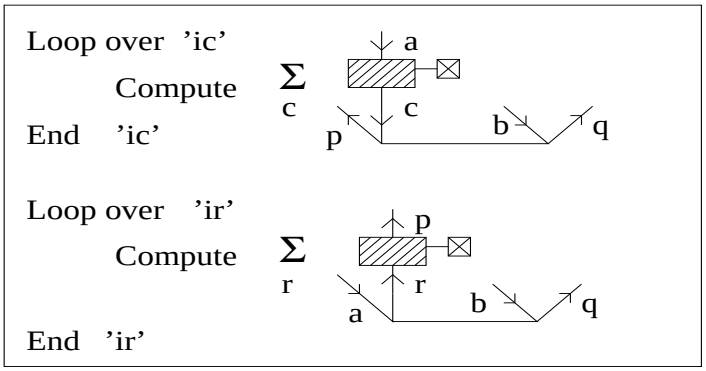

End of doubles loop

End 'iq'
End 'ib'
End 'ip'
End 'ia'

Figure C.5: Loop structure for inclusion of IMS diagrams in driver routine and computing the cluster amplitudes using the IMS

```
Loop over  'ia'
Loop over  'ip'
        Loop over  'ib'
        Loop over  'iq'
            Loop over  'ir'
```

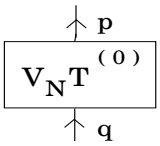


```
            Loop over 'ic'
```

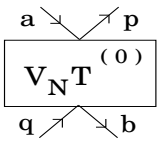

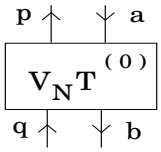


```
            End 'ic'
            Loop over  'is'
```

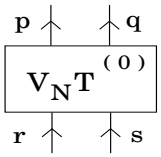


```
            End 'is'
            End  'ir'
            Loop over  'ic'
```

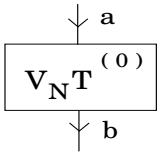


```
            Loop over  'id'
```

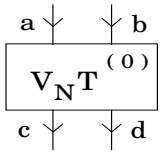


```
            End 'id'
            End 'ic'
        End 'iq'
        End 'ib'
End 'ip'
End 'ia'
```

Figure C.6: Loop structure for one-body and two-body Coulomb IMS diagrams in the routine *coulims.f*.

Loop over 'ia'
Loop over 'ip'

EDM diagrams arising from $(D_{eff})_{Z1}$

Zeroth order contribution = edm_order0

Loop over 'ib'
Loop over 'iq'

EDM diagrams arising from
$(D_{eff})_{Z1} T_1^{(0)}$ & $(D_{eff})_{Z2\ (b)}$

end 'iq'
end 'ib'
end 'ip'
end 'ia'

Loop over 'ia'
Loop over 'ip'

Loop over 'ib'
Loop over 'iq'

Effective diagrams at first order arising from F1(A)

Contribution of first order effective
diagrams = edm_eff1(indx)

end 'iq'
end 'ib'
end 'ip'
end 'ia'

Loop over 'ia'
Loop over 'ip'

Loop over 'ib'
Loop over 'iq'

Loop over 'ir'
Loop over 'ic'

Effective diagrams of F1(B)
No. of diagrams = 22

Contribution of first order effective
diagrams = edm_eff1(indx)

Effective diagrams of F2(A)
No. of diagrams = 11

end 'ic'
end 'ir'

end 'iq'
end 'ib'

end 'ip'
end 'ia'

Effective diagrams of F2(B)
Call 'coulims.f' routine

Figure C.7: F2(A) and F2(B) diagrams in the routine $compute_edm.f$

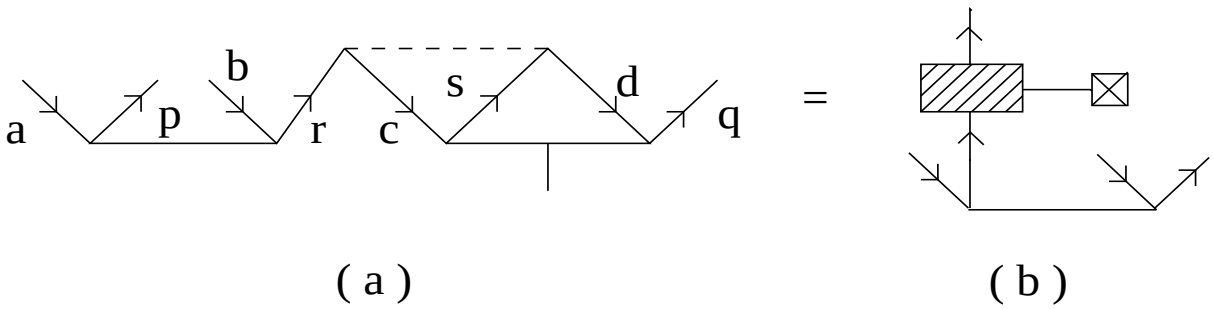

Figure C.8: EDM IMS diagram (particle-particle type) contracted with $T_2^{(0)}$.

Appendix D

The tensor-pseudotensor H_{EDM} matrix element

Consider the general matrix element of H_{EDM} between $|\Phi_a\rangle$ and $|\Phi_b\rangle$, $\langle\Phi_a|H_{EDM}|\Phi_b\rangle$ where H_{EDM} has the form given in Eq.2.8. Keeping the constants aside for the moment, consider

$$\langle\Phi_a|H_{EDM}|\Phi_b\rangle = \langle\Phi_a|i\beta\alpha_z I_z \rho_N(r)|\Phi_b\rangle$$

Consider the Z-axis as the axis of quantisation.

$$\langle\Phi_a|H_{EDM}|\Phi_b\rangle = iI_z\langle\Phi_a|i\beta\alpha_z \rho_N(r)|\Phi_b\rangle \tag{D.1}$$

The wavefunctions $|\Phi_a\rangle$ and $|\Phi_b\rangle$ can be represented in terms of the two-component Dirac wavefunctions given by,

$$|\Phi_a\rangle = \frac{1}{r}\begin{pmatrix} P_a(r)\chi_{\kappa_a,m_a}(\theta,\phi) \\ iQ_a(r)\chi_{-\kappa_a,m_a}(\theta,\phi)\end{pmatrix}$$

and

$$|\Phi_b\rangle = \frac{1}{r}\begin{pmatrix} P_b(r)\chi_{\kappa_b,m_b}(\theta,\phi) \\ iQ_b(r)\chi_{-\kappa_b,m_b}(\theta,\phi)\end{pmatrix}$$

The Dirac matrices, β and α are given by

$$\beta = \begin{pmatrix} I & 0 \\ 0 & -I\end{pmatrix}; \alpha = \begin{pmatrix} 0 & \sigma \\ \sigma & 0\end{pmatrix}$$

Substituting for β, α_z in Eq.D.1, we get

$\langle \Phi_a | H_{EDM} | \Phi_b \rangle =$

$$\int \frac{1}{r^2} \left[\begin{array}{cc} P_a(r)\chi^{\dagger}_{\kappa_a,m_a}(\theta,\phi) & -iQ_a(r)\chi^{\dagger}_{-\kappa_a,m_a}(\theta,\phi) \end{array} \right] \begin{pmatrix} 0 & \sigma_z \\ -\sigma_z & 0 \end{pmatrix} \left[\begin{array}{c} P_b(r)\chi_{\kappa_b,m_b}(\theta,\phi) \\ iQ_b(r)\chi_{-\kappa_b,m_b}(\theta,\phi) \end{array} \right]$$

$$\times \rho_N(r) r^2 dr d\Omega(iI_z)$$

$$= \int \left[\begin{array}{cc} P_a(r)\chi^{\dagger}_{\kappa_a,m_a}(\theta,\phi) & -iQ_a(r)\chi^{\dagger}_{-\kappa_a,m_a}(\theta,\phi) \end{array} \right] \left[\begin{array}{c} \sigma_z(i)Q_b(r)\chi_{-\kappa_b,m_b}(\theta,\phi) \\ -\sigma_z(i)P_b(r)\chi_{\kappa_b,m_b}(\theta,\phi) \end{array} \right]$$

$$\rho_N(r) dr d\Omega(iI_z)$$

Simplifying further,

$\langle \Phi_a | H_{EDM} | \Phi_b \rangle =$

$$= \int \left[P_a(r)\chi^{\dagger}_{\kappa_a,m_a}(\theta,\phi)\sigma_z Q_b(r)\chi_{-\kappa_b,m_b}(\theta,\phi)(i) \right] +$$

$$\left[Q_a(r)\chi^{\dagger}_{-\kappa_a,m_a}(\theta,\phi)\sigma_z P_b(r)\chi_{\kappa_b,m_b}(\theta,\phi)(i) \right] \rho_N(r) dr d\Omega(iI_z)$$

Separating the integrals for radial and angular parts,

$$\int P_a(r)Q_b(r)\rho_N(r)dr \underbrace{\int \chi^{\dagger}_{\kappa_a,m_a}(\theta,\phi)\sigma_z\chi_{-\kappa_b,m_b}(\theta,\phi)d\Omega(i)}_{I1}(iI_z) \tag{D.2}$$

$$+ \int Q_a(r)P_b(r)\rho_N(r)dr \underbrace{\int \chi^{\dagger}_{-\kappa_a,m_a}(\theta,\phi)\sigma_z\chi_{\kappa_b,m_b}(\theta,\phi)d\Omega(i)}_{I2}(iI_z)$$

To calculate the specific angular matrix elements corresponding to $\langle \Phi_{Ks_{1/2}} | H_{EDM} | \Phi_{K'p_{1/2}} \rangle$ and $\langle \Phi_{Ks_{1/2}} | H_{EDM} | \Phi_{K'p_{3/2}} \rangle$ we evaluate the respective angular parts, I1 and I2 in Eq.$D.2$.

Consider the first integral, I1 for $\langle \Phi_{Ks_{1/2}} | H_{EDM} | \Phi_{K'p_{3/2}} \rangle$:

$$I1 = \int \chi^{\dagger}_{\kappa_a,m_a}(\theta,\phi)\sigma_z\chi_{-\kappa_b,m_b}(\theta,\phi)d\Omega$$

$\chi^{\dagger}_{\kappa_a,m_a}(\theta,\phi)$: κ_a = -1 $J_a = 1/2$ This angular wave function is for the upper component of $\Phi_a\rangle$. Hence, $l_a = (J_a + Sign(\kappa_a) \times 1/2) = 0$. =¿$m^l_a = 0$ and $s_a = 1/2$. Choose the projection of the total angular momentumi to be the highest value. $M_a = 1/2 = 0 + 1/2$.

The state $|J_a, M_a\rangle = |\frac{1}{2}, \frac{1}{2}\rangle = |0,0\rangle|\frac{1}{2}, \frac{1}{2}\rangle$ in the L-S basis. Writing $\chi^{\dagger}_{\kappa_a, m_a}(\theta, \phi)$ in the uncoupled basis,

$$\chi_{\kappa_a, m_a}(\theta, \phi) = \sum_{m_a^l, m_a^s} |l_a, m_a^l\rangle \times |s_a, m_a^s\rangle \langle l_a, m_a^l, s_a, m_a^s | J_a, M_a\rangle$$

$$= |0,0\rangle|0,0\rangle = Y_0^0 |\alpha\rangle$$

where $|\alpha\rangle$ represents the wavefunction of a spin-up particle and Y_0^0, the spherical harmonics.

Consider $\chi_{-\kappa_b, m_b}(\theta, \phi)$: This corresponds to the lower component of $|\Phi_b\rangle$. The orbital angular momenta of the upper and lower components l and l' respectively are related as $l' = 2J - l$. We now have, $\kappa_b = -2$ $J_b = 3/2$ The kappa for the lower component, $-\kappa_b = 2$. Therefore, $l'_b = 2J_b - l_b$ and $l_b = 1$. Hence, $l'_b = 2$. From Wigner-Eckart theorem, the multipole moments, M_a, M_b and q satisfy $-M_a + q + M_b = 0$. Hence, $M_a = M_b$. Hence choose $M_b = 1/2$. Therefore,

$$\chi_{-\kappa_b, m_b}(\theta, \phi) = |2,0\rangle|\tfrac{1}{2}, \tfrac{1}{2}\rangle\langle 2, 0; \tfrac{1}{2}, \tfrac{1}{2} | \tfrac{3}{2}, \tfrac{1}{2}\rangle +$$

$$|2,1\rangle|\tfrac{1}{2}, -\tfrac{1}{2}\rangle\langle 2, \tfrac{1}{2}, -\tfrac{1}{2} | \tfrac{3}{2}, \tfrac{1}{2}\rangle$$

$$= Y_2^0 |\alpha\rangle\langle 2, 0; \tfrac{1}{2}, \tfrac{1}{2} | \tfrac{3}{2}, \tfrac{1}{2}\rangle + Y_2^1 |\beta\rangle\langle 2, 1; \tfrac{1}{2}, -\tfrac{1}{2} | \tfrac{3}{2}, \tfrac{1}{2}\rangle$$

Now,

$$\sigma_z \chi_{-\kappa_b, m_b}(\theta, \phi) = Y_2^0 |\alpha\rangle\langle 2, 0; \tfrac{1}{2}, \tfrac{1}{2} | \tfrac{3}{2}, \tfrac{1}{2}\rangle - Y_2^1 |\beta\rangle\langle 2, 1; \tfrac{1}{2}, -\tfrac{1}{2} | \tfrac{3}{2}, \tfrac{1}{2}\rangle$$

The integral I1 becomes,

$$I1 = \int \chi^{\dagger}_{\kappa_a, m_a}(\theta, \phi) \sigma_z \chi_{-\kappa_b, m_b}(\theta, \phi) d\Omega = 0$$

Consider I2:

$\chi_{\kappa_b, m_b}(\theta, \phi)$:

$\kappa_b = -2$, $J_b = \frac{3}{2}$, $l_b = \frac{3}{2} - \frac{1}{2} = 1 \rightarrow m_b^l$=-1, 0, 1. Fix $M_b = \frac{1}{2}$.

$$\chi_{\kappa_b, m_b}(\theta, \phi) = Y_1^0 |\alpha\rangle\langle 1, 0; \tfrac{1}{2}, \tfrac{1}{2} | \tfrac{3}{2}, \tfrac{1}{2}\rangle + Y_1^1 |\beta\rangle\langle 1, 1; \tfrac{1}{2}, -\tfrac{1}{2} | \tfrac{3}{2}, \tfrac{1}{2}\rangle$$

$$\sigma_z \chi_{\kappa_b, m_b}(\theta, \phi) = Y_1^0 |\alpha\rangle \langle 1, 0; \tfrac{1}{2}, \tfrac{1}{2} | \tfrac{3}{2}, \tfrac{1}{2}\rangle - Y_1^1 |\beta\rangle \langle 1, 1; \tfrac{1}{2}, -\tfrac{1}{2} | \tfrac{3}{2}, \tfrac{1}{2}\rangle$$

$\chi_{-\kappa_a, m_a}(\theta, \phi)$:

$\kappa_a = -1$, $-\kappa_a = 1$, $J_a = 1/2$, $l'_a = 2J_a - l_a = 1$. Hence, $m_a^l = -1, 0, 1$. Fix $M_a = \frac{1}{2}$.

$$\chi_{-\kappa_a, m_a}(\theta, \phi) = Y_1^0 |\alpha\rangle \langle 1, 0; \tfrac{1}{2}, \tfrac{1}{2} | \tfrac{1}{2}, \tfrac{1}{2}\rangle + Y_1^1 |\beta\rangle \langle 1, 1; \tfrac{1}{2}, -\tfrac{1}{2} | \tfrac{1}{2}, \tfrac{1}{2}\rangle$$

Using the orthogonality property(??) of the Spherical tensors Y_l^m and Clebsch-Gordan coefficients, we get I2=$-\frac{2}{3}\sqrt{2}$. The EDM matrix element,

$$\left\langle \Phi_{K s_{1/2}} \middle| H_{EDM} \middle| \Phi_{K' p_{3/2}} \right\rangle = (i^2)(I_z) \left(-\frac{2}{3}\sqrt{2} \right) \int Q_a(r) P_b(r) \rho_N(r) dr \qquad \text{(D.3)}$$

Appendix E

Radial Matrix elements of the Nuclear Schiff moment

Consider the matrix element of the Schiff moment interaction $H_{\rm SM}$ between two states, $\langle \Phi_a | H_{\rm SM} | \Phi_b \rangle$. The wavefunctions $|\Phi_a\rangle$ and $|\Phi_b\rangle$ can be represented in terms of the two-component Dirac wavefunctions given by,

$$\Phi(\mathbf{R}) = \frac{1}{r} \begin{pmatrix} P_a(r)\chi_{\kappa_a,m_a}(\theta,\phi) \\ i\, Q_a(r)\chi_{-\kappa_a,m_a}(\theta,\phi) \end{pmatrix} \tag{E.1}$$

Expressing $|\Phi_b\rangle$ in a similar form and setting up of the matrix element of $H_{\rm SM}$ gives,

$$\left\langle \Phi_a \middle| H_{\rm SM} \middle| \Phi_b \right\rangle = \int \begin{bmatrix} P_a(r)\,\chi^{\dagger}_{\kappa_a,m_a} & - & i\,Q_a(r)\,\chi_{-\kappa_a,m_a}(\theta,\phi)^{\dagger} \end{bmatrix} (-3\,S\,e)$$

$$\begin{bmatrix} P_b(r)\,\chi_{\kappa_b,m_b}(\theta,\phi) \\ i\,Q_b(r)\,\chi_{-\kappa_b,m_b}(\theta,\phi) \end{bmatrix} \frac{\rho(\vec{R})}{B}\, dR\, d\Omega \tag{E.2}$$

where $d\Omega = sin\theta\, d\theta\, d\phi$ and $B = \int R^4 \rho(\vec{R}) dR$. Multiplying the matrices,

$$\int_0^{\infty} \Big[\underbrace{P_a(r)\;\; P_b(r)\,\chi^{\dagger}_{\kappa_a,m_a}\;\chi_{\kappa_b,m_b}}_{\mathcal{A}} + \underbrace{Q_a(r)\;\; Q_b(r)\,\chi^{\dagger}_{-\kappa_a,m_a}\;\chi_{-\kappa_b,m_b}}_{\mathcal{B}} \Big]$$

$$\left(-3\,S\,e\,\frac{1}{B}\right) \rho(\vec{R})\; R\, cos\theta\; dR\, d\Omega \tag{E.3}$$

Consider,

$$\mathcal{A} = (-3\,S\,e) \int \Big[P_a(r)\;\; P_b(r)\,\chi^{\dagger}_{\kappa_a,m_a}\;\chi_{\kappa_b,m_b} \Big] \frac{\rho(\vec{R})}{B}\; R\, cos\theta\; dR\, d\Omega$$

and

$$\mathcal{B} = (-\,3\,S\,e) \int \left[Q_a\,(r)\;Q_b\,(r)\,\chi^{\dagger}_{-\kappa_a,m_a}\;\chi_{-\kappa_b,m_b} \right] \frac{\rho(\vec{R})}{B}\;R\;cos\theta\;dR\;d\Omega$$

We now evaluate the angular parts of the specific integrals between $s_{1/2}$ and $p_{1/2}$ orbitals. First consider the angular part of,

$$\langle \Phi_{ks_{1/2}} | H_{\rm SM} | \Phi_{mp_{1/2}} \rangle$$

given by,

$$\int \chi^{\dagger}_{\kappa_a,m_a}\;cos\theta\;\chi_{\kappa_b,m_b}\;\sin\theta\;d\theta\;d\phi$$

$\kappa_a \;=\; -1\,;\; J_a \;=\; 1/2 \Rightarrow\; l_a \;=\; \big(J_a + \text{sign}(\kappa_a) \times 1/2\big) \;=\; 0$

Using the above expression for l_i, the values of κ_i are calculated by fixing the projection of the total angular momentum $J_a = 1/2$ and $J_b = 1/2$ as $M_a = 1/2$ and $M_b = 1/2$ and tabulated in Table.E.

κ_a	m^l_a	κ_b	m^l_b
-1	0	1	-1, 0, 1

Table E.1: $\hat{P}$,$\hat{T}$ violation for a non-zero EDM

The angular part χ_{κ_a,m_a} is expressed in terms of the spherical harmonics and the spin functions α(up-spin) and β(down-spin) as,

$$\begin{aligned}
\chi_{\kappa_a,m_a} &= \sum_{m^l_a,m^s_a} |l_a\;m^l_a\rangle \otimes |s_a\;m^s_a\rangle \times \langle l_a\;m^l_a\;s_a\;m^s_a \mid J_a\;M_a\rangle \\
&= \mathcal{Y}^0_0\;\;|\,\alpha\rangle\;\;\langle 0\;0\;\tfrac{1}{2}\;\tfrac{1}{2} \mid \tfrac{1}{2}\;\tfrac{1}{2}\rangle \\
&= \mathcal{Y}^0_0\;\;|\,\alpha\rangle\;\;\langle \tfrac{1}{2}\;\tfrac{1}{2}\;0\;0\;\mid \tfrac{1}{2}\;\tfrac{1}{2}\rangle \\
&= \mathcal{Y}^0_0\;\;|\,\alpha\rangle
\end{aligned} \tag{E.4}$$

Now consider, $\kappa_b \;=\; 1$ and $J_b \;=\; 1/2, \Rightarrow l_b \;=\; 1$ and $m^l_b \;=\; -1\;,0\;,1.$ Fix $M_b = 1/2$, and using $m^s_b + m^l_b \;=\; M_b$, the possible values of $m^s_b \;=\; \pm 1/2$. Hence,

$$\begin{aligned}
\chi_{\kappa_b,m_b} &= \mathcal{Y}^1_1 \mid \beta\rangle\langle 1\;1\;\tfrac{1}{2}\;-\tfrac{1}{2} \mid \tfrac{1}{2}\;\tfrac{1}{2}\rangle + \mathcal{Y}^0_1 \mid \alpha\rangle\langle 1\;0\;\tfrac{1}{2}\;\tfrac{1}{2} \mid \tfrac{1}{2}\;\tfrac{1}{2}\rangle \\
&= \mathcal{Y}^1_1 \mid \beta\rangle \left(\sqrt{2/3}\right) \;-\; \mathcal{Y}^0_1 \mid \alpha\rangle \left(\sqrt{1/3}\right)
\end{aligned} \tag{E.5}$$

after substituting for the Clebsch-Gordon coefficients. Combining $E.4$ and $E.5$, the angular part of (A) becomes,

$$\int \chi^{\dagger}_{\kappa_a,m_a}\ cos\theta\ \chi_{\kappa_b,m_b}\ \sin\theta\ d\theta\ d\phi\ =\ \int\ [\mathcal{Y}^0_0\langle\ \alpha|]\ (cos\theta)$$

$$\left[\mathcal{Y}^1_1\ |\ \beta\rangle\left(\sqrt{2/3}\right)-\ \mathcal{Y}^0_1|\ \alpha\rangle\left(\sqrt{1/3}\right)\right]\sin\theta\ d\theta\ d\phi$$

$$\begin{aligned}&=\ \int -\ \mathcal{Y}^0_0\mathcal{Y}^0_1\ \left(\sqrt{1/3}\right)\cos\theta\ \sin\theta\ d\theta\ d\phi\\ &=\ -\left(\frac{1}{3}\right)\end{aligned}\qquad\text{(E.6)}$$

The integral $(\mathcal{A})$ becomes,

$$\mathcal{A}=(-\ 3\ S\ e)\ \left(\frac{-1}{3}\right)\int P_a\,(r)\ \ P_b\,(r)\,\frac{\rho(\vec{R})}{B}\ R\ \ dR$$

We now evaluate the angular part of (B) given by,

$$\int \chi^{\dagger}_{-\kappa_a,m_a}\ \cos\theta\ \chi_{-\kappa_b,m_b}\ \sin\theta\ d\theta\ d\phi$$

Consider, $\kappa_a\ =\ -1\ \Rightarrow\ -\kappa_a\ =\ 1$ and $J_a=1/2$. Hence, $l_a\ =\ 1$ and $m^l_a\ =\ -1,\ 0,\ 1$. Fixing $M-a=1/2$, $m^s_a\ =\ \pm 1/2$. Therefore,

$$\begin{aligned}\chi_{-\kappa_a,m_a}\ &=\ \mathcal{Y}^0_1\ |\alpha\rangle\ \langle 1\ 0\ \tfrac{1}{2}\ \tfrac{1}{2}\ |\ \tfrac{1}{2}\ \tfrac{1}{2}\rangle+\ \mathcal{Y}^1_1\ |\ \beta\rangle\langle 1\ 1\ \tfrac{1}{2}\ -\tfrac{1}{2}\ |\ \tfrac{1}{2}\ \tfrac{1}{2}\rangle\\ &=\ \mathcal{Y}^0_1\ |\alpha\rangle\ \left(-\sqrt{1/3}\right)\ +\ \mathcal{Y}^1_1\ |\ \beta\rangle\left(\sqrt{2/3}\right)\end{aligned}\qquad\text{(E.7)}$$

Consider, $-\kappa_b=-1,\ J_b=1/2\ \Rightarrow l_b=0\ \ \Rightarrow m^l_b=0$. Fix $M_b=1/2\ \ \Rightarrow m^s_b=1/2$. Hence,

$$\chi_{-\kappa_b,m_b}\ =\ \mathcal{Y}^0_0\ |\alpha\rangle$$

We now obtain the angular part of (B),

$$\begin{aligned}&=\ \int\left[\mathcal{Y}^{0*}_1\langle\alpha|\left(-\sqrt{1/3}\right)\ +\ \mathcal{Y}^{1*}_1\langle\beta|\left(\sqrt{2/3}\right)\right]\ cos\theta\ \left[\mathcal{Y}^0_0\ |\alpha\rangle\right]\ \sin\theta\ d\theta\ d\phi\\ &=\ \int\mathcal{Y}^{0*}_1\,\mathcal{Y}^0_0\ \left(-\sqrt{1/3}\right)\cos\theta\ \sin\theta\ d\theta\ d\phi\\ &=\ \left(\frac{-1}{3}\right)\end{aligned}\qquad\text{(E.8)}$$

Substituting in $(\mathcal{B})$,

$$\mathcal{B} = (-\ 3\ S\ e)\ \left(-\frac{1}{3}\right)\ \int Q_a\,(r)\ Q_b\,(r)\,\frac{\rho(\vec{R})}{B}\ R\,dR$$

Combining $(\mathcal{A})$ and $(\mathcal{B})$,

$$\langle \Phi_{ks_{1/2}} | H_{\rm SM} | \Phi_{mp_{1/2}} \rangle = (-\ 3\ S\ e)\ \left(\frac{-1}{3}\right)$$

$$\int_0^\infty [P_a\,(r)\ P_b\,(r)\ +\ Q_a\,(r)\ Q_b\,(r)]\,\frac{\rho(\vec{R})}{B}\ R\,dR \tag{E.9}$$

The matrix element of the Schiff moment operator between the states $|mp_{1/2}\rangle$ and $|ks_{1/2}\rangle$ can be derived in similarly and is given by,

$$\left\langle \Phi_{mp_{1/2}} \middle| H_{\rm SM} \middle| \Phi_{ks_{1/2}} \right\rangle = (-\ 3\ S\ e)\ \left(\frac{-1}{3}\right)$$

$$\int_0^\infty \left[P_a\,(r)\ P_b\,(r)\ +\ Q_a\,(r)\ Q_b\,(r)\right]\frac{\rho(\vec{R})}{B}\ R\,dR \tag{E.10}$$

which is exactly same as for $\left\langle \Phi_{ks_{1/2}} \middle| H_{\rm SM} \middle| \Phi_{mp_{1/2}} \right\rangle$.

Appendix F

Matrix elements of the $\hat{P}$ and $\hat{T}$ violating nuclear potential

We start with the derivation of a general P,T - odd electrostatic potential inside the nucleus, take the electronic matrix element of this potential and show that it is related to the nuclear Schiff moment.

The nuclear electrostatic potential is

$$\Phi(\mathbf{R}) = \int_0^\infty \frac{e\rho(\mathbf{r})}{|\mathbf{R}-\mathbf{r}|} d^3r + \frac{1}{Z}(\mathbf{d}.\nabla) \int_0^\infty \frac{\rho(\mathbf{r})}{|\mathbf{R}-\mathbf{r}|} d^3r \tag{F.1}$$

where $e\rho(\mathbf{r})$ is the nuclear charge density, $\int \rho(\mathbf{r}) d^3r = Z$, $\mathbf{d} = e\int \rho(\mathbf{r}) d^3r = e\langle \mathbf{r} \rangle$ is the nuclear EDM. The definitions of the vectors $\mathbf{R}$ and $\mathbf{r}$ are given in fig.1.

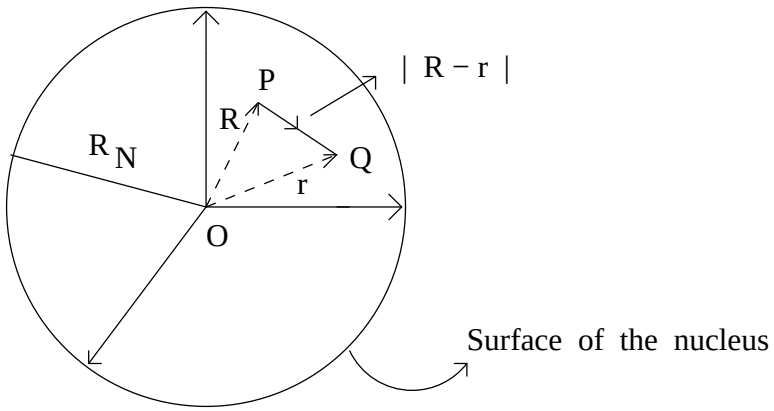

Note that both $\mathbf{R}$ and $\mathbf{r}$ are lying within the nucleus and R_N is the nuclear radius. The second term cancels the dipole long range electric field in the multipole expansion

of $\Phi(\mathbf{R})$. Consider the multipole expansion of $\Phi(\mathbf{R})$ around $\mathbf{R} = \mathbf{R}_0$

$$\Phi(\mathbf{R}) = \Phi(\mathbf{R}_0) + (\mathbf{R} - \mathbf{R}_0)\Phi'(\mathbf{R}_0) + \frac{(\mathbf{R} - \mathbf{R}_0)^2}{2!}\Phi''(\mathbf{R}_0) + ...$$

which is equivalent to Eq.F.1 at $\mathbf{R} = \mathbf{R}_0$ except that the second term in Eq.F.1 is defined per nucleon. Expanding $\frac{1}{|\mathbf{R}-\mathbf{r}|}$

$$\frac{1}{|\mathbf{R} - \mathbf{r}|} = \sum_l \frac{r_<^l}{r_>^{l+1}} P_l(cos\theta)$$

where θ is the angle between $\mathbf{R}$ and $\mathbf{r}$ and $P_l(cos\theta)$ are the Legendre Polynomials. Consider the first term of Eq.F.1.

$$\int_0^\infty \frac{e\rho(\mathbf{r})}{|\mathbf{R} - \mathbf{r}|} d^3r = \int_0^R \frac{e\rho(\mathbf{r})}{|\mathbf{R} - \mathbf{r}|} d^3r + \int_R^\infty \frac{e\rho(\mathbf{r})}{|\mathbf{R} - \mathbf{r}|} d^3r$$

Only odd multipoles of l give rise to P,T-odd potential. All values beyond l=1 give negligible contribution. Hence, in the $\sum_l$ only l=1 is retained for the first term. Using $P_l(\cos\theta) = \cos\theta$ we get

$$= \frac{1}{R^2} \int_0^R e\mathbf{r}\rho(\mathbf{r}) cos\theta d^3r + R \int_R^\infty \frac{e\rho(\mathbf{r})}{r^2} cos\theta d^3r$$

$$\int_0^\infty \frac{e\rho(\mathbf{r})}{|\mathbf{R} - \mathbf{r}|} d^3r = \frac{\mathbf{R}}{R^3} \cdot \int_0^R e\mathbf{r}\rho(\mathbf{r}) d^3r + \mathbf{R} \cdot \int_R^\infty \frac{e\mathbf{r}\rho(\mathbf{r})}{r^3} d^3r. \tag{F.2}$$

Consider the second term in Eq.F.1. Retaining only the l=0 term

$$\frac{1}{Z}(\mathbf{d} \cdot \nabla) \int_0^\infty \frac{\rho(\mathbf{r})}{|\mathbf{R} - \mathbf{r}|} d^3r = \frac{1}{Z}\mathbf{d} \cdot \nabla \left(\frac{1}{R}\right) \int_0^R \rho(\mathbf{r}) d^3r + \frac{1}{Z}(\mathbf{d} \cdot \nabla) \int_R^\infty \frac{\rho(\mathbf{r})}{\mathbf{r}} d^3r \tag{F.3}$$

Consider the first term in the Eq.F.2 in the limit $R \to$ inf

$$e\frac{\mathbf{R}}{R^3} \cdot \int_0^\infty \mathbf{r}\rho(\mathbf{r}) d^3r = e\frac{\mathbf{R}}{R^3}\langle\mathbf{r}\rangle.$$

Similarly in the limit $R \to$ inf first term in Eq.F.3 becomes

$$-\frac{\mathbf{R}}{ZR^3}e\langle\mathbf{r}\rangle\int_0^\infty \rho(\mathbf{r})d^3r = -\frac{e\langle\mathbf{r}\rangle}{R^3}\mathbf{R}.$$

These two terms cancell each other. Hence the integral limits in the first terms of Eq.F.2 and Eq.F.3 can be changed using

$$\int_0^R = \int_0^\infty - \int_R^\infty = -\int_R^\infty$$

Eq.F.1 becomes

$$\Phi(\mathbf{R}) = \frac{-e\mathbf{R}}{R^3}\int_R^\infty \mathbf{r}\rho(\mathbf{r})d^3r + e\mathbf{R}\int_R^\infty \frac{\rho(\mathbf{r})\mathbf{r}d^3r}{r^3} + \frac{e\langle\mathbf{r}\rangle}{ZR^3}\cdot\mathbf{R}\int_R^\infty \rho(\mathbf{r})d^3r$$

Rewriting the above equation

$$\Phi(\mathbf{R}) = e\mathbf{R}\left[\int_R^\infty \left(\frac{\langle\mathbf{r}\rangle}{ZR^3} - \frac{\mathbf{r}}{R^3} + \frac{\mathbf{r}}{r^3}\right)\rho(\mathbf{r})d^3r\right] \tag{F.4}$$

This nuclear potential goes to zero when $\rho(\mathbf{r})$ becomes zero for $\mathbf{R} > \mathbf{R}_N$.

Physical significance of the different terms in Eq.F.4:

- Consider the first term

$$\int_R^\infty e\mathbf{R}\frac{\langle\mathbf{r}\rangle}{ZR^3}\rho(\mathbf{r})d^3r$$

  Rearranging,

$$\int_R^\infty \frac{e\langle\mathbf{r}\rangle}{Z}\frac{\mathbf{R}}{R^3}\rho(\mathbf{r})d^3r$$

  This term represents the interaction of the average nuclear electric dipole moment per nucleon due to a charge distribution at a distance of $\mathbf{r}$ between $\mathbf{R}$ and $\mathbf{R}_N$ with the electric field due to a point charge at a distance $\mathbf{R}$ from the centre of the nucleus.

- Consider the second term

$$\int_R^\infty e\mathbf{r}\cdot\frac{\mathbf{R}}{R^3}\rho(\mathbf{r})d^3r$$

This term is the interaction of the nuclear electric dipole moment produced due to a charge distribution $\rho(\mathbf{r})$ in the region between $\mathbf{R}$ and $\mathbf{R}_N$ with the electric field due to a unit charge at a distance $\mathbf{R}$ from the centre of the nucleus.

- The third term

$$\int_R^\infty \mathbf{R}\frac{e\mathbf{r}}{r^3}\rho(\mathbf{r})d^3r$$

represents an interaction of an electric field produced due to a charge distribution between $\mathbf{R}$ to $\mathbf{R}_N$ with the nuclear dipole moment produced at a distance $\mathbf{R}$ from the centre of the nucleus. The nuclear electrostatic potential, Eq. *F*.4 mixes the electron wavefunctions of opposite parity. We consider only the $s_{1/2}$ and $p_{1/2}$ electron wavefunctions as only these have a non-zero probability density inside the nucleus. We are interested in the matrix element

$$\langle\Psi_s|-e\Phi(\mathbf{R})|\Psi_p\rangle.$$

Using the relativistic form of the electron wavefunctions

$$\Psi(\mathbf{R})=\begin{pmatrix} f(\mathbf{R})\Omega(jlm) \\ -i(\sigma\cdot\mathbf{n})g(\mathbf{R})\Omega(jlm)\end{pmatrix} \tag{F.5}$$

in the above matrix element and simplifying

$$\int_0^\infty (f_sf_p+g_sg_p)\left(\Omega_s^\dagger\mathbf{n}\Omega_p\right)\left[\Phi(\mathbf{R})\right]R^2dR\sin\theta d\theta d\phi$$

Using

$$\int_0^\infty dR\int_R^\infty dr=\int_0^\infty dr\int_0^r dR$$

and $U_{sp}=f_sf_p+g_sg_p$, the above term reduces to

$$=-e^2\langle s|\mathbf{n}|p\rangle\int_0^\infty\left[\frac{\langle\mathbf{r}\rangle}{ZR^3}-\frac{\mathbf{r}}{R^3}+\frac{\mathbf{r}}{r^3}\right]\rho(\mathbf{r})d^3r\int_0^r R^2U_{sp}dR$$

$$= -e^2\langle s|\mathbf{n}|p\rangle \left\{ \int_0^\infty \left[\left(\frac{1}{Z}\langle \mathbf{r}\rangle - \mathbf{r} \right) \int_0^r U_{sp} dR + \frac{\mathbf{r}}{r^3} \int_0^r U_{sp} R^3 dR \right] \rho(\mathbf{r}) d^3r \right\}$$

Now expand $U_{sp} = f_s f_p + g_s g_p = \sum_k b_k R^k$ and substituting in the above equation

$$= -e^2\langle s|\mathbf{n}|p\rangle \sum_k \left\{ \left[\int_0^\infty \left(\left(\frac{1}{Z}\langle \mathbf{r}\rangle - \mathbf{r} \right) b_k \frac{r^{k+1}}{k+1} + \frac{\mathbf{r}}{r^3}\frac{r^{k+4}}{k+4} b_k \right) \right] \rho(\mathbf{r}) d^3r \right\}$$

$$= -e^2\langle s|\mathbf{n}|p\rangle \sum_k \frac{b_k}{k+1} \left\{ \left[\frac{1}{Z}\langle \mathbf{r}\rangle\langle r^{k+1}\rangle - \frac{3}{k+4}\langle \mathbf{r} r^{k+1}\rangle \right] \right\}$$

where $\langle s|\mathbf{n}|p\rangle = \int \Omega_s^\dagger \mathbf{n} \Omega_p d\phi \sin\theta d\theta$.

In the non-relativistic case, ($Z\alpha \to 0$), only $b_1 \neq 0$. Hence,

$$\langle s| - e\Phi^{(1)}|p\rangle = -\frac{e^2 b_1}{2}\langle s|\vec{n}|p\rangle \cdot \left[\frac{1}{Z}\langle \vec{r}\rangle\langle r^2\rangle - \frac{3}{5}\langle \vec{r} r^2\rangle \right]$$

$$= 4\pi e \vec{S} \cdot \left(\nabla \Psi_s^\dagger \Psi_p \right)_{R\to 0}$$

where the Schiff moment $\vec{S}$ is defined as

$$\vec{S} = \frac{e}{10}\left[\langle \vec{r} r^2\rangle - \frac{5}{3Z}\langle r^2\rangle\langle \vec{r}\rangle \right] = S\vec{I}/I \tag{F.6}$$

where $\vec{I}$ is the nuclear spin. The above form of the Schiff moment defines the non-relativistic expression for the $\hat{P}$ and $\hat{T}$ violating nuclear potential arising due to the Schiff moment. Note that the quantities defining S refer to the nuclear coordinates.

Appendix G

Additional Notes

G.1 Matrix elements of the Coulomb operator

The term representing the two-body Coulomb interaction can be expanded as [25, 26]

$$\frac{1}{r_{12}} = \sum_k U^k(1,2) \sum_q (-1)^q C_q^k(1) C_{-q}^k(2) \tag{G.1}$$

where

$$U^k(1,2) = \frac{r_<^k}{r_>^{k+1}},$$

$$C_q^k = \sqrt{4\pi/2k+1} Y_q^k(\theta, \phi)$$

The two-electron matrix element is given by,

$$\langle ab|\frac{1}{r_{12}}|cd\rangle = \delta(m_a + m_b, m_c + m_d) \sum_k d^k(j_a m_a; j_c m_c) d^k(j_b m_b; j_d m_d) R^k(a,b,c,d,k)$$

The 'd^k' coefficients are the angular factors and $R^k(a,b,c,d,k)$ is a two-electron radial integral dependent on the large and small components of the orbitals a,b,c,d and the multipole k. This can written as,

$$\left\langle ab\left|\frac{1}{r_{12}}\right|cd\right\rangle = \sum_{\substack{j_a,j_c,j_b,j_d \\ m_a,m_c,m_b,m_d,k,q}} X_q^k(j_a,j_b,j_c,j_d)(-1)^{(j_a-m_a+j_d-m_d)} \begin{pmatrix} j_a & k & j_c \\ -m_a & q & m_c \end{pmatrix} \begin{pmatrix} j_d & k & j_b \\ -m_d & q & m_b \end{pmatrix} \tag{G.2}$$

where

$$X_q^k\left(j_a, j_b, j_c, j_d\right) = (-1)^{(k-q)}\,(-1)^{(j_a-\frac{1}{2}+j_b-\frac{1}{2})} \begin{pmatrix} j_a & k & j_c \\ \frac{1}{2} & 0 & -\frac{1}{2} \end{pmatrix} \begin{pmatrix} j_d & k & j_b \\ \frac{1}{2} & 0 & -\frac{1}{2} \end{pmatrix}$$

$$\left[j_a, j_c, j_b, j_d\right]^{\frac{1}{2}} R^k\left(a, b, c, d, k\right)$$

and

$$R^k\left(a, b, c, d, k\right) = \int_0^\infty \int_0^\infty \Big[P_a(r_1)P_c(r_1) + Q_a(r_1)Q_c(r_1)\Big] \times \frac{r_<^k}{r_>^{k+1}}$$

$$\times \Big[P_b(r_2)P_d(r_2) + Q_b(r_2)Q_d(r_2)\Big]\, dr_1\, dr_2$$

With the selection rules,

$$(-1)^{l_a+l_c+k} = (-1)^{l_b+l_d+k} = 1$$

G.2 Matrix elements of the Induced Dipole Operator

Consider the angular matrix element of the induced dipole operator between the states of angular momenta (J_a, M_a) and (J_b, M_b),

$$\left\langle \Psi_{J_a,M_a} \middle| D^k_{\rm ind} \middle| \Psi_{J_b,M_b} \right\rangle = \Big(-1\Big)^{J_a-M_a} \begin{pmatrix} J_a & k & J_b \\ -M_a & 0 & M_b \end{pmatrix} \times \left\langle J_a \middle\| D^k_{\rm ind} \middle\| J_b \right\rangle$$

where the reduced matrix element is

$$\left\langle J_a \middle\| D^k_{\rm ind} \middle\| J_b \right\rangle = \Big(-1\Big)^{J_a+\frac{1}{2}} \Big[(2J_a+1)\,(2J_b+1)\Big] \begin{pmatrix} J_a & 1 & J_b \\ \frac{1}{2} & 0 & -\frac{1}{2} \end{pmatrix} \times \left\langle \Psi_a(r) \middle| D_{\rm ind} \middle| \Psi_b(r) \right\rangle$$

and $D_{\rm ind} = e\,\mathbf{r}$.

Bibliography

[1] C.S.Wu, E. Ambler, R. W. Hayward, D. D. Hoppes, and R. P. Hudson. *Phys. Rev.*, 105:1413–1415, 1957.

[2] J.R. Christensen, J.W. Cronin, V.L. Fitch, and R.Turlay. *Phys. Rev. Lett.*, 138(13), 1964.

[3] E. D. Commins. *Advances in Atomic, Molecular and Optical Physics*, 40(1), 1999.

[4] S. M. Barr and W. J. Marciano. In cp violation. World Scientific, Singapore, 1989. edited by C. Jarlkog.

[5] M. V. Romalis, W. C. Griffith, J. P. Jacobs, and E. N. Fortson. *Phys. Rev. Lett.*, 86:2505, 2001.

[6] J.P. Jacobs, W.M. Klipstein, S.K. Lamoreaux, B.R. Heckel, and E.N. Fortson. *Phys. Rev. Lett.*, 71(23):3782, 1993.

[7] Ann-Marie Martensson-Pendrill. *Phys. Rev. Lett*, 54(11), 1985.

[8] Toby Falk, Keith A. Olive, Maxim Pospelov, and Radu Roiban. *Nucl.Phys. B*, 560:3–22, 1999.

[9] A.M. Martensson-Pendrill and E. Lindroth. *Europhys. Lett.*, 15(2):155–160, 1991.

[10] V. A. Dzuba, V.V. Flambaum, and J. S. M. Ginges. *Phys. Rev. A*, 66:012111, 2002.

[11] J. S. M. Ginges and V.V. Flambaum. *Physics Reports*, 397:63–154, 2005.

[12] V. V. Flambaum, I. B. Khriplovich, and O. P. Sushkov. *Nucl. Phys. A*, 449:750, 1986.

[13] W. C. Haxton. *Chinese Journal of Physics*, 32(S-11), 1994.

[14] M. Pospelov. *Phys. Lett. B*, 530:123, 2002.

[15] V. F. Dmitriev and R. A. Senkov. *Phys. Rev. Lett*, 91:21, 2003.

[16] Norval Fortson, Patrick Sandars, and Stephen Barr, 2003.

[17] V.V. Flambaum and J. S. M. Ginges. *Phys. Rev. A*, 65:032113(1)–032113(9), 2002.

[18] I. Lindgren and J. Morrison. *Atomic Many-Body Theory.* Springer-Verlag, 1985.

[19] Raymond F. Bishop and Hermann Kummel, 1987.

[20] R. F. Bishop. *Microscopic Quantum Many-Body Theories and their Applications (Lecture notes in Physics).* Springer-Verlag-Berlin, 1998. J. Navarro and A. Polls.

[21] R. J. Bartlett. *Modern Electronic Structure Theory*, volume III. World Scientific, Singapore, 1995. edited by D. R. Yarkony.

[22] Hermann Kummel. Origins of the coupled cluster method. *Theoretica Chemica Acta*, 80:81–89, 1991.

[23] Geetha K.P. *Relativistic Many-body Studies of Parity Non-Conservation (PNC) in Heavy Atomic Ions.* PhD thesis, Bangalore University, 2001.

[24] A. Szabo and N.S. Ostlund. *Modern Quantum Chemistry.* Dover Publications.

[25] I.P. Grant. *Adv. Phys.*, 19:747, 1970.

[26] I.P. Grant. *Proceedings. Royal. Society A*, 262:555, 1961.

[27] Angom Dilip Kumar Singh and K.V.P. Latha. *Calculation of Atomic Electric Dipole Moment of Closed-shell Atoms using Coupled-cluster Method.* http://www.iiap.res.in/research/NAPP/main.html, 2006. unpublished.

[28] I. Lindgren and J. Morrisson. *Atomic Many-Body Theory.* Springer-Verlag, Berlin, 2nd. ed edition, 1986.

[29] A.K. Mohanty and E. Clementi. *Chemical Physics Letters*, 157:348–352, 1989.

[30] Thomas M. Miller and Benjamin Bederson. *Advances in Atomic, Molecular Physics*, 13(1), 1977.

[31] R. J. Crewther, P. Di Vecchia, G. Veneziano, and E. Witten. *Phys. Lett*, 91B:487(E), 1980.

[32] R. J. Crewther, P. Di Vecchia, G. Veneziano, and E. Witten. *Phys. Lett*, 88B:123, 1979.